Universidad Autónoma de Madrid

Facultad de Ciencias

Departamento de Biología Molecular

Cell Competition in heart development and homeostasis.

Doctoral thesis

Cristina Villa del Campo

Diciembre 2014

Director: Miguel Torres Sánchez
Tutor: Pablo Gómez del Arco

This work was performed in Miguel Torres' laboratory in the Cardiovascular Developmental Biology and Repair Department at the Centro Nacional de Investigaciones Cardiovasculares (CNIC) in Madrid

This study was funded by grants RD06/0010/0008 (TerCel RETICS), RD12/0019/0005 (TerCel RETICS), BFU2009-08331 (MICINN), S2010/BMD-2315 (Comunidad de Madrid) and BFU2012-31086 (MINECO).

Cristina Villa del Campo has a FPI fellowship from the MINECO (BFU2009-08331)

The only way to make sense out of change is to
move with it and join the dance
(Alan Watts)

INDEX

INDEX of FIGURES

Figures

Tables

Abbreviations

AHF: Anterior heart field
ANP: Atrial Natriuretic peptide (also Nppa)
AVC: Atrioventricular canal
Bcl2: B cell leukemia/lymphoma 2
Bmp: Bone morphogenetic protein
Bst: Belly spot and tail
Cdk4: Cyclin-dependent kinase 4
Cnc: Cardiac neural crest
Dpp: Decapentaplegic
ECFP: Enhanced cyan fluorescent protein
ECM: Extracellular matrix
EGF: Epidermal growth factor
EMT: epithelial to mesenchymal transition
EPDCs: Epicardial derived cells
EYFP: Enhanced Bellow fluorescent protein
FHF: First heart field
Fwe: Flower
iMOS: Inducible mosaics
ISH: In situ hybridization
IVS: Interventricular septum
LV: Left Ventricle
MEF2C: Myocyte enhancer factor 2C
mESC: Mouse embryonic stem cell
MI: Myocardial infarction
Myc: Myelocytomatosis oncogene
Mycn: v-myc myelocytomatosis viral related oncogene, neuroblastoma derived
Myh6: myosin, heavy polypeptide 6, cardiac muscle, alpha
Nppa: See ANP
OFT: Outflow tract
PE: Proepicardium
PHH3: Phosfohistone 3
Pi3K: Phosphatidylinositol 3-kinase

Tbx18: T-box18

TGFb: Transforming Growth Factor beta

VFW: Ventricular free wall

WT: Wild-type

Wt1: Wilms tumor 1 homolog

SUMMARY

It is my ambition to say in ten sentences what others say in a whole book
(Friedrich Nietzsche)

Heterogeneous anabolic capacity in cell populations can trigger a phenomenon known as cell competition, through which less active cells are eliminated. Cell competition has been induced experimentally in stem/precursor cell populations in insects and mammals and takes place endogenously in early mouse embryonic cells. Here we show that cell competition can be efficiently induced in mouse cardiomyocytes by mosaic overexpression of Myc both during gestation and adult life. The expansion of the Myc-overexpressing cardiomyocyte population is driven by the elimination of wild type cardiomyocytes, which happens through apoptosis in the embryonic heart and autophagic cell death in the adult cardiomyocytes. Importantly, this cardiomyocyte replacement is phenotypically silent and does not affect heart anatomy or function. Myc overexpression in the adult heart induces a cardioprotective response through the reactivation of fetal programs.

Moreover, cell competition induction in the epicardium during development shows an increased contribution of this lineage to cardiac myocytes. These results show that capacity for cell competition in mammals is not restricted to stem cell populations and suggest that stimulated cell competition has potential as a cardiomyocyte replacement strategy.

La heterogeneidad en la eficiencia anabólica de una población celular desencadena un fenómeno que se conoce como Competición Celular, mediante el cual las células metabólicamente menos activas son eliminadas. La competición celular se ha inducido experimentalmente en poblaciones de células madre/progenitoras en insectos y mamíferos y se ha demostrado que ocurre de forma endógena en células madre embrionarias de ratón. En esta tesis demostramos que la competición celular puede inducirse en cardiomiocitos de ratón mediante sobreexpresión en mosaico de Myc, tanto en desarrollo como en el corazón adulto. La expansión de los cardiomiocitos que sobreexpresan Myc tiene lugar debido a la eliminación de los cardiomiocitos salvajes.

Cabe resaltar que este reemplazo de cardiomiocitos ocurre de manera fenotipicamente silenciosa y no afecta a la anatomía o función cardiacas.

Aún más, la inducción de competición celular en el epicardio (que ha demostrado ser una población celular con características de células progenitoras) durante el desarrollo da lugar a un aumento en la contribución de dicho linaje a cardiomiocitos.

Estos resultados demuestran que la capacidad de competir en células de mamífero no se restringen a poblaciones de células madre y se propone que el estímulo de esta capacidad celular podría tener potencial en estrategias de reemplazo de cardiomiocitos.

INTRODUCTION

The journey of a thousand miles begins with one step (Lao Tzu)

Cell competition has only recently been described to be a mechanism that ensures cell fitness during mammalian development (Claveria et al., 2013).

However, whether it is a universal feature to all cells and tissues in the embryo or restricted to pluripotent cells in the epiblast, remains to be determined. In this thesis we address how cell competition can be induced in the developing heart as well as in adult cardiomyocytes in homeostatic conditions.

Moreover, we explore the possibility of inducing cell competition among heart lineages with regenerative potential; thus addressing the putative use of cell competition in heart regeneration approaches.

Cell competition

During evolution, multicellular organisms have evolved different ways to ensure the proper development of their organs and tissues. Such mechanisms rely on complex interactions between cells and depend on the integration of different signals that will lead to cell survival or cell death. If cells fail to receive appropriate signals from their neighbours they undergo programmed cell death (Raff 1992).

Such dependence on specific survival signals provides a way to eliminate misplaced cells, to regulate cell numbers and, perhaps, to select for the fittest cells; ensuring the mainteinance of the homeostasis of the whole organism.

One such mechanism that has been proposed to ensure homeostasis is cell competition, a mechanism by which fitter cells in a given context colonize the tissue at the expense of viable but less fit cells, which are eliminated by induction of apoptosis. Therefore, cell competition is acting as a quality control system to eliminate suboptimal cells.

Cell competition has been defined under various contexts and comprises different types of competitive interactions; but a main feature that underlies cell competition is the elimination of cells that are viable on their own but actively eliminated when confronted with more competitive cells.

Broadly, cell competition can be classified in three types regarding the characteristics of the cells that are in competition (figures 1 y 3).

- Canonical cell competition (Morata and Ripoll, 1975): In this type of cell competition wild-type (WT) cells outcompete neighbouring cells that are somehow defective in their competitive ability; but that are viable when growing

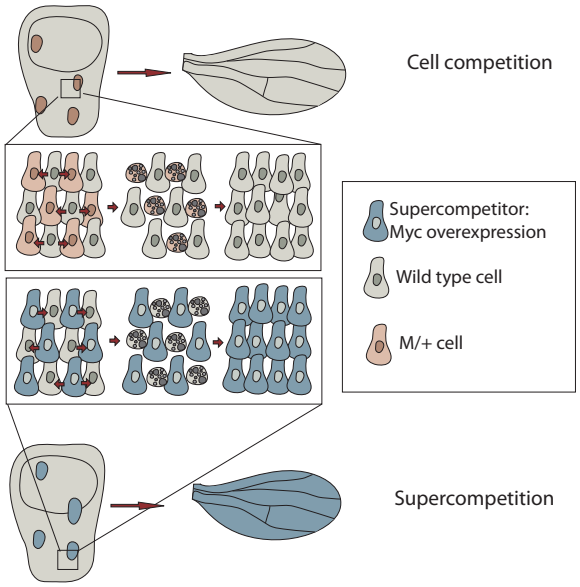

Figure 1. Cell competition and supercompetition in *Drosophila*'s wing disc

Schematic representation of cell competition as was first described in *Drosophila*'s experiments. In cell competition model, *Minute/+* cells were confronted with WT fitter cells and undergo apoptotic elimination. Wild-type cells overproliferated at the expense of *Minute/+* loser cells colonizing the final wing.
In supercompetition induced by Myc, (Moreno and Basler 2004) dMyc clones are generated in a wild-type bakground; and these dMyc cells overproliferate at the expense of WT loser cells that are eliminated by apoptosis. Arrows represent an unknown signal that drives apoptosis-driven cell competition after fitness comparison.

in an homotypic enviroment.

- Supercompetition: (Moreno and Basler 2004) Supercompetitor cells have been genetically modified; and this modification confers them a competitive advantage over wild-type cells; which are outcompeted when growing in a mosaic fashion.

- Endogenous cell competition: (Claveria, et al. 2013)

Endogenous cell competition has only very recently been described, in contrast with the previously mentioned types. It has been proposed to select for fitter cells in an homeostatic context; without being experimentally-induced.

The studies leading to the description of these three types of cell competition as well as factors implicated in one or more competitive interactions is described further down; but all three types share the non-cell-autonomous elimination of "loser cells", that are only defined by the tissue context.

A little bit of history: lessons from the fly

First observation of the phenomenon now termed cell competition was reported almost 40 years ago by Ginés Morata and Pedro Ripoll (Morata and Ripoll, 1975)(reviewed in Diaz and Moreno, 2005) using *Drosophila*'s wing disc, where two different cell populations that differed in metabolic rates were confronted; and it was shown that cells that would have otherwise been viable were eliminated when growing in the presence of cells that were metabolically more active. This experiment was performed using *Minute* flies, which carry a mutation in ribosomal proteins, lacking full ribosome machinery.

Homozygous *Minute* flies are lethal, but when the mutation is carried in heterozigosity, they are viable and develop forming normal flies of the right size, albeit at a slower rate.

However, when *Minute/+* (*M/+*) cells were

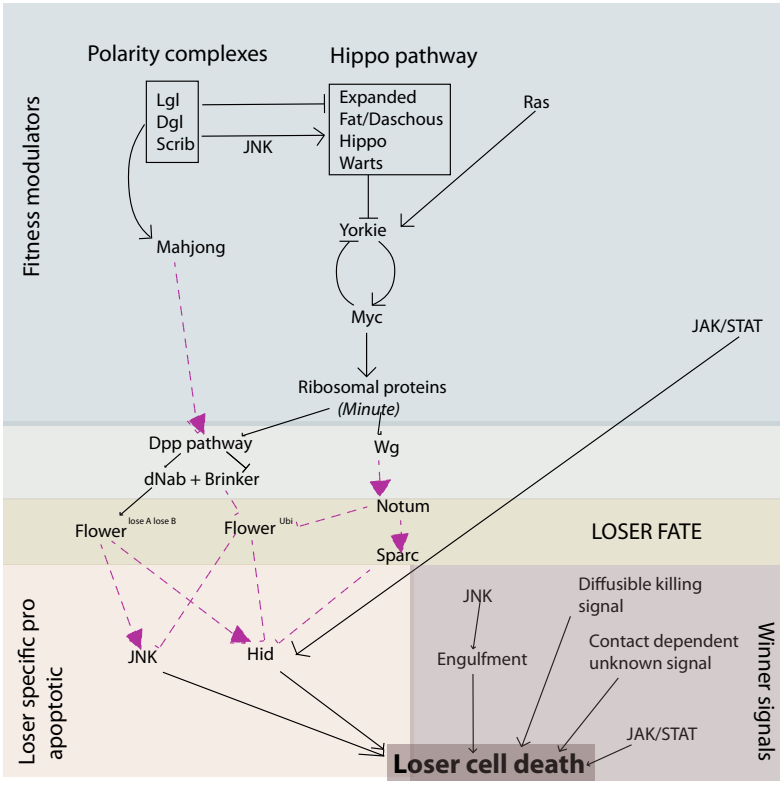

Figure 2. Cell competition and cell selection are multistep processes.

Schematic of the regulation of loser cell elimination, that includes all described pathways involved in cell competition. Coloured rectangles show different layers of regulation. Cell selection is initiated by mutations or pathways that lead to a gain or a loss of fitness (light blue). This modulation of fitness leads to the deficit or gain of some limiting factors for which cells are competing (grey). This then activates cell fitness markers (Flower, Sparc; green). Eventually, loser cell death is induced by different cell autonomous signal (JNK, Hid; Dark brown: LOSER FATE), and by non-cell autonomous signals emitted by winner cells (light brown). Hypothetical relationships are marked by dashed lines that are highlighted in purple.
(Modified from (Levayer and Moreno 2013).

growing in a mosaic wing in direct confrontation with wild type cells, they were completely eliminated (Morata and Ripoll 1975). The conclusion from this was that *Minute* cells, although viable on their own, were eliminated when they had to grow among wild-type cells, metabolically more active.

This model was supported by several studies that followed. Simpson (Simpson, 1979) used a starvation model, that allowed to reduce growth rates in the wing disc. It was described that, in starvation conditions, *M/+* cell elimination happened at a slower rate, and their final proportion in the disc was higher.

This way it was demonstrated that differences in growth rates driven by metabolic activity (abolished upon starvation) underlaid *Minute/+* cell elimination (Simpson, 1979 ; reviewed in de Beco et al., 2012).

It wasn't until many years later that some light was shed on the phenomenon of cell competition. In 2002 a study was published reporting that cells in the imaginal disc could be competing for survival or growth factor signals and that differences in ligand capture mediated the elimination of *M/+* cells.

In the model proposed, cells compete for a secreted protein involved in cell survival, Decapentaplegic (Dpp; member of the TGFb family) (Moreno et al., 2002; reviewed in Gallant, 2005, Milan, 2002). They reproduced classic experiments using *Minute* mutants and defined that *M/+* cells were eliminated by apoptosis when confronted with a WT population. This was confirmed by showing how blocking apoptosis using the baculoviral inhibitor p35 reduced cell competition. It was described that in *Minute* cells, uptake of Dpp signal is defective, leading to apoptotic cell death. In this model, suboptimal cells would have a reduced Dpp uptake, which would lead to their elimination.

Despite the relevance of this study and the description of the ligand capture model, many mechanistic questions remained unanswered. The relevance of the ligand-capture model and other trophic theories for cell competition is still disputed; since, besides the condition of a limiting amount of survival factor; a system that enables the comparison of cell fitness is needed. (Adachi-Yamada and O'Connor, 2002, Gibson and

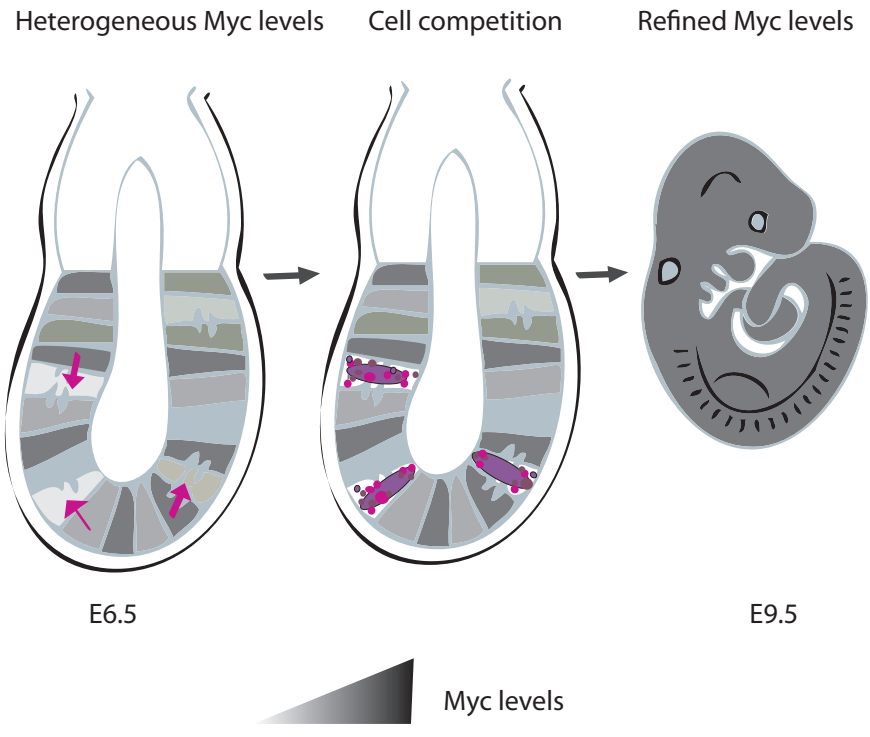

Figure 3. Model depicting how endogenous cell competition was defined

In the Mouse epiblast during normal development, Myc levels are intrinsically heterogeneous and endogenous cell competition refines the epiblast cell population through the elimination of cells with low relative Myc levels. Thus, cell competition naturally contributes to the selection of the epiblast cell pool. (Modified from (Claveria et al., 2013)

Perrimon, 2005, Shen and Dahmann, 2005).

Supercompetition

In 2004 two papers linking cell competition to the proto-oncogen *dMyc* generated a new wave of interest in this process. *dMyc* is a fly homolog of the mammalian family of *Myc* transcription factors (which includes *Myc*, *Mycn* and *L-Myc*), and it is able to regulate the expression of many genes involved in cell proliferation, growth, and the cell's anabolic machinery, including ribosome biogenesis (reviewed in de la Cova and Johnston, 2006; Bellosta and Gallant, 2010).

These two papers studied the role of *dMyc* in cell competition and its implications by inducing clonal dMyc overexpression in the wing disc (de la Cova et al., 2004, Moreno and Basler, 2004). Clones expressing high levels of dMyc were able to expand at the expense of wild type cells until they filled the compartment. This expansion required the elimination of wild-type cells by apoptosis. In this context wild-type cells behaved as "losers" and thus dMyc overexpressing cells were termed "supercompetitors".

It was also shown that these supercompetitor cells (expressing two additional copies of dMyc) behaved as "winners" when confronted with wild type cells but were "losers" if confronted with cells expressing four extra *dMyc* copies (Moreno and Basler, 2004).

This supported the idea that it's not absolute dMyc levels that drive cell competition but rather the relative dMyc in a given cell population.

Moreover, cell competition was not a simple outcome of cell overproliferation, since overexpression of different known factors inducing cell growth (Pi3K, Dp110) or cell cycle regulators (CyclinD and Cdk4) was unable to eliminate wild-type cells however much the clone expanded (Moreno and Basler, 2004; de la Cova et al., 2004).

In this context, *dMyc* deficient cells can be comparable to *Minute/+* cells, suggesting that the force driving cell competition is dMyc control over the cell's anabolic machinery. As in *Minute* classic experiments, dMyc-overexpressing clones only expanded within their compartment until final growth was reached.

There are, however, some differences between classic cell competition and supercompetition, since it has been described that *Minute*-driven cell competition required cell-cell contact (Martin et al., 2009) and dMyc-driven cell competition could be triggered about 10 cell diameters away (de la Cova et al., 2004).

This is consistent with an *in vitro* study performed using *Drosophila's* cells in which conditioned media from cell competition could induce a competitive response (Senoo-Matsuda and Johnston, 2007).

All of these data further support the idea that it is the relative anabolic activity (fitness) between neighbouring cells what drives cell competition and that some sensing mechanism has to allow cells to communicate their fitness status to its neighbours.

Other players involved in cell competition in *Drosophila*

Recently other pathways have been linked to cell competition, either more players in the already described cell competition or novel pathways that affect cell competition in different ways (shown in full detail in figure 2), adding more factors that trigger cell competition, more mediators or cell-cell signals implicated.

We will only mention some of them since in-depth analysis of these pathways falls out of the scope of this thesis.

Regarding which factors are able to induce cell competition; they can roughly be characterized in two groups:

1.- Those that involve differences in ana-

bolic ability, resulting in different growth rates; which were the first shown triggers of cellcompetition (Morata and Ripoll, 1975, Moreno et al., 2002, Simpson and Morata, 1981).

2.- Those in which epithelial integrity is altered. Cells lacking basolateral proteins such as Scribble, undergo apoptosis in the presence of wild-type cells. (Norman et al., 2012).

Even if we will not describe this in detail, loss of epithelial integrity has been described both in *Drosophila* (Igaki et al., 2006, Froldi et al., 2010) and in mammalian models (Norman et al., 2012) (Tamori et al., 2010) to be a trigger of cell competition.

Engulfment as a requirement for cell competition?

Studies of cell competition performed using *Minute* mutants showed that competitive cell death of *M/+* cells by WT clones that expanded at their expense, usually happened where both cell populations were adjacent.

This suggested the existence of winner/loser contact-dependent induction of cell death, and hinted for a requirement of loser cell engulfment by winner cells for cell competition to occur (Li and Baker, 2007; reviewed in Li and Baker, 2007). It also addressed the question of the fate of the outcompeted bodies and how they are eliminated from the tissue, since initial observations claimed that apoptotic cells were extruded from the tissue and accumulated basally (Moreno and Basler, 2004).

It was described that *M/+* cells adjacent to WT population were 5-10x more likely to undergo apoptosis than cells that weren't in contact. Moreover, corpses of *M/+* cells were typically found within the cytoplasm of WT cells. This led to the thought that engulfment played a major role in loser cell corpse clearance. To test this, genes involved in engulfment were mutated, which resulted in an abrogation of cell competition (Li and Baker, 2007).

However, these results have not been reproduced (Lolo et al., 2012; reviewed in Lolo et al., 2013), and it has also been proposed that engulfment was only required for the elimination of already delaminated cells and mostly performed by haemocytes since winner cells didn't need to express engulfment genes forcell competition to occur.

This reopened the question of the mechanism responsible for the elimination of loser cell corpses and also of the meaning of loser cell increased apoptosis at clonal boundaries.

The Flower code

A possible mechanism that could explain apoptosis of loser cells in clonal boundaries would be a cell-cell communication of the cell's fitness status that would lead to the elimination of the less fit cell. Such mechanism would require the presence of a fitness marker that would allow cells to compare each other's anabolic status.

Using gene expression arrays, several genes that were expressed during cell competition were identified. One of those genes was a membrane calcium channel involved in endocytosis and exocytosis. Further assays lead to propose it as a mechanism that would allow neighbouring cells to report their fitness: *Flower* (*fwe*) (Rhiner et al., 2010). Fwe protein contains 3 to 4 transmembrane domains and it is found in three isoforms, which express different C-terminal regions exposed to the extracellular space. One of Flower's isoforms is predominant and it is expressed in WT cells: fwe^{Ubi}. By induction of supercompetition driven by dMyc overexpression, WT loser clones were found to express two other isoforms: $fwe^{Lose\text{-}A}$ and $fwe^{Lose\text{-}B}$.

These isoforms were also expressed in loser cells in *Minute* induced cell competition (Rhiner et al., 2010).

If Fwe^{Lose} isoforms were forcedly expressed in wild-type cells homogenously, no effect was observed. However, when they were expressed in clones, they strongly induced apoptosis.

Moreover, upon reduction of the Fwe^{Ubi} levels in clones, this effect was also observed, suggesting that the ability of Fwe to induce cell death is strongly context dependent, relying on the cell-cell differences in Fwe isoform expression.

Loss of Fwe expression doesn't affect non-competititive growth of the tissue; therefore Fwe is proposed to be a downstream effector of cell competition, labelling loser cells and leading to their elimination.

The regulation mechanism by which *fwe* mRNA is alternatively spliced into *Ubi* or *Lose* forms is still to be determined, as well as how this extracellular code is interpreted in order to lead to cell death or cell survival.

Cell competition relevance for cancer

All of these studies leave an open question on whether cell competition is a universal feature in metazoans, since it could have potential implications in homeostasis, cancer and regeneration. Several studies have linked cell competition to genes implicated in cancer, such as *Myc* but also the tumor suppressor pathway Hippo (Tyler et al., 2007; Chen et al., 2012), Jak/Stat signalling pathway (Rodrigues et al., 2012) and tumor suppressor p53 (de la Cova et al., 2014).

It is thought that cell competition could be implicated in the growth of tumour cells, linking supercompetition with the precancerous fields model, in which these lesions could colonize the tissue by eliminating surrounding cells (Rhiner and Moreno, 2009, de Beco et al., 2012; reviewed in Baker and Li, 2008).

However, the role of cell competition in cancer is still unclear, since it has also been proposed to be a mechanism involved in tumor supression, by driving the elimination of faulty cells; and, when disrupted, promoting the accumulation of cells carrying mutations (Martins et al., 2014; Ballesteros-Arias et al.)

It was then necessary to elucidate the role of cell competition in mammalian models to further understand its possible implications and relevance for cancer.

Cell competition in mammals

A couple of early studies had suggested that cell competition could be an extended mechanism among metazoans:

The 'Belly spot and tail' (*Bst*) mutation is a mouse equivalent of the fly *Minute* mutants, since these mice are defective in the ribosomic protein L24. As in *Drosophila Minutes*, homozygous *Bst* mice are not viable, whereas heterozygous show decreased pigmentation and a kinked tail, along with some other deficiencies (Oliver et al., 2004). By generating chimaeras it was shown that *Bst/+* cells had a significant growth and survival disadvantage in the presence of wild-type cells (Oliver et al., 2004), however this study did not address whether the observed differences resulted from cell-autonomous features or from cell competition.

A further study was published, suggesting a role for cell competition in liver regeneration (Oertel et al., 2006). Upon partial resection of adult rat liver, fetal liver was transplanted; and it was shown that fetal hepatocytes grafted and proliferated in the host for long periods being able to replace up to 23% of the liver mass. Moreover it was also shown that this repopulation was associated with increased apoptosis of host hepatocytes immediately adjacent to the transplanted fetal ones (Oertel et al., 2006).

Two studies published later assessed the role of the tumour suppressor gene *p53*. A form of cell competition based on stress and mediated by p53 was described, being res-

tricted to the hematopoietic compartment. In this case, cell competition induced a senescence-like phenotype in outcompeted cells rather than their apoptotic elimination (Bondar and Medzhitov, 2010, Marusyk et al., 2010). When mixed with irradiated wild-type cells, cells with mutant *p53* have an advantage and become winners, repopulating hosts more efficiently. In this context, cell competition selects for less damaged cells by comparing p53 levels (Bondar and Medzhitov, 2010).

Loss of epithelial polarity has also been related with cell competition *in vitro* in several studies (Tamori et al., 2010) which describe for the first time epithelial-integrity related cell competition in mammals. More recently, it has been reported in a mammalian model *in vitro* how loss of *Scribble* in clones induced them to be eliminated (Norman et al., 2012).

All of the mentioned assays performed in mammalian systems suggested that cell competition could be a universal characteristic of metazoans.

The reports of cell competition commented, however, involved the experimental introduction of stress or mutations and did not address the potential roles of natural cell competition in normal developmental or tissue homeostasis processes. Clavería and colleagues approached the study of cell competition in mammals by developing a system of inducible mosaics based on Cre recombination (Clavería et al., 2013). Recombination generates two different labelled cell populations; one of which overexpresses Myc under the control of the *Rosa26* promoter. Using this system, it was demonstrated that supercompetition could be induced in the mouse epiblast and that it provoked the phenotypically silent replacement of wild type cells.

This replacement relied on apoptosis of WT loser cells that was shown to be contact dependent, as WT cells in direct contact with Myc overexpressing ones showed higher apoptotic rates. Moreover, it was demonstrated that cell competition occurred endogenously in the epiblast. Epiblast pluripotent cells were shown to have high number of naturally occurring apoptotic events and express Myc in an heterogeneous fashion, which was not observed with other pluripotency markers.

It was shown that those epiblast cells undergoing apoptosis were the ones that expressed lower relative Myc levels, and thus, elimination of these cells refined Myc levels of the developing embryo. Rescuing cells by p35 expression showed that their Myc levels were relatively lower than those of the rest of the population (they were “loser” cells), indicating that cells that were eliminated in normal conditions were those which expressed less Myc.

This study also explored cell competition in vitro in mouse embryonic stem cells (mESC).

It was reported for the first time not only that cell competition could be induced in mESC cultures but also that these cultures were also subject to endogenous cell competition, dependent on their differences in endogenous Myc levels. The mechanism for the elimination of loser cells both in the epiblast and in mESC cultures was also explored, and it was shown that those cells with relative lower Myc levels were engulfed by their winner neighbours, shedding some light on the mechanism by which loser cell corpses are eliminated and why cell contact could be a key mechanism in this elimination.

This study was the first to report anabolic endogenous cell competition happening naturally in the developing embryo and proposed a model in which epiblast cells compare their anabolic ability and eliminate those with relative lower fitness, thus refining the overall fitness of the cells that will generate the em-

bryo. Parallel studies have also identified Flower-mediated endogenous cell competition in *Drosophila* for the elimination of supernumerary neurons (Merino et al., 2013).

A second study in mESCs demonstrated cell competition dependent of BMP receptor and Myc levels (Sancho et al., 2013). It is not clear, however, that the phenomena reported are equivalent, since in the Claveria study, Myc-induced cell competition took place in undifferentiated mESCs and required close contact; while in the Sancho et al. study, induced differentiation was required for competition and cell competition could be induced by transferring the supernatant of the cultures.

A more recent example of endogenous cell competition has been reported for T-cell progenitors in the thymus (Martins et al., 2014). It was shown that resident progenitor cells were outcompeted by bone-marrow-derived colonizing cells upon competition for the survival factor Interleukin7 (IL7) and that cell competition is required to replace thymus-resident progenitors with fresh cells from the bone marrow; since abolishment of cell competition in this context led to a cancerous transformation of thymic cells; again suggesting cell competition could play a role in eliminating faulty cells and thus preventing oncogenic responses.

These studies open the door to understanding the role of cell competition in normal organism development and physiology.

Despite the universality of cell competition mechanism (shown to be conserved across metazoans) the studies performed in insects and specially those in mammals seem to link cell competition to cellular stemness or progenitor states, but this hypothesis remains to be tested experimentally.

In this thesis we explore this issue by asking whether cell competition could be induced in one of the first lineages to differentiate in the mammalian embryo, the cardiac lineage.

Heart development

The heart is the first organ to form in the embryo; and its development is a complex process that involves the integration of many different cell populations that must be incorporated into an already functional organ.

Heart progenitor cells arise from the splanchnic mesoderm that migrate anteriorly during gastrulation to give rise to two regions or fields of cardiac progenitor cells, located at both sides of the midline (reviewed in Rana et al., 2013; Vincent and Buckingham, 2010).

Around day E7.5, these two bilateral regions then fuse at the midline to give rise to what is commonly termed ‘the cardiac crescent’ (figure 4). These cardiac crescent cells migrate to fuse into a heart tube that detaches from the splanchnic mesoderm, and remains only connected to the dorsal pericardial walls by its ends, the arterial and the venous poles.

This primary heart tube mostly contains left ventricle (LV) and atrial precursors, and is referred to as first heart field (FHF), composed by a myocardial layer lined by an internal endocardial layer. However, the majority of the precursors that will form the heart remain in an undifferentiated state medially and posteriorly to the primary cardiac tube.

This second source of cardiac progenitors is commonly termed second heart field (SHF) due to its later contribution to the developing heart, although the nature of the dynamics and molecular mechanisms underlying the restrictions between these two fields of progenitors is still debated.

The first heart field cells upon differentiation lower their proliferation rate and growth of the heart tube at this stage relies mostly on incorporation of SHF progenitors at both poles of the tube (de Boer et al., 2012). These progenitors remain highly proliferative and undifferentiated, and are progressively added

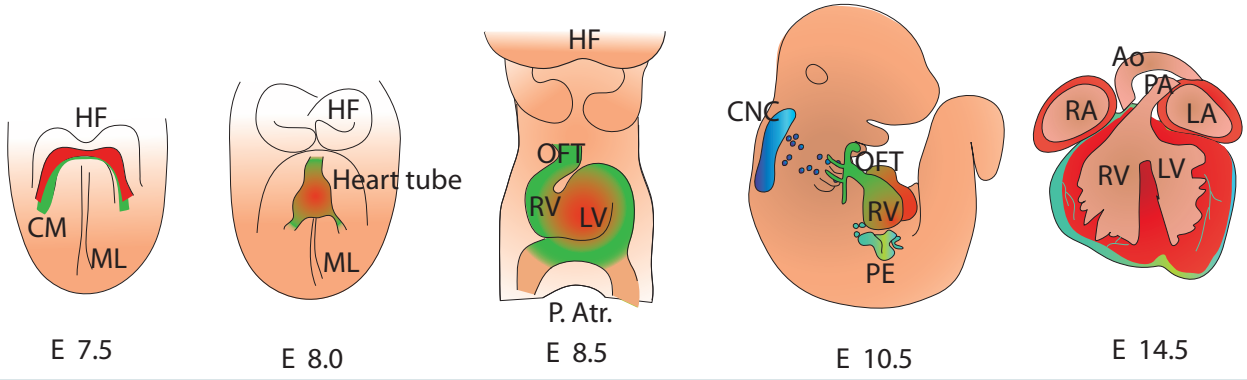

Figure 4. Overview of early heart development

Ventral views of the developing mouse embryo and embryonic heart. At E7.5 cardiac progenitors (CM, red) migrate to the midline (ML) of the embryo to form the cardiac tube. At E7.5 two cardiac fields are distinguished: the first heart field (FHF red) and the second heart field (SHF, green). By E8.0 a cardiac tube is formed where endocardium and myocardium are already present. At E8.5, the tube loops and the different cardiac regions become apparent: atrium (left and right LA, RA), ventricle (left and right LV, RV), outflow tract (OFT).

By E10.5 cells have been added to the heart from the second heart field region and new cells are incorporated from the cardiac neural crest (CNC; blue) and from the proepicardium (turquoise), which gives rise to the epicardial layer, tah upon EMT will contribute to the coronary vasculature. (as seen at E14.5). HF: head folds; Ao: Aorta. (Modified from Buckingham *et al.* 2005)

to the heart tube allowing its expansion. At the arterial pole, SHF cells give rise to the outflow tract (OFT), the right ventricle and the ventricular septum (Zaffran et al., 2004), whereas at the venous pole, SHF progenitors contribute to atria (although the majority of cells in the atria come form FHF) and atrial septum (Snarr et al., 2008).

While this addition is taking place, the heart undergoes a rightward looping that positions the forming chambers that are being specified, the atria become displaced cranial to the ventricles.

At this point, chamber regions (LV, RV, atria) are specified and undergo a ballooning process increasing their proliferation rate locally; as opposed to valve forming regions, namely atrio-ventricular canal (AVC) which will give rise to mitral and tricuspid valves and outflow tract (OFT), where pulmonary and aortic valves are formed.

During this phase, the chambers reach their final organization and the myocardial layer thickens forming a layer of projections that invade the heart lumen (the trabecules), which allow the myocardium to meet the cardiac pumping needs and still allow for proper nutrition and gas exchange before the formation of the coronary vessels.

This trabecules emerge at around day E9.5 and last until approximately day E14.5, when the myocardium undergoes compaction, the trabeculae stop growing and thicken, merging with the compact layer of the myocardium.

As these process takes place, the space between trabeculae forms capillaries (reviewed in Samsa et al., 2013).

Afterwards, septation of both atria and ventricles occurs. Cells from neural crest (cardiac neural crest or CNC) also become added to the developing heart and give rise to the separation of the OFT into aorta and pulmonary vein (Kirby and Hutson, 2010).

Epicardium and its contribution to the developing heart

The epicardium is the outermost layer of the heart. It derives from an extracardiac structure, the proepicardium (PE), a mass of cells from the coelomic epithelium that forms at the posterior dorsal pericardial wall, near the venous pole of the heart, protruding to

the pericardial cavity, at around E9.5 (reviewed in Perez-Pomares and de la Pompa, 2011).

The proepicardial cells then migrate onto the looping heart and attach to the myocardial surface, where they flatten and adopt their characteristic "cobble-stone" morphology. The epicardium then undergoes a process of EMT (epithelial to mesenchymal transition) and gives rise to EPDCs (epicardial derived cells) that invade the myocardial layer and differentiate into several cell types within the developing heart. EPDCs contribute mostly to form the coronary vessels and interstitial heart fibroblasts (figure 5).

EPDCs have been reported to give rise to endothelial cells (Perez-Pomares et al., 2002) and vascular smooth muscle cells (Mikawa and Gourdie, 1996) in the coronary vessels and to cardiac fibroblasts (Gittenberger-de Groot et al., 1998). Contribution of the epicardium to the cardiomyocyte population has also been reported (Zhou et al., 2008, Cai et al., 2008); but this is still a controversial issue (Christoffels et al., 2009) and remains to be elucidated.

Despite the controversy, EPDCs have been shown to be a multipotent progenitor within the heart (Wessels and Perez-Pomares, 2004).

Moreover, studies in adult mice in a myocardial infarction context upon priming have shown that epicardial cells are able to recapitulate an embryonic program and give rise to new vasculature (Smart et al., 2007) and cardiomyocytes (Smart et al., 2011), which supports the notion that EPDCs in the adult heart can be a source of progenitor cells (Chong et al., 2011) with multiple potentials, and evidences the need for further studies regarding epicardium both in embryonic and in adult context.

Maintaining the numbers: cell proliferation/renewal in the developing and adult heart

As mentioned previously, during development, the linear heart tube is a slow proliferating structure and during this phase the heart grows by addition of cells from the SHF; whose high proliferation rates lower upon differentiation (Kelly et al., 2001).

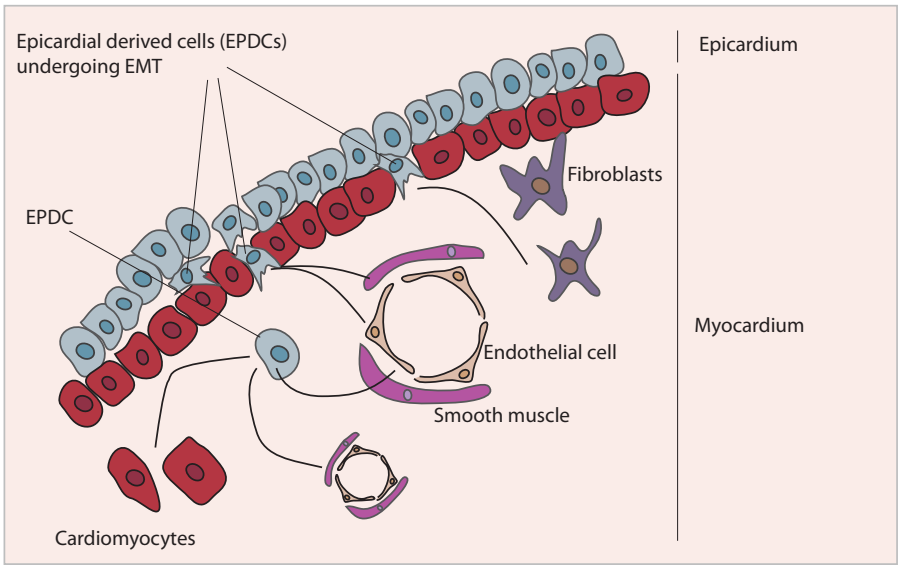

Figure 5. Epicardium and its contribution to the developing heart.

Schematic representation of epicardium contribution to different cell types in the developing heart. Epicardial cells cover the heart surface and then undergo ETM, delaminate from the epicardium, invade the underlying myocardium and these EPDCs subsequently differentiate into smooth muscle, fibroblast, endothelial cells and maybe to cardiomyocytes. (Modified from Epicardial Lineages and Cardiac Repair Manvendra K. Singh and Jonathan A. Epstein)

An increase in cell proliferation takes place in the chamber forming regions during the ballooning phase (de Boer et al., 2012).

After that, the fetal heart grows through continuous proliferation. In postnatal stages, proliferation declines and cardiomyocytes undergo binucleation. Thus, there are two distinct cycling phases: the fetal one, resulting in cell division and the postnatal one, which takes place after birth and results in cardiomyocytes entering a quiescent state and undergoing binucleation through lack of cytokinesis. (Soonpaa et al., 1996; Li et al., 1996).

This switch from hyperplastic to hypertrophic growth is tightly linked to binucleation and "terminal differentiation" of cardiomyocytes. Caryokinesis without cytokinesis is therefore associated with the loss of the proliferative capacity.

Moreover, lower vertebrate species in which cardiomyocytes do not undergo binucleation, have been long shown to be able to regenerate part of the heart. In amphibians and fish the ventricle is undivided, and the animal can survive removal of the apex.

It was shown in 1974 that newt heart could undergo a resection of its ventricle and grow it back; while DNA synthesis was detected close to the wound (Oberpriller and Oberpriller, 1974). More recently, the zebrafish has been stablished as a cardiac regeneration model (Poss et al., 2002, Raya et al., 2003).

The fact that mammalian heart underwent a phase of hypertrophic growth and binucleation associated with the loss of proliferative capacity, led to the long-standing belief that the heart was a fully "post-mitotic organ" and unable to regenerate. While this view holds true for the most part of the postnatal life, it has been shown that postnatal heart retains regenerative ability until P7 (postnatal day 7) (Porrello, Mahmoud et al. 2011), coinciding with the cessation of developmental proliferation of cardiomyocytes (Soonpaa et al., 1996).

The question on adult cardiomyocyte turnover rate remains controversial, although it is widely accepted now that some degree of cardiomyocyte renewal takes place in the mammalian adult heart.

Several studies report a low rate of cardiomyocyte renewal in homeostatic conditions both in humans (Bergmann et al., 2009, Kajstura et al., 2010) and rodents (Soonpaa and Field, 1997, Senyo et al., 2013, Ali et al., 2014); and after heart injury, proliferation of cardiomyocytes and cardiomyocyte renewal is increased near the border of the infracted zone (Senyo et al., 2013).

Despite intensive research regarding this topic, the results are intensely debated and proliferation rates of existing cardiomyocytes in the adult heart differ, ranging from 1% (Soonpaa and Field, 1994, Bergmann et al., 2009) to 40% per year (Kajstura et al., 2010).

Interestingly, it has also been shown that inducing cardiomyocyte-restricted Cyclin D2 expression resulted in regenerative growth in injured hearts (Pasumarthi et al., 2005). The proliferative activation of cardiomyocytes led to a clear reduction in scarring and an increased number of cardiomyocytes, concomitant with improved heart function and anatomy following myocardial infarction (MI).

Therefore, new insight on the heart capacity to replenish cardiomyocytes in homeostatic conditions is an interesting lead; and the implications of further studies addressing this issue would be very relevant for the future of cardiovascular medicine.

Dealing with stress: how the heart responds to physiological and pathological challenges

In the adult heart, growth of the organ usually corresponds to its functional load. In

responses to changes in demand, the heart triggers a hypertrophic response to counterbalance the increase in wall stress (reviewed in (McMullen and Jennings, 2007).

Hypertrophic responses in the adult heart are broadly classified in physiological and pathological, and although they both share common features they are caused by different stimuli and associated with different molecular and cellular responses (Iemitsu et al., 2001).

Pathological cardiac hypertrophy is associated with hypertension, valve disease, myocardial infarction and genetic causes; whereas physiological hypertrophy occurs during development or early postnatal stages and in response to exercise (Fagard, 1997).

Both of them concur with an increase in myocyte volume and the pathological response involves also a depressed cardiac function. Pathological hypertrophy is usually accompanied by fibrosis and extracellular matrix (ECM) accumulation (Brower et al., 2006), although both types involve remodelling of the ECM.

In pathological hypertrophy there is usually a reactivation of fetal genes, which show an increased expression, such as atrial natriuretic peptide (ANP) (Saito et al., 1987).

The fetal gene program also triggers significant changes in metabolic programs. Myocardial energy metabolism during cardiac hypertrophy presents a shift in fuel consumption similar to that seen in fetal heart tissue: the heart muscle decreases fatty-acid oxidation and increases glucose utilization.

This metabolic change appears to be advantageous by delaying the transition to heart failure (Lopaschuk et al., 2010).

The understanding of the molecular pathways activated under pathological stress conditions will help developing new cardioprotective therapies; and along with further insight in cardiomyocyte turnover promotion, will provide tools for myocyte replenishment.

OBJECTIVES

Only the most naïve of questions are truly serious
(Milan Kundera)

OBJECTIVES

At the light of recent studies pointing to a role of cell competition in refining fitness in pluripotent epiblast cells and the potential relevance of cell competition to cancer, we decided to explore the role of cell competition in differentiated cells, the cardiomyocytes; both during embryonic development and in adult homeostatic conditions. Moreover we addressed the potential role of cell competition in a pool of cardiac cells with potential regenerative ability, the epicardium.

In this study we have induced cell competition in embryonic cardiomyocytes by generating heterogeneity in Myc levels.

Specific aims:

Determine whether induced heterogeneous Myc levels induce cell competition in developing cardiomyocytes and study the mechanisms involved

Determine whether induced heterogeneous Myc levels induce cell competition during cardiac tissue homeostasis in adult cardiomyocytes and study of the implications for cardiac function.

Determine how cell cardiomyocyte competition affects cardiac adaptation to physiological stress.

Determine the changes in the expression profile upon Myc mosaic expression in cardiomyocytes.

Determine how the epicardium and epicardial-derived lineages respond to Myc-induced cell competition.

OBJECTIVES

MATERIALS AND METHODS

Men have become the tools of their tools
(H.D. Thoreau)

MATERIALS AND METHODS

Animal models

iMOS lines. The mosaic lines used in this thesis have been previously described: (Claveria et al., 2013) and are shown in figure 6.

iMOS^{WT} in which both labelled cell populations are WT.

iMOS$^{T1\text{-}Myc}$ in which EYFP population overexpresses Myc and ECFP population is WT.

iMOS$^{T1\text{-}Myc/T2\text{-}p35}$ in which EYFP population overexpresses Myc and ECFP population expresses apoptosis inhibitor p35.

iMOS$^{T2\text{-}p35}$ in which EYFP population is WT and ECFP population expresses the apoptosis inhibitor p35.

Cre lines:

Nkx2.5-Cre (Stanley et al., 2002)

Islet1-Cre (Cai et al., 2003)

Mef2C-AHF-Cre (Verzi et al., 2005)

My6-merCremer (Sohal et al., 2001)

Wt1-Cre (Wessels et al., 2012)

Wt1 CreERT2 (Zhou et al., 2008)

Tie2-Cre (Kisanuki et al., 2001)

nMyc flox (Knoepfler et al., 2002)

Embryo harvest

Mice embryos were extracted at different developmental stages. Females from different genotypes (usually *iMOS* positive females) were mated with males (usually carrying the Cre recombinase).

To estimate the developmental stage, vaginal plugs were checked every morning. Midday of the day when the vaginal plug was detected was considered gestational day 0.5 (E0.5). Females were sacrificed by CO_2 inhalation and abdominal cavity was opened to expose the

A

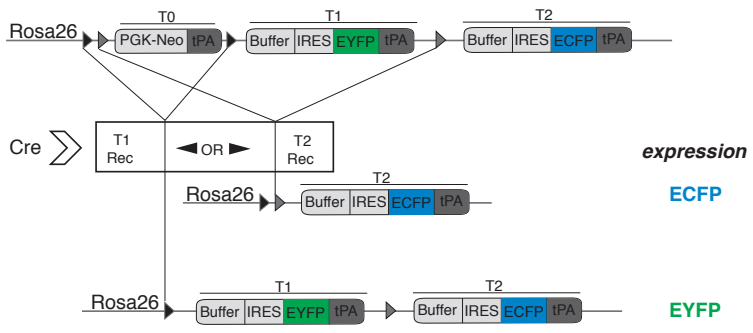

B

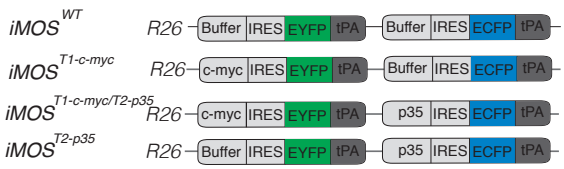

Figure 6. A. Squematic representation of the *iMOS* system construction.
In this system two pairs of modified lox sites are used, so that upon recombination either of the two possible recombinations will take place at random. Upon *Cre* expression, either T0 cassette is excised, leading to the expression of T1 (EYFP). Because of the presence of the triple polyadenilation sequence, expression doesn't progress to T2. If T2 recombination takes place both T0 and T1 are excised leading to the expression of T2 (ECFP). Recombination of this system gives rise to a mosaic, generating at random two labeled cell populations, Expresion is under the control of *Rosa26* promoter and will give rise to a policistronic mRNA expressing a buffer sequence or a protein of interest and a fluorescent reporter protein, either the yellow fluorescent protein (EYFP) or the cyan fluorescent protein (ECFP).

B Squematic representation of the different *iMOS* Mouse lines used in this thesis.
In *iMOS* ^{WT}, both labeled cell populations are random, *iMOS* $^{T1\text{-}c\text{-}Myc}$ generates a EYFP Myc overexpressing population and ECFP WT population. In *iMOS* $^{T1\text{-}C\text{-}Myc/T2\text{-}p35}$, EYFP population overexpresses *Myc* and ECFP population expresses p35. In *iMOS* $^{T2\text{-}p35}$, EYFP population is WT whereas ECFP population expresses p35.

uterus, which was removed by dissection.

In cold PBS under the scope in a Petri dish, muscular uterine wall and decidual layer were carefully ripped to expose the embryo, covered which the yolk sac. Yolk sac and Reichter membrane were teared apart and the embryos harvested.

Yolk sac was recovered to use for genotyping purposes in small embryos (in bigger ones, pieces of the embryo such as limbs or tails were preferentially used). This procedure was only done when fluorescent analysis couldn't be performed or wasn't sufficient to know the embryo's genotype.

Embryos were fixed in PFA (Merck) 2% in PBS overnight at 4ºC.

Adult heart dissection

After sacrificing the mouse by CO2 inhalation, thoracic cavity was opened and ribs cut apart to expose the heart. Heart was dissected and collected in a Petri Dish on cold PBS.

After dissection, cannulation through the aorta was performed and new cold PBS was infused through coronary vessels to remove the blood. If hearts were collected for cryosectioning they were infused through the cannula afterwards with PFA 2%, cut in half and fixed overnight at 4º C.

If fresh confocal imaging was performed, hearts were cut into slices using a blade and imaged directly in PBS on a MatTek Glass Bottom Microwell Dish.

BrDU and tamoxifen administration

BrDU (5mg/ml) was administered to pregnant females by intraperitoneal injection 2 hours prior to embryo collection. When using and inducible Cre, recombination was induced by tamoxifen administration by oral gavage (from 2 to 6 mg/female).

BrDU 0.5 mg/ml was administered to adult mice through the drinking water for one month

Tamoxifen (40g/kg Teklad TD.07262) pellets were fed to adult mice at whining for one month to induce recombination in *My6-merCremer.*

Whole mount embryo staining

Whole mount embryo staining: TUNEL

When E8.5, E9.5 and 10.5 embryos were harvested, most often staining was performed on the whole embryo to further analyse performing confocal sections. In some cases, heart was dissected previous to the staining; and in other, whole embryos were stained. Following overnight fixation embryos were washed in PBS several times and permeabilized using 0.5% Triton X-100 (Calbiochem) for 30 minutes.

TUNEL staining was performed by pretreating embryos after permeabilization in TUNEL solution (PBS, TdT buffer and $CoCl_2$ –TdT kit from Roche) for one hour and then terminal transferase and Biotin-16-dUTPs were added (accordingly to manufacturers' directions) and incubated for 1h at 37ºC. Afterwards, reaction was stopped in Citrate buffer 10mM pH6 for 20 minutes at room temperature. After PBS washes, blocking step in 10% goat serum (Gibco-BRL Life-Technologies) for one hour was performed and developing took place by overnight incubation at 4ºC, using fluorofore coupled with streptavidins (1:500) and DAPI (1:200). On the following day, after several washes embryos were stored in Vectashield solution at 4ºC until visualization took place.

Cy-3 and Cy-5 conjugated streptavidins (Jackson ImmunoResearch) were used.

Whole mount embryo staining: Immunofluorescence

For immunofluorescence stainings, same procedure was followed as mentioned in the previous paragraph but after permeabilization (performed in 0.25% to 0.5% depending on the antibody), blocking was performed in 10% goat serum for one hour and then incubation

with the primary antibody was performed overnight at 4ºC. Following day and after several washes, embryos were incubated with a secondary antibody coupled with a fluorescent protein overnight at 4ºC. On the third day, after several washes embryos were ready to be imaged and store, which was performed in Vectashield mounting medium (Vector Laboratories, USA).

Specifically, for BrDU staining, a treatment with DNAse I 1:20 (Roche) for 1h at 37ºC was performed after permeabilization.

Primary antibodies used were:

Rabbit anti-phosphohistone 3 polyclonal (Millipore) 1:300

Rabbit anti-GFP polyclonal (Living Colors) 1:150

Rabbit anti-LC3 polyclonal (Abgent) 1:100

Rabbit anti-Beclin polyclonal (Cell signalling) 1:50

Mouse anti-Troponin T monoclonal (Thermo Scientific) 1:300

Mouse anti-BrDU monoclonal (Invitrogen) 1:50

Rabbit anti-Myc polyclonal (Millipore) 1:300

Rabbit anti-Wt1 polyclonal (SantaCruz) 1:100

Chick anti-GFP polyclonal (Abcam) 1:200

Rabbit anti Beclin-1 polyclonal (cell signalling) 1:100

Rabbit anti Nppa polyclonal (Millipore) 1:200

Mouse anti Mycn monoclonal (Abcam)

Secondary antibodies used were:

Cy3-goat anti rabbit 1:500 (Jackson)

Cy5-goat anti rabbit 1:500 (Jackson)

Cy3-goat anti mouse 1:500 (Jackson)

594-goat anti mouse 1:500 (Invitrogen)

488-goat anti chicken 1:500 (Invitrogen)

Whole mount staining: In situ hybridization

Whole mount in situ hybridization was performed on E9.5 embryos to detect *Myc* mRNA (probe used in Claveria et al., 2013). Embryos fixed overnight in PFA 4% at 4ºC were bleached with H_2O_2 and then treated with protei-nase K at 20ug/ml for 8 minutes. After that, they were refixed in 0.25% glutaraldehide in 4% PFA. After incubation in prehybridization solution (50% formamide, 4xSSC pH4.5, 50ug/ml heparine, 20ug/ml tRNA, 7% blocking reagent solution, 1% SDS), probe hybridization was done in that solution overnight at 65ºC.

After hybridization, several washes were performed in posthybridization solution I (50% formamide, 5x SSC, 1% SDS) and posthybridization solution II (50% formamide, 2xCCS, 0.1%SDS). Afterwards, embryos were washed in TBST (50mM Tris-HCl pH 7.5, 150 mM NaCl, 10 mM KCl, 0.1% Tween20). Next step was blocking in goat serum and incubating in anti Digoxigenin antibody overnight at 4ºC. After that, the embryos were washed in NTMT solution (NaCl 100mM, Tris HCl 0.1M, 50mM MgCl2, 0.1% Tween20) and developing of the signal was performed adding BM Purple substrate.

Tissue processing for cryosectioning

After overnight fixation, tissue (embryos or adult hearts) was wash in PBS several times and then left in 15% sucrose in PBS overnight at 4ºC. Following that, samples were included in a sucrose 15% and gelatin 7.5% (Sigma Aldrich) at 37ºC. After that, gelatin blocks are made and cooled at 4ºC. Gelatin blocks are frozen at -70ºC in isopentane for 1 minute and stored at -80ºC.

Cryosections (8 or 10um) were made using a Leica CM1950 Automated Cryostat.

Immunostaining on gelatin sections

Gelatin must be removed from the sections by incubating them at 37ºC in PBS for 15 minutes. After that, sections were washed and

permeabilized using 0.2% Triton X-100 in PBS for 10 minutes. Blocking was performed in PBS with 10% goat serum for one hour.

Primary antibody was incubated overnight at 4ºC. On the following day, sections were washed and DAPI and secondary antibody incubation was done for 45 minutes to 1 hour at room temperature. Afterwards, sections were washed again and mounted in Vectashield to preserve fluorescence.

All antibodies used have been mentioned previously. Other stainings performed were membrane staining through incubation with wheat germ agglutinin (WGA) coupled with Cy3 or 633 (Invitrogen) to analyze cell diameter.

Embryonic heart digestion: plating and citometry

After embryos were harvested, embryonic hearts from stages E11.5 and E14.5 were dissected carefully, removing lungs and vessels in cold PBS under the scope. Hearts were disaggregated in small pieces using microscissors. Small pieces were incubated in 5-10ml of a digestion buffer containing Colagenase II (Worthington) at 4mg/ml and 2.5% trypsin in PBS. Incubation was performed at 37ºC from 15 to 45 minutes depending on size of the heart.

When the pieces appeared digested by visual inspection, solution was pipetted carefully to terminally disaggregate the pieces without inducing bubble formation. Solution was then transferred to a 50ml falcon tube through a 40um cell strainer (BD Biosciences). Then, 10ml of Complete DMEM (DMEM (cc) + FBS 10% + Penicillium/Streptoptomycin 1% (Cambrex Bioscience) was added to stop enzymatic reaction.

Afterwards, digestion mix was centrifuged for 5 minutes at 1200 rpm to pellet the cells. Supernatant was removed by aspiration and cells resuspended in a volume of complete DMEM medium depending on the purpose of the isolation.

If cells were going to be analyzed by flow cytometer, samples were resuspended in 500ul-1ml of complete DMEM. Cells were also plated in MatTek glassbottom dishes or in glass coverslips (either way coated with 0.1% gelatin in PBS). In this case, cells were resuspended in 1-2 ml of DMEM complete medium.

Flow cytometer

Isolated cardiac cells from embryonic hearts were analyzed by flow cytometry to quantify EYFP population since ECFP wasn't detected by flow cytometry. Propidium Iodide was added to the cells to asses viability (1:5000). An LSR Fortessa 4L Flow Cytometer was used for the analysis (Laser wavelengths 488, 640, 405, 561). For the analysis, FACSDiva and FlowJo softwares were used.

Adult cardiomyocyte isolation

Mice were injected with 200ul heparine 30 minutes - 1h before being sacrificed to ensure no clots were formed in the coronary vessels during the procedure.

After sacrificing the mouse by CO_2 inhalation, thoracic cavity was opened and ribs cut apart to expose the heart. Hearts were dissected and collected in a Petri Dish on cold Perfussion Buffer. (For buffers used in this protocol refer to Table1A.) After dissection, hearts were cannulated through the aorta and cannula secured with surgical thread.

To digest the matrix and isolate de cardiomyocytes different buffers were subject to Langerdorff perfusion through the aorta (Obame 2008, Sambrano 2002, Zhou 2000). A system that enabled the buffer to enter the heart through the aorta achieved a constant flux by gravity and maintained a constant temperature of 37ºC throughout the whole digestion procedure.

After 15 minutes of introducing Perfusion Buffer through the aorta, the solution was chan-

ged to Digestion Buffer (See table 1A) and this solution perfuses the heart for about 10-15 minutes.

After being perfused with digestion Buffer the heart matrix was digested and cardiomyocytes could be collected in a Petri Dish carefully, finishing disaggregation with a Pasteur pipette.

From this point onwards, steps were carried out at room temperature. These isolated cardiomyocytes were transferred to a 50ml Falcon Tube through a 100um strain net, to remove all the remaining matrix.

After that, Stopping Buffer I was added to the cells and incubated for 15-20 minutes (or until all the cardiomyocytes reached the bottom). Supernatant was discarded and cells newly resuspended in Stopping Buffer II in a 15ml Falcon tube. Cells were incubated in Stopping Buffer II about 15-20 minutes or until cardiomyocytes reached the bottom. Supernatant was discarded and then several steps of calcium reintroduction were performed (T1-T5) at 15ºC. Cardiomyocytes were then ready to be plated. This was done on laminin-coated MatTek glass bottom dishes or in laminin (BD Biosciences) coated glass round

A

	REAGENT	Company	Final concentration
PERFUSSION BUFFER	Sodium chloride	Sigma - Aldrich	113mM
	Potassium choride	Sigma - Aldrich	4,7mM
	Potassium phosphate monobasic	Sigma - Aldrich	0,6mM
	Sodium phosohate dibasic	Sigma - Aldrich	0,6mM
	Magnesium sulphate heptahydrate	Sigma - Aldrich	1,2mM
	Sodium bicarbonate	Sigma - Aldrich	12mM
	Potassium bicarbonate	Sigma - Aldrich	10mM
	Phenol Red	Sigma - Aldrich	0,032mM
	HEPES salt	Sigma - Aldrich	10mM
	Taurine	Sigma - Aldrich	30mM
	Butanodione monoxime (BDM)	Sigma - Aldrich	10mM
	Glucose	Sigma - Aldrich	5,5mM
	H2O		
DIGESTION BUFFER	Perfussion buffer	-	1X
	Liberase TM 100mg	Roche Appl. Biosc	0,2mg/ml
	Trypsin 2,5%	Gibco	0,14mg/ml
	Calcium Chloride 100mM	Sigma - Aldrich	12,5uM
	H2O		
STOPPING BUFFER I	Perfussion buffer	-	1X
	Fetal Bovine Serum	Gibco	5%
	Calcium Choride 10mM	Sigma - Aldrich	12,5uM
STOPPING BUFFER II	Perfussion buffer	-	1X
	Fetal Bovine Serum	Gibco	10%
	Calcium Choride 10mM	Sigma - Aldrich	12,5uM

Table 1. Tables that summarize the reagents and Solutions used in the adult cardiomyocyte isolation protocol.

A Solutions prepared during the isolation procedure

B

	Tube	SBII	$CaCl_2$
CALCIUM REINTR.	T1	1X	62uM
	T2	1X	112uM
	T3	1X	212uM
	T4	1X	500uM
	T5	1X	1mM

Table 1. Tables that summarize the reagents and Solutions used in the adult cardiomyocyte isolation protocol.

B Calcium reintroducing solutions (T1-T5) in increasing Ca^{2+} concentrations

C

	REAGENT	Company	Final concentration
PLATING MEDIUM	Medium 199	Invitrogen	
	PEN-STREPT	Lonza	100U/ml
	L-Glutamine	Lonza	1%
	BSA	Sigma-Aldrich	0,20%
	NaHCO3	Sigma-Aldrich	22mM
	FBS	GIBCO	0,05
	ITS-A Liquid Media 100x		0,00%
	BDM		10mM
	Blebistatin		25uM
CULTURE MEDIUM	Medium 199	Invitrogen	
	PEN-STREPT	Lonza	100U/ml
	L-Glutamine	Lonza	1%
	BSA	Sigma-Aldrich	0,20%
	NaHCO3	Sigma-Aldrich	22mM
	FBS	GIBCO	0,20%
	ITS-A Liquid Media 100x		0,00%
	BDM		10mM
	Blebistatin		25uM

Table 1. Table that summarize the reagents and solutions used in the adult cardiomyocyte isolation protocol.

C Culture medium for adult cardiomyocytes.

coverslips. Firstly, cardiomyocytes were plated using plating medium and then, after one hour that medium was removed and culture medium was added (again, refer to the table for full composition of buffers and culture mediums). These cardiomyocytes were usually imaged straight after plating but also were fixed overnight at 4ºC in 2% PFA to perform immunostaining.

Adult physiological cardiac stress induced by exercise

To induce physiological stress in adult mouse hearts, we submitted mice to exercise through swimming for a two month period. Animals were swimming for increasing lengths of time everyday in a thermostatized water tank, kept at 37ºC. Table 2 summarizes the swimming times that were followed throughout the experiment and figure 7 illustrates the protocol.

Echocardiography

Mice were anesthetized by isofluorane inhalation (1.25%) and examined with a 30-MHz transthoracic echocardiography probe. Images were obtained with Vevo 770 (VisualSonics, Toronto, Canada). Short-axis, long-axis, B-mode and two-dimensional M-mode views were obtained as previously described (Cruz-

WEEK	Monday	Tuesday	Wednesday	Thursday	Friday	S	S
1	5	10	15	20	25	Rest	Rest
2	25	30	35	40	45	Rest	Rest
3	45	45	45	45	45	Rest	Rest
4	60	60	60	60	60	Rest	Rest
5	75	75	75	75	75	Rest	Rest
6	90	90	90	90	90	Rest	Rest
7	90	90	90	90	90	Rest	Rest
8	90	90	90	90	90	Rest	Rest

Table 2. Table that summarizes the swimming protocol followed for the physiological hypertrophy protocol created through exercise.
Animals were subjected to exercise during 8 weeks at increasing times, ranking from 5 to 90 minutes.

Adalia et al., 2010). Left ventricle function was estimated from the ejection fraction, obtained from M-mode echocardiographic images by a blinded echocardiography expert. For these measurements, a long- or short-axis view of the heart was selected to obtain an M-mode registration in a line perpendicular to the left ventricular septum and posterior wall at the level of the mitral chordae tendinea.

Ex vivo assays. Explants

Epicardium

Following method described in (Chen et al., 2002).

To derive primary epicardial cells, embryos from different developmental stages were harvested.

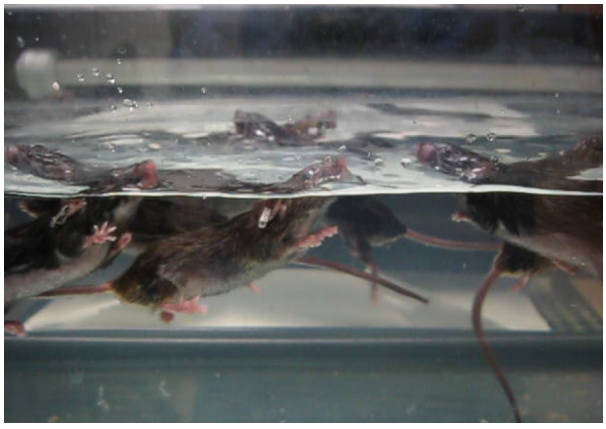

Figure 7. Excersice protocol
Photograph showing how the exercise protocol was performed.

To isolate epicardial cells from E10.5 and E11.5 embryos, hearts were dissected, both atria and the outflow tract region were removed and the ventricles were each cut into two pieces.

Each piece was placed with the epicardial epicardial outermost part facing down onto a gelatin covered MatTek Glass bottom Dish (0.1%Gelatin in PBS). These myocardial pieces were cultured in DMEM containing 10% FBS and 1% Penicillium Streptomycin. After 24 to 48 hours, epicardial cells had migrated from the explant and form a monolayer.

At this point, the myocardial explant was removed using forceps and epicardial cells were left to grow for 3-5 days, at which point they were visualized by confocal microscopy and/or fixed for immunostaining in 2%PFA overnight at 4ºC.

In order to derive epicardial cells from embryonic hearts from E15.5 to P0, a different technique was used, involving the manual peeling of the outermost epicardial layer from the heart surface and posterior placing of these cells on a gelatin coated MatTek glass bottom dish. Isolated epicardial layers were cultured for 5-7 days in DMEM+FBS 10% + Pen Strept 1%.

Migrating epicardial cells were either analyzed directly in the confocal or fixed in 2%PFA overnight at 4ºC for immunostaining.

Proepicardium

This method is extensively described in (Garriock et al., 2014).

Embryos for proepicardium explants were harvested at E9.0, since after E9.5 much of the proepicardium had already transferred onto the heart.

After the embryos were removed from decidual layer and yolk sac, the pericardium was removed using fine forceps. The proepicardium was identified just under the heart as a "grape-like" clustering of cells. Heart tube was removed and discarded to have better access and proepicardial cells were removed using forceps.

Proepicardial explants were cultured in DMEM 10% FBS 1% Pens-Strept for 48h on gelatin coated MatTek Glass bottom dishes.

Embryonic myocardium

In some cases, coexplant assays were performed by culturing epicardium (E10.5) with myocardium (E9.0-9.5). Epicardial explant was performed as described previously but in this case, close to the myocardium from the E10.5 heart, the whole heart from a E9.0 embryo was placed, trying to orient the atrioventricular canal region facing the E10.5 explant. After 2-5days these coexplants were fixed in 2% PFA overnight at 4ºC for immunostaining.

RNA isolation from adult hearts

In order to perform RNA differential expression analysis, RNA from whole hearts was isolated. Hearts were dissected and washed thoroughly to eliminate blood residue; PBS was run through the aorta by cannulation to ensure coronary vessels were also as free as possible from blood residue.

Hearts were then cut into pieces and homogenised in cold trizol reagent (Life Technologies) using the Tissue Lyser. Settings for the tissue lyser were 500 oscilations/second in 1minute cycles. About 4 cycles were needed until complete homogenization of the tissue. Then 0.2 ml of chloroform were added to homogeneized sample. After shaking and centrifuging for 12.000 x g for 15 minutes two phases formed; Aqueous fase was collected and transferred to a new tube.

RNA was afterwards cleaned by using QIAGEN RNeasy colums following manufacturers' directions. RNA purity was assessed by Nanodrop plots and agarose gel profile.

Isolated RNA was then handed to Genomic Unit in CNIC to proceed with sequentiation.

RNASeq. Data analysis

RNASeq library production

In order to assess the gene expression changes in iMOST1-Myc hearts upon mosaic Myc overexpression, total RNA was extracted from hearts induced to recombine with tamoxifen at t1, according to the scheme in figure 20.

Two hearts from *iMOS$^{T1\text{-}Myc}$*; *My6-merCremer* were used while two hearts from *iMOS$^{T1\text{-}Myc}$* littermates without Cre expression were used as control. RNA was isolated using standard procedures and analyzed using RNA-Seq. Total RNA was quantified by absorbance at 260 nm in a NanoDrop spectrophotometer and its integrity was determined using an Agilent Bioanalyzer (Santa Clara, CA).

Total RNA (1 µg) was used with the TruSeq RNA Sample Preparation v2 Kit (Illumina, San Diego, CA) to construct index-tagged cDNA libraries. The quality, quantity and the size distribution of the Illumina libraries were determined using the DNA-1000 Kit (Agilent Bioanalyzer).

Prepared cDNA libraries were applied to an Illumina flow cell for cluster generation (True Seq SR Cluster Kit V2 cBot) and sequence-by-synthesis single reads of 75 base length using the TruSeq SBS Kit v5 (Illumina) were generated on the Genome Analyzer IIx following the standard RNA sequencing protocol.

RNASeq data analysis

Sequencing adaptor contaminations were removed from reads using cutadapt software (http://code.google.com/p/cutadapt/) and the resulting reads were mapped and quantified on the transcriptome (Ensembl gene-build 70) using RSEM v1.2.3 (Li and Dewey, 2011).

Only genes with at least 2 counts per million in at least 1 sample were considered for statistical analysis. Data were then normalized and deferential expression tested using the bioconductor package EdgeR (Robinson et al., 2010). We considered as differentially expressed those genes with a Benjamini-Hochberg adjusted p-value ≤0.05.

Analysis of the data was performed using Gene set enrichment analysis and Ingenuity pathways analysis software (Biobase International).

Image acquisition

Images were acquired using a Nikon A1R confocal microscope using 405,458,488,568 and 633 nm wavelengths and 20x/0.75 dry and 40x/1.30 oil objectives. Tile scan, Z-stacks and large image acquisitions were performed using NIS software (version).

Acquisitions were commonly 1024x1024 px, A.U. set to 1 (except for adult cardiomyocyte imaging and Z-stacks steps as recommended by the optical configuration).

Image analysis

Myc levels

To quantify Myc protein expression ImageJ (http://rsb.info.nih.gov/ij) was used. Nucleai were detected by DAPI staining and segmented using threshold tool to create a mask.

When nucleai were too close, manual correction was applied to ensure segmentation detected only individual cells. Segmentation generated a mask that was used to measure mean intensity within the defined nucleus.

Mask was applied to Cy3 red channel staining (detecting Myc protein) and measure tool gave the mean intensity for every single object.

These intensity values were then classified into intervals and represented as interpolated curves derived from the original frequencies.

EYFP/ECFP proportion

EYFP/ECFP proportion was also quantified using ImageJ software. In cases when both EYFP and ECFP were clearly detected, both cell populations were quantified either by measuring the occupied area (using thresholding tool) for each cell type or counting cells (using cell counter plugin).

In those cases where ECFP was not detectable (in adults or neonate hearts), EYFP was quantified as previously mentioned and to estimate ECFP proportion, antiGFP staining was used to determine whole recombination.

EYFP levels

EYFP levels were quantified in adult isolated cardiomyocytes by determining cell area using threshold tool in ImageJ on a background channel. These areas were used to generate a mask that enabled to measure average intensity in EYFP channel. This was represented in arbitrary units. Values were classified into intervals and assigned to EYFP-negative, -medium or –high expression categories, which were defined identically for all experiments.

Cell area

Cell area was defined using ImageJ. Isolated adult cardiomyocytes' area was measured using background green channel to detect objects and then 'analyze particles' tool from Image J to detect every cell as an object. Measure tool would give area for any given cell.

To measure area of cells stained with WGA (wheat germ agglutinin) on sections, Image J manual free hand selection was used.

3D Recontructions

Z-stacks from embryonic hearts were reconstructed using Imaris x64 software. Imaris allowed to generate different isosurfaces (EYFP positive and negative cells) and detect those nucleai within isosurfaces.

A parameter 'distance to EYFP' was set to each TUNEL event and those within a cell diameter from a EYFP expressing cell where quantified as "in contact".

Statistical analysis

To compare percentages of ECFP cells/ area between more than two groups, Kurskall-Wallis test was used (assuming non-normal distributions).

For comparisons of two groups, Man-Whitney test was used. To test the correlation between cell size and EYFP expression levels, a linear regression model was used.

The significance of BrdU+ frequency and mononucleated cardiomyocyte frequency comparisons from adult hearts was analyzed using a proportions test as implemented in R.

All comparisons (and graphs) were made using Prism 5.0 statistical analysis software.

RESULTS

Knowledge is a treasure, but practice is key to it
(Lao Tzu)

RESULTS

Cell competition in the developing heart

Myc family expression in the developing heart.

To explore cell competition in the developing heart, we firstly addressed the role of Myc in the embryonic myocardium, as it has been shown to be a regulator of cell anabolism. *Myc* mRNA was not detected at E9.5 in the developing heart by in situ hybridization (ISH) (Figure 8 A, A'); as it had been previously reported. (Moens, Stanton et al. 1993).

We then decided to delete both *Myc* alleles in the developing heart to discard a role of Myc in myocardium development; and to do so we took advantage of *Nkx2.5-Cre* line to recombine *Myc* floxed alleles. Nkx2.5 is expressed in cardiac progenitors as early as E7.5 and Cre recombination takes place in myocardium derived from primary heart tube and from second heart field derivatives, as well as the endocardium and valve mesenchyme (Stanley et al. 2002).

Deletion of *Myc* gene using this driver did not produce any apparent cardiac embryonic phenotype (figure 8 B and C) and the proportion of adult cardiac-specific Myc knockout animals was according to expected (figure 8 D). This result is in agreement with the expression pattern of Myc. We therefore focused on *Mycn*, a member of the *Myc* family expressed in the developing heart (figure 8 E, E'), specially in the compact layer of the myocardium (Davis et al. 1993,

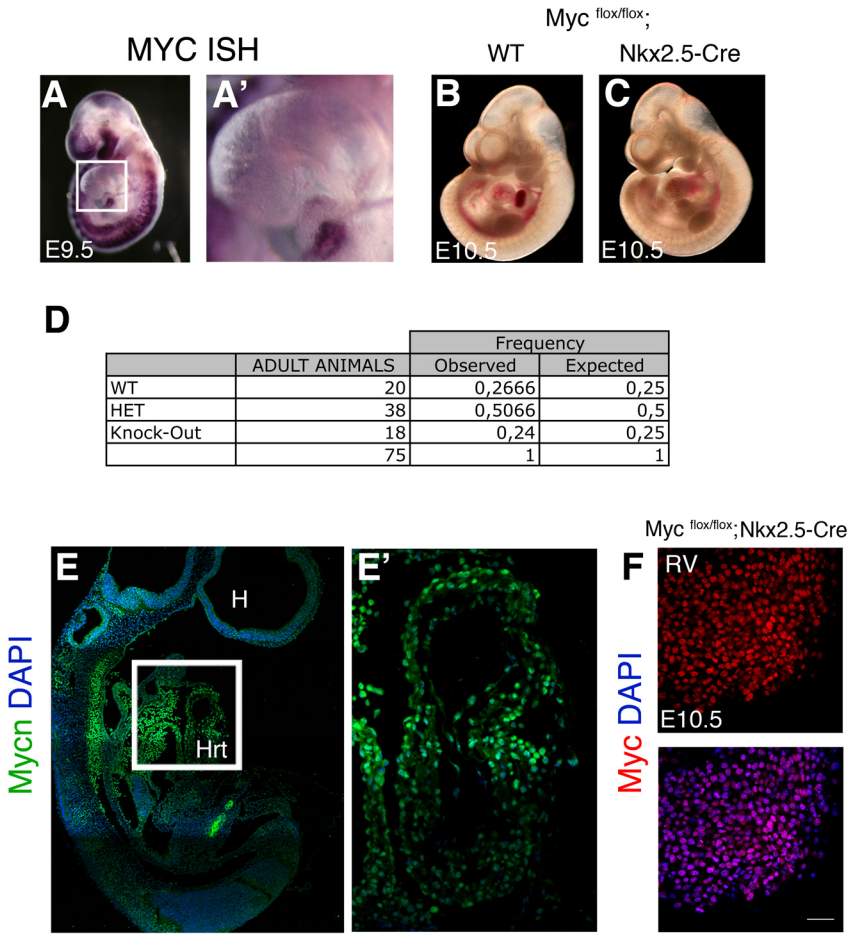

D

		Frequency	
	ADULT ANIMALS	Observed	Expected
WT	20	0,2666	0,25
HET	38	0,5066	0,5
Knock-Out	18	0,24	0,25
	75	1	1

Figure 8. Myc is dispensable for heart development

A. Whole mount in situ hybridization in E9.5 WT embryo for *Myc*, showing no expression of Myc in the developing heart (boxed area of A and A'). **B.** Whole mount image from a E10.5 WT embryo. **C.** Whole mount image from a E10.5 *Myc flox/flox;Nkx2.5-Cre*. **D.** Table showing the observed and expected proportion of adult animals from the three different genotypes: *MycWT;Nkx-2,5*; *MycFlox/WT;Nkx2.5-Cre* and *MycFlox/Flox; Nkx2.5-Cre*. **E.** Confocal section of a E9.5 embryo (sagital view) showing Mycn immunodetection. **E'.** Magnification of the heart, from boxed area in **E**. **F.** Confocal section of a whole E10.5 right ventricle showing staining for Myc (upper panel) and Myc merged with DAPI (lower panel). Bar, 50 µm. H: Head, Hrt: Heart, RV: Right ventricle.

Moens, Stanton et al. 1993). It has been reported that *nMyc* deletion in the heart, using *TnT-Cre* (expressed specifically in cardiac myocytes) produces a defect in myocardium proliferation and does not yield live embryos past E12.5, with most of them being recovered alive only up to E11.5 (Harmelink et al. 2013). Interestingly, Myc and Mycn proteins are very similar and are able to functionally replace each other in mice in which *Mycn* has been knocked-in replacing endogenous *Myc* (Malynn et al. 2000). Myc overexpression through the *iMOS* system should therefore be functionally equivalent to Mycn expression, recapitulating and contributing to its function in the developing myocardium.

Moreover, using anti-Myc antibodies in wild-type, heterozygous and knock-out embryos, nuclear signal was still detected in the myocardium, indicating that the antibody also recognizes Mycn expression in the myocardium (figure 8 F).

Generation of random genetic mosaics in the developing heart through the *iMOS* system. Overexpression of Myc under the *Rosa26* promoter

To study cell competition in the developing heart we used *Nkx2.5-Cre* to induce *iMOS* recombination in early cardiac progenitors. This approach is expected to generate random mosaics in cardiac lineages during development.

We first generated mosaics recombining the *iMOS*^{WT} transgene, which gives rise to

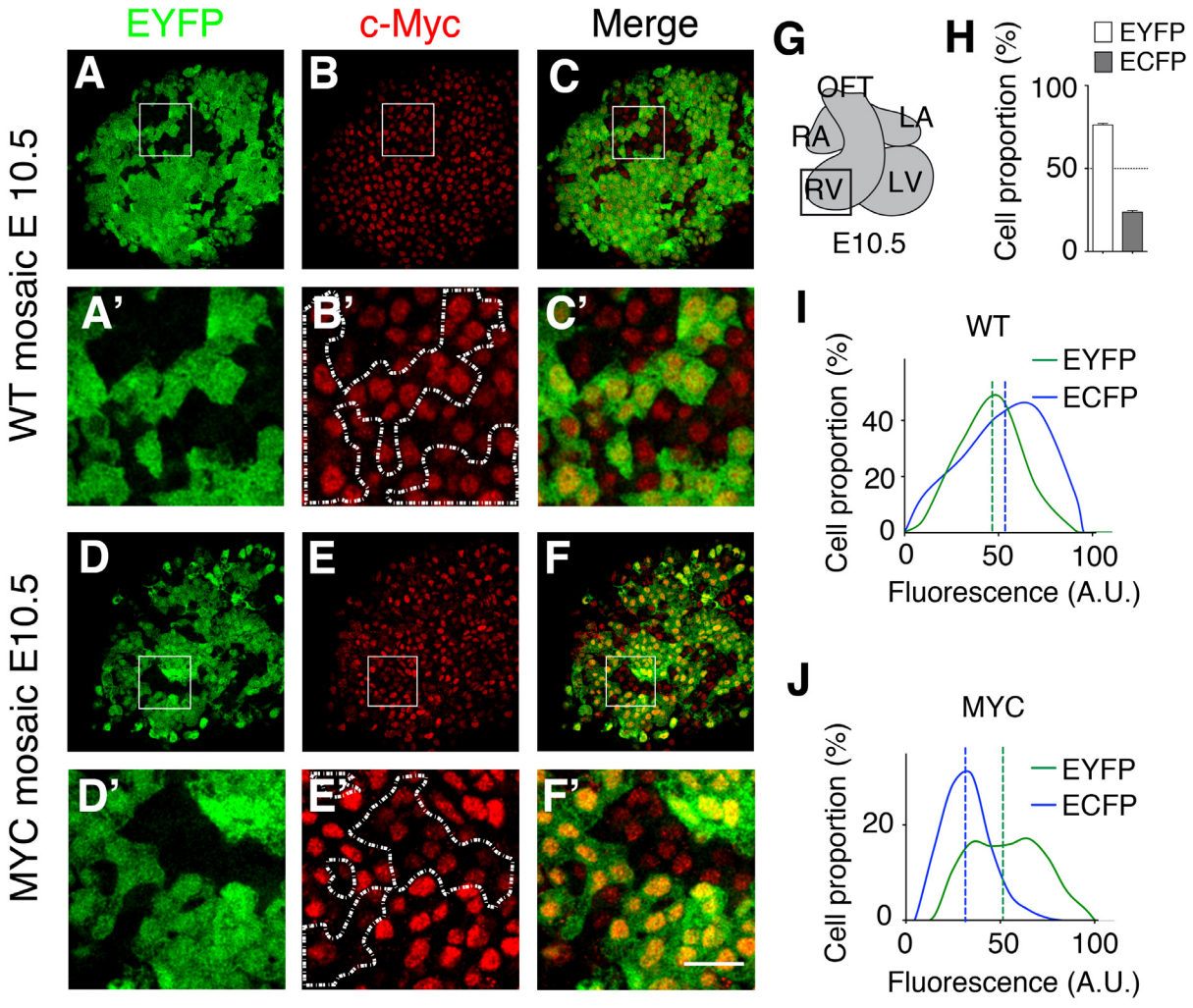

random mosaics of ECFP- and EYFP-WT cell populations.

Quantitative confocal analysis of recombination at E10.5 in *iMOS^{WT};Nkx2.5-Cre* hearts confirmed the mosaic expression pattern of the two reporter proteins in embryonic cardiomyocytes at a reproducible cell population ratio, as previously described (EYFP:ECFP = 3:1)(Claveria et al. 2013) (figure 9 A-C, G, H).

As had been shown for the *Nkx2.5-Cre* line (Stanley et al., 2002), the fluorescent protein distribution pattern showed *iMOS* activation throughout the embryonic heart (figure 9 A-C').

We then generated *Nkx2.5-Cre*-induced *iMOS$^{T1\text{-}Myc}$* mosaics, in which the EYFP cell population moderately overexpresses Myc under the *Rosa26* promoter (see methods figure 6) (Figure 9 D-F').

To address functional Myc overexpression we analyzed Myc protein levels through immunodetection on confocal sections in both mosaics. This analysis showed that Myc levels in *iMOS^{WT}* mosaics were comparable between the two mosaic populations; and, in contrast to what had been observed in the epiblast in the context of endogenous cell competition (Claveria et al. 2013), levels were cell-to-cell homogeneous. In the EYFP cell population of *iMOS$^{T1\text{-}Myc}$* mosaic hearts an expected increase in Myc expression levels in the EYFP cell population was observed (figure 9 I, J).

This increase is attributable presumably to the simultaneous detection by the antibody of exogenous Myc and endogenous Mycn.

Mosaic Myc overexpression induces cardiomyocyte population expansion in the developing heart

To test the effect of Myc overexpression in a mosaic fashion during heart development, we analyzed neonatal hearts from *iMOS^{WT}* and *iMOS$^{T1\text{-}Myc}$* mosaics. Confocal analysis showed a strong reduction of the ECFP-WT cell population in *iMOS^{T1Myc}* mosaics, where these cells are confronted with Myc overexpressing ones.

At birth, the contribution of WT cardiomyocytes in *iMOS$^{T1\text{-}Myc}$* mosaics had dropped to 25% of its original contribution to the heart (figure 10 A, B, D, E and G).

To understand the temporal dynamics of the shift in the contribution of the EYFP-Myc and ECFP-WT cell populations, we quantified by confocal analysis the contribution of the mosaic cell populations at different stages of the developing heart, using again *Nkx2.5-Cre* to induce the *iMOS* system.

In *iMOS$^{T1\text{-}Myc}$* mosaics we found a progressive reduction in the contribution of the ECFP-WT cell population (and a correlatively increased contribution of the EYFP-

Figure 9. Mosaic Myc overexpression driven by *Nkx2.5-Cre* in the developing heart

A-C. Confocal sections showing EYFP+ cardiomyocyte distribution and Myc expression by immunofluorescence in the right ventricle of a whole-mount *Nkx2.5-Cre*-recombined *iMOS^{WT}* E10.5 heart (WT), as depicted in **G**. **A'-C'** show magnified details of the boxed areas in **A-C. D-F'** Similar data for the *Nkx2.5Cre*-recombined *iMOS$^{T1\text{-}Myc}$* E10.5 heart (MYC). Bar, 50 µm. Dashed lines in **B'** and **E'** outline the frontiers between EYFP+ and EYFP- cells. ECFP fluorescence is lost upon Myc immunodetection; however, all EYFP- cells are ECFP+ (see Figure 10).
G. Schematic representation of an E10.5 heart identifying the area shown in **A-F'**. OFT, outflow tract; RA, right atrium; LA, left atrium; RV, right ventricle; LV, left ventricle. **H.** Graph showing the proportions observed of EYFP and ECFP cardiomyocytes in *Nkx2.5Cre*-recombined *iMOS^{WT}* E10.5 whole hearts (N=7). **I, J.** Distribution of Myc protein levels in the EYFP and ECFP cell populations of *iMOS^{WT}* (I) and *iMOS$^{T1\text{-}Myc}$* (J) mosaic whole hearts at E10.5; Myc protein levels were quantified from the immunofluorescence images similar to those in A-F'. (N=425 cells in I and 449 in J). Dashed vertical lines indicate the mean for each distribution.

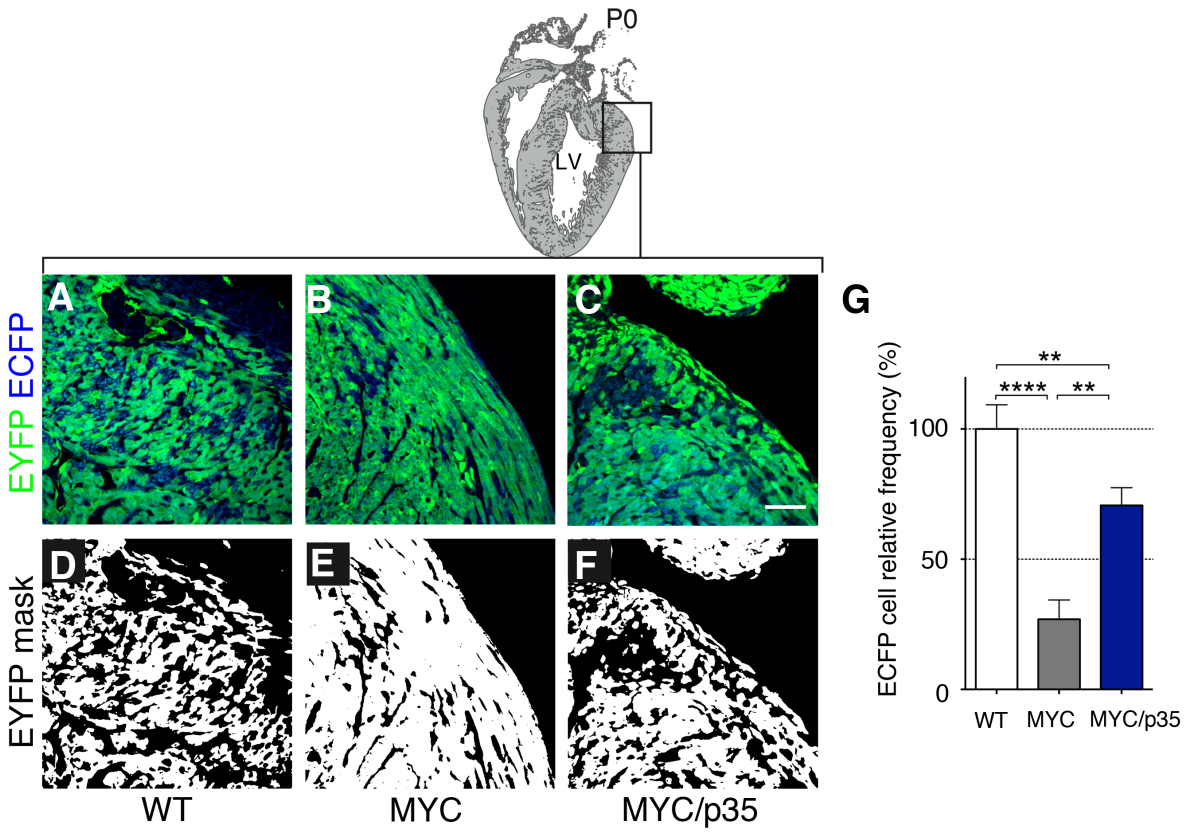

Figure 10. Myc-overexpressing population shows an expansion at P0

A-C. Confocal detection of EYFP+ and ECFP+ cardiomyocyte distributions in histological sections of the left ventricle of P0 hearts from *Nkx2.5-Cre* recombined *iMOS*^{WT} (WT) (**A**), *iMOS*$^{T1\text{-}Myc}$ (MYC) (**B**) and *iMOS*$^{T1\text{-}Myc/T2\text{-}p35}$ (MYC/p35) mice (**C**). Bar, 50 µm. **D-F.** show masks of the EYFP detection in **A-C**. **G.** Percentage of ECFP+ cells observed at P0 in whole hearts of the *iMOS*$^{T1\text{-}Myc}$ (MYC) and *iMOS*^{WT} (WT) mosaics relative to that observed in the *iMOS*^{WT} (WT) mosaics, which was normalized to 100%. Data in **G** are means ±SEM; * p<0,05; **p<0,01; ***p<0,001.

Myc population) that was not observed in the *iMOS*^{WT} mosaics (figure 11 A-G).

The reduction in the proportion of ECFP-WT cardiomyocytes in *iMOS*$^{T1\text{-}Myc}$ mosaic hearts compared with *iMOS*^{WT} hearts was detected already at E9.5, although this decrease was not found to be significant.

However, from this developmental stage on, the contribution of ECFP-WT population in *iMOS*$^{T1\text{-}Myc}$ hearts was progressively reduced during development, with elimination of 75% of the normal ECFP-WT population contribution at birth. The reduction was 40% of the *iMOS*^{WT} value at E10.5, 60% at E11.5 and 75% at P0 (figure 11 G).

This indicates that the shift in cell populations probably takes place constantly during the period observed but it does so more intensely in a two-day window between E9.5 and E11.5.

Mosaic Myc overexpression in the embryonic heart provokes no pathological hyperplasia of cardiomyocytes

Previous studies showed that Myc overexpression in cardiomyocytes during fetal life can lead to pathological cardiac hyperplasia (Jackson et al., 1990).

However, in these studies Myc overexpression was 20-fold above normal. Myc-overexpression levels through the *Rosa26* promoter had been shown to be mild in the quantitative analysis performed initially to test *iMOS* sys-

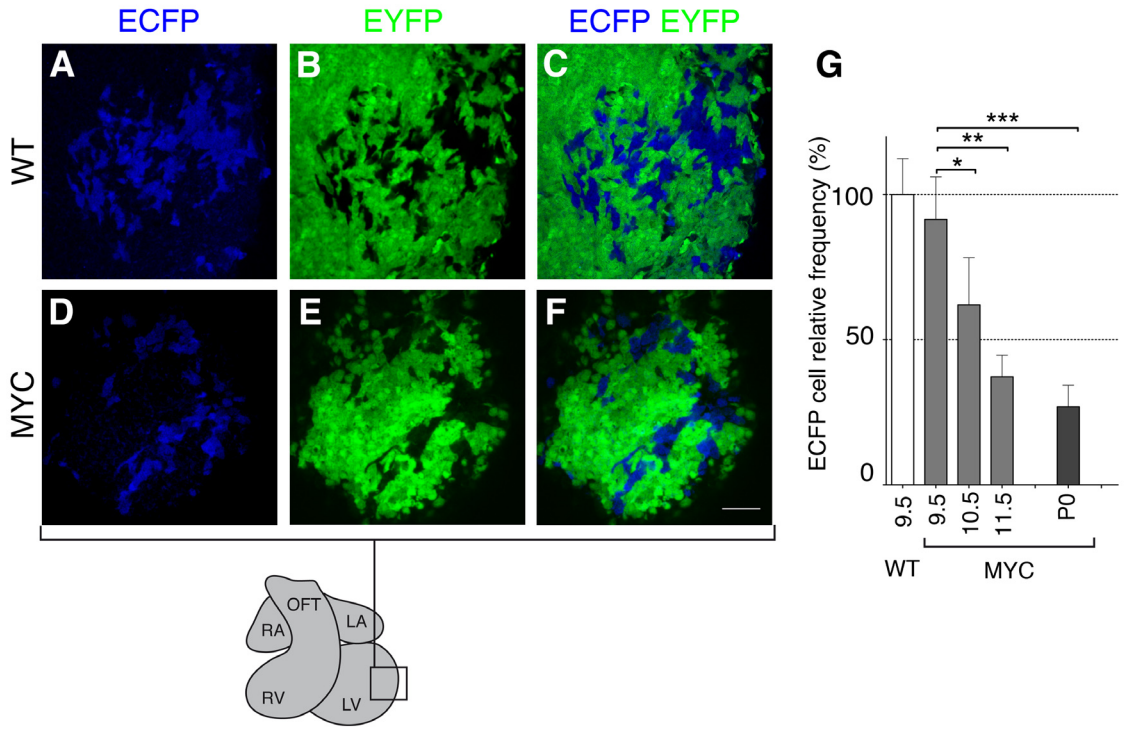

Figure 11. Myc-overexpressing cardiomyocyte population expands in the developing heart

A-F. Confocal sections showing EYFP+ and ECFP+ cardiomyocyte distributions in the left ventricle of whole-mount E10.5 hearts from *Nkx2.5Cre*-recombined *iMOS*^{WT} (WT) (**A-C**) and *iMOS*$^{T1\text{-}Myc}$ (MYC) (**D-F**) embryos. Bar, 50 µm. **G.** Percentage ECFP+ area at different embryonic stages in whole hearts of the *iMOS*$^{T1\text{-}Myc}$ (MYC) mosaics relative to that observed in the *iMOS*^{WT} (WT) mosaics, which was normalized to 100%. Numbers on the X-axis indicate the day of embryonic development; P0 indicates postnatal day 0 (N≥5 embryos). Data in **G** are means ±SEM; * p<0,05; **p<0,01; ***p<0,001.

tem recombination (Claveria et al. 2013) and in agreement with the observations in early embryos, we find that Myc overexpression levels approximate to the addition of one WT *Mycn* copy in the heart (figure 9 J).

To determine whether this overexpression levels could lead to cardiac hyperplasia we characterized postnatal heart anatomy and cardiomyocyte size. P0 hearts from *Nkx2.5-Cre*-recombined *iMOS*$^{T1\text{-}Myc}$ and *iMOS*^{WT} mice were of normal size and anatomy (not shown), and cardiomyocytes from the *iMOS*$^{T1\text{-}Myc}$ hearts were of a similar size to those from *iMOS*^{WT} hearts in area, as measured in histological sections (figure 12).

The shift in the cell population proportion observed in *iMOS*$^{T1\text{-}Myc}$ mosaics thus results from expansion of the EYFP Myc-overexpressing cardiomyocyte population at the expense of the ECFP-WT population, without involving modifications in cardiomyocyte number or size or heart anatomy.

These results also indicate that the levels of Myc overexpression from the *iMOS*$^{T1\text{-}Myc}$ allele through *Rosa26* promoter are within the limits that allow normal cardiac development and cardiomyocyte function and do not lead to hyperplasia.

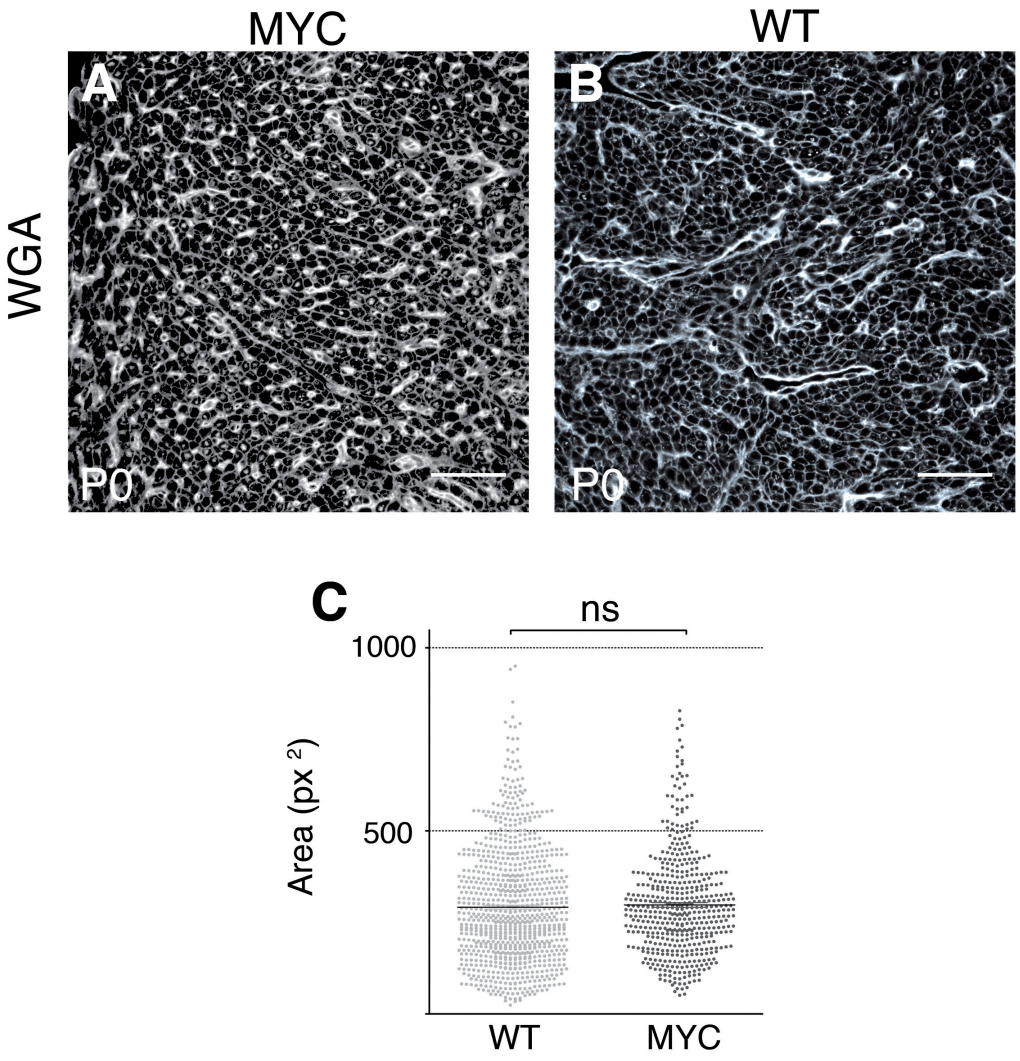

Figure 12. Morphometric analysis in newborn mice of cardiomyocytes exposed to Myc overexpression during gestation

A and **B.** Confocal sections showing wheat germ agglutinin (WGA) staining of P0 hearts from *Nkx2.5-Cre* recombined *iMOS*^{WT} (WT) (**A**) and *iMOS*$^{T1\text{-}Myc}$ (MYC) (**B**) mosaics. Bar, 50 µm. **C.** Analysis of 2-D cardiomyocyte size in *iMOS*^{WT} (WT) and *iMOS*$^{T1\text{-}Myc}$ (MYC) mosaics (N= 507 and 902 cells, respectively).

Islet1 progenitors are highly sensitive to Myc-induced cell competition

We then explored whether this expansion would take place in specific compartments of the developing heart; and to do so we took advantage of *Islet1-Cre*, to induce recombination in second heart field progenitors, since Islet1 is a specific marker of SHF derivatives (Yang et al. 2006).

We wanted to test whether Islet1+ second heart field progenitors were also sensitive to Myc-induced cell competition, and the impact of inducing mosaicism in this particular cell population.

To test this, we generated *iMOS*^{WT} mosaics in the second heart field (SHF) using Islet1 to drive Cre expression. This driver provides partial interspersed recombination in the SHF population resulting in a 7% con-

tribution of EYFP cardiomyocytes to the right ventricle (RV) in the neonatal heart. (figure 13 A, E, E').

Interestingly, Myc mosaic overexpression in this SHF population dramatically increased the contribution of EYFP-Myc cells to the RV, which was 40% of the RV at P0, which represents a 6-7-fold expansion of the original EYFP cardiomyocyte population during development (figure 13 B, D F, F'). Moreover, the ECFP-WT cardiomyocyte population was almost completely eliminated from the RV in *iMOS*$^{T1\text{-}Myc}$ mosaic hearts, indicating a very active elimination of the ECFP-WT population and a continued expansion of the Myc-overexpressing cardiomyocyte popula-

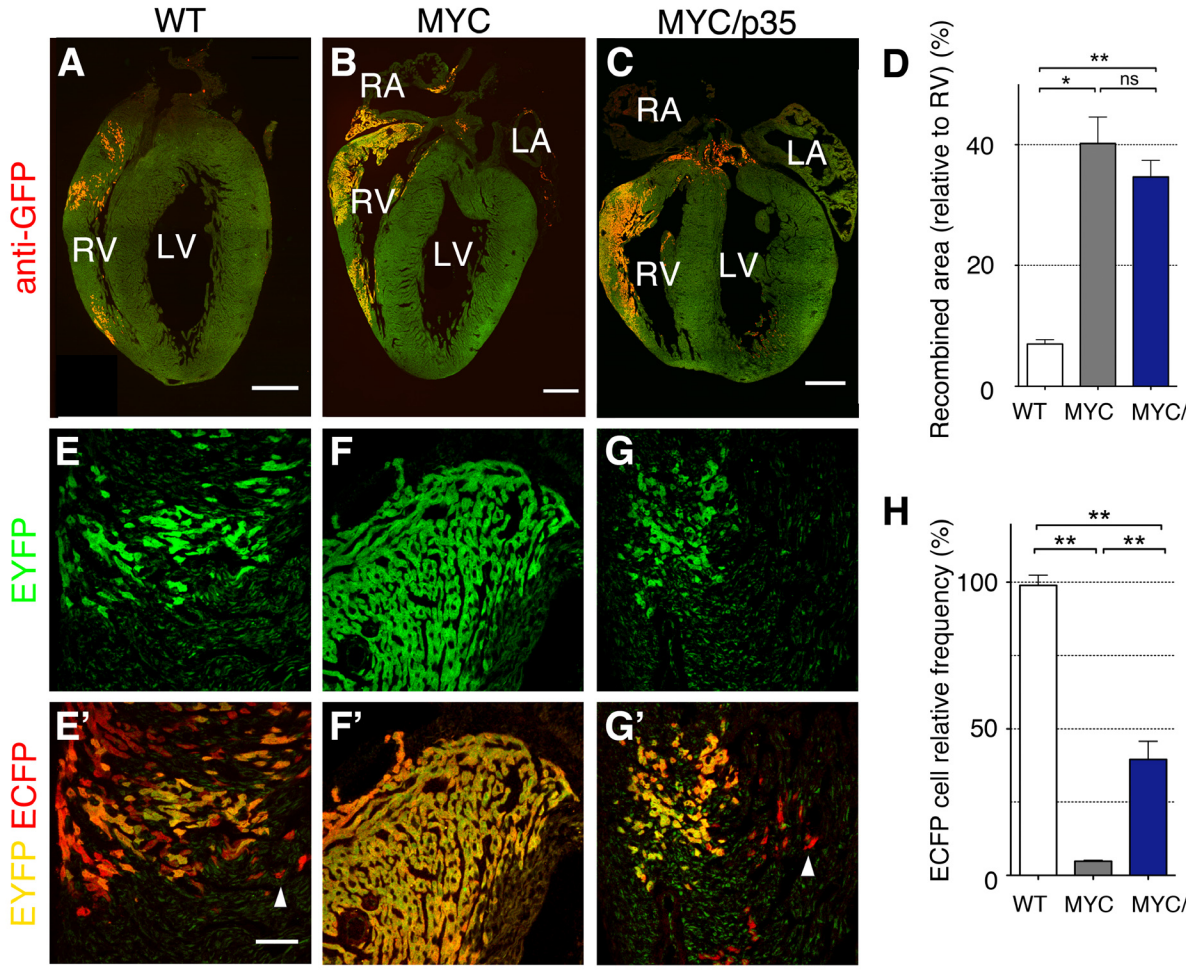

Figure 13. Myc-overexpressing cardiomyocytes upon mosaic induction in Islet1+ progenitors show an enhanced expansion at P0

A-G'. Confocal detection of EYFP+ **(A-C)**, anti-GFP immunofluorescence (detecting both EYFP and ECFP) **(E-G)** and co-localization of both signals **(E'-G')** in histological sections from *Islet1-Cre* recombined *iMOS*^{WT} (WT) **(A, E, E'),** *iMOS*$^{T1\text{-}Myc}$ (MYC) **(B, F, F')** and *iMOS*$^{T1\text{-}Myc/T2\text{-}p35}$ (MYC/p35) newborn mice. In **E'-G'**, EYFP+ cells are yellow because they are positive for both EYFP and anti-GFP, and ECFP+ cells are detected in red, as they are only positive for anti-GFP. Bar, 100 µm for **A** to **C** and 50 µm for **E'.** RA: right atrium, LA left atrium, RV right ventricle; LV left ventricle. **D.** Percentage of the RV area positive for anti-GFP immunofluorescence in *Islet1Cre* recombined *iMOS*^{WT} (WT), *iMOS*$^{T1\text{-}Myc}$ (MYC) and *iMOS*$^{T1\text{-}Myc/T2\text{-}p35}$ (MYC/p35) newborn mice (N=4). **H.** Percentage of ECFP+ recombined area with respect to the total EYFP+ECFP- recombined area observed at P0 in the *iMOS*$^{T1\text{-}Myc}$ (MYC) and *iMOS*$^{T1\text{-}Myc/T2\text{-}p35}$ (MYC/p35) mosaics relative to that observed in the *iMOS*^{WT}(WT) mosaics, which was normalized to 100% (N≥4).Data in **D**, **H** are means ±SEM. *p<0.05; **p<0.01; ***p>0.001.

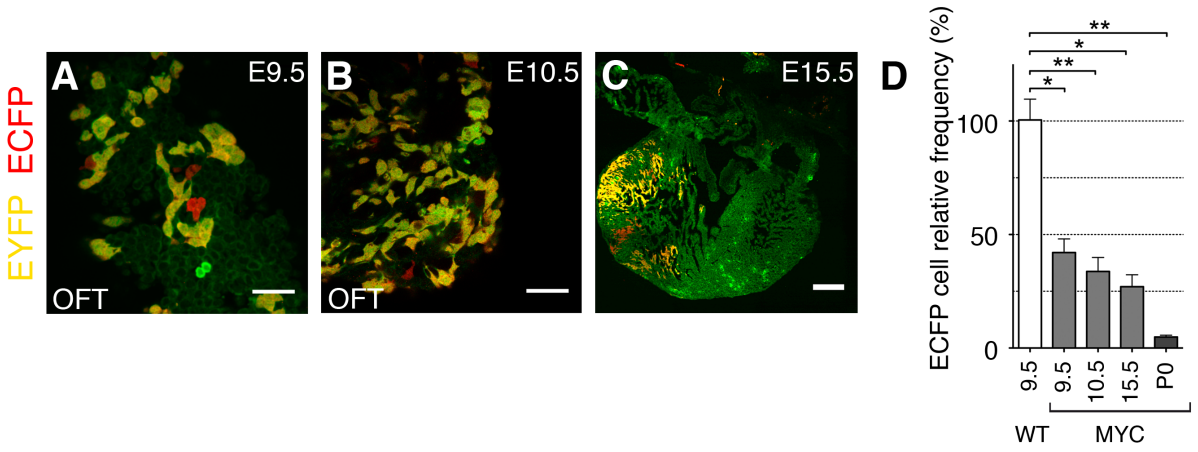

Figure 14. Myc-overexpressing cardiomyocytes upon induction in Islet1 progenitors, show an early expansion

A-C. Confocal sections of the E9.5 (**A**) and E10.5 (**B**) OFT and the E15.5 RV (**C**) from *Islet1-Cre* recombined *iMOS*$^{T1\text{-}Myc}$ hearts, showing overlays of EYFP and anti-GFP signals. Bar, 50 µm for **A** and **B** and 100 µm for **C**. Percentage of ECFP+ area with respect to the total EYFP+ECFP-recombined area observed at different stages in the *iMOS*$^{T1\text{-}Myc}$ (MYC) mosaics relative to that observed in the *iMOS*^{WT} (WT) mosaics, which was normalized to 100%. Numbers on the X-axis indicate the day of embryonic development; P0 indicates postnatal day 0 (N=4). Data in **D** are means ±SEM. *p<0.05; **p<0.01; ***p>0.001.

tion during fetal life, in a context in which it is continuously confronted with WT cardiomyocytes (figure 13 H).

To further understand how this expansion takes place, we characterized the temporal progression of the ECFP-WT cardiomyocytes in *iMOS*$^{T1\text{-}Myc}$ mosaics; and found that as early as E9.5 this population is already decreased to 40% of its normal contribution in the *iMOS*^{WT} mosaic; with a further progressive reduction until the near-complete elimination found at birth (figure 14 A-D).

This enhanced early elimination of ECFP-WT cells indicates that the undifferentiated Islet1 progenitors are especially sensitive to Myc mosaic overexpression.

Cell proliferation does not account for the expansion of the Myc-overexpressing cardiomyocyte population

We then studied which mechanisms could underlie Myc-overexpressing cardiomyocyte expansion; and firstly we addressed the role of cell proliferation in this process.

To do so, we performed Phosfohistone3 (PHH3) staining in E10.5 hearts, when the shift in the cell population is taking place. We determined the percentage of proliferating cells in both *iMOS*^{WT}; and *iMOS*$^{T1\text{-}Myc}$; *Nkx2.5-Cre* recombined hearts (figure 15 A, B).

We found no significant differences between the overall rates of PHH3+ cells in WT and Myc overexpressing mosaics (figure 15C). Similarly, we did not find differences in the proportion of PHH3+ cells between the two cell populations in the *iMOS*$^{T1\text{-}Myc}$ mosaic (figure 15 D, E).

To confirm these observations, we also performed BrDU staining and results were similar, with no differences in BrDU+ cell frequency between *iMOS*^{WT} and *iMOS*$^{T1\text{-}Myc}$ (figure 15 F-H) or between the EYFP-Myc and ECFP-WT populations of the *iMOS*$^{T1\text{-}Myc}$ mosaic hearts (figure 15 I-J).

These results fit with previous studies

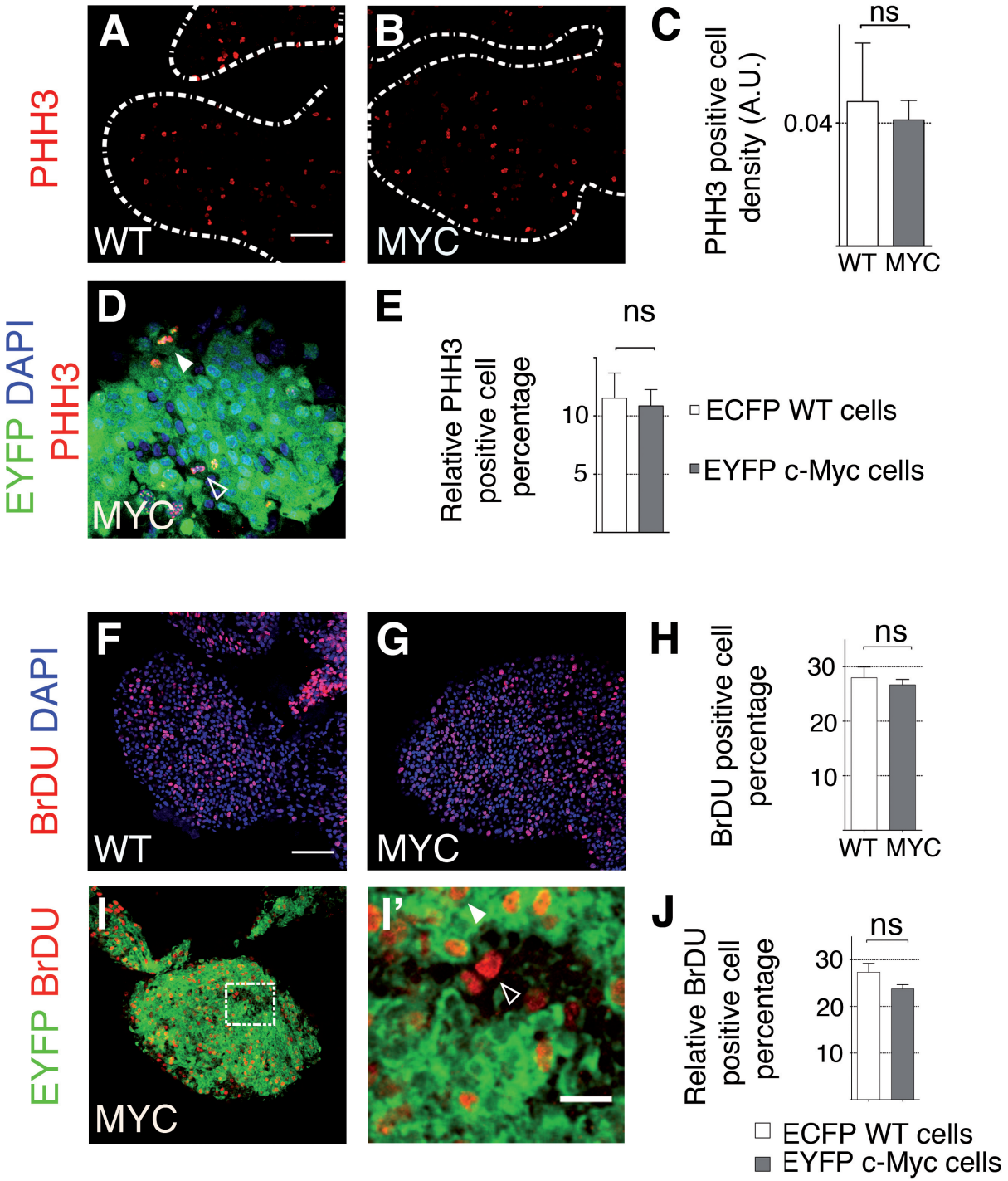

Figure 15. Analysis of cell proliferation upon Myc mosaic overexpression in the developing heart

A, B. Z-projections from 30 µm confocal stacks obtained from E10.5 left ventricles of *iMOS*^{WT} (WT) and *iMOS*$^{T1\text{-}Myc}$ (MYC) mosaics, showing anti PHH3 staining to mark cell division. Bar, 50 µm. **C.** Total PHH3 density measured as number of positive cells per arbitrary area units at E10.5 in *iMOS*^{WT} (WT) and *iMOS*$^{T1\text{-}Myc}$ (MYC) mosaics (N=4 hearts, N≥20 positive cells/heart). **D.** Confocal section of a MYC mosaic left ventricle at E10.5, showing the distribution of EYFP+, ECFP+ and PHH3+ cells. Bar, 50 µm. **E.** PHH3+ nuclei frequency in the EYFP and ECFP populations of *iMOS*$^{T1\text{-}Myc}$ mosaics (N=5 embryos and ≥ 680 nuclei). The filled arrowhead marks an EYFP+, PHH3+ cell and the empty arrowhead, an ECFP+, PHH3+ cell. Data are means ± SEM.*p<0.1; **p<0.05; ***p<0.001. **F,G.** Confocal sections from E10.5 left ventricles of *iMOS*^{WT} (WT) and *iMOS*$^{T1\text{-}Myc}$ (MYC) mosaics showing anti BrDU staining. **H.** BrDU+ cardiomyocyte frequency analyzed at E10.5 in *iMOS*^{WT} (WT) and *iMOS*$^{T1\text{-}Myc}$ (MYC) mosaics (N=4 hearts,N≥20 positive cells/heart). **I.** Confocal section of an *iMOS*$^{T1\text{-}Myc}$ mosaic (MYC) E10.5 left ventricle showing the distribution of EYFP+ and BrDU+ cells. **I'.** detailed image of the boxed area in **I**. **J.** BrDU+cardiomyocyte frequency in the EYFP-Myc (MYC) and ECFP-WT (WT) populations of the *iMOS*$^{T1\text{-}Myc}$ mosaic (N=4). Bar, 20µm. Filled arrowhead shows an EYFP+, BrDU+ cell and empty arrowhead, an ECFP+, BrDU+ cell. Data are mean ± SEM.*p<0.1; **p<0.05; ***p<0.001

showing that the *Myc* dosage induced by a single *Rosa26* allele does not increase proliferation rates in most tissues (Clavería et al., 2013; Murphy et al., 2008) and indicate that differences in cell proliferation do not account for the shift in cardiomyocyte populations.

Myc-overexpressing cardiomyocyte population expands by apoptosis-driven cell competition

Then we decided to evaluate the role of apoptotic cell death in the depletion of WT

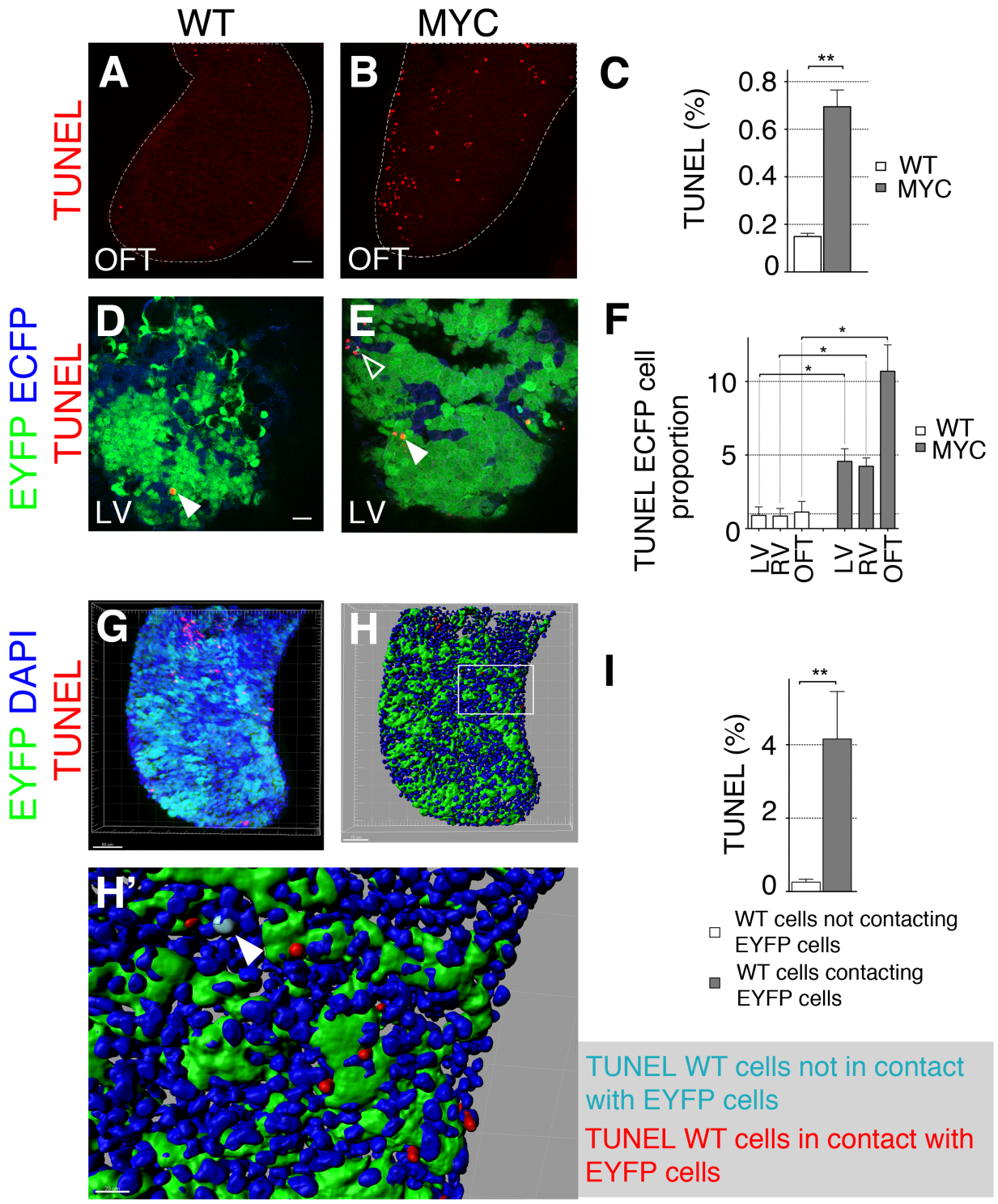

cardiomyocytes.

To do so, we generated a third mosaic line; *iMOS*$^{T1\text{-}Myc/T2p35}$, which generates random mosaics upon recombination. In these mosaics, an ECFP-p35 cell population is confronted with an EYFP-Myc population.

P35 is a baculoviral caspase inhibitor that prevents apoptosis both in insects and mammals (Claveria et al., 2013, Hay et al., 1994).

Quantitative confocal analysis of neonatal hearts induced with *Nkx2.5-Cre* showed that these mosaics retained at birth 70% of the original p35-expressing ECFP cell (figure 10 C, F, G). This contrasts with the 25% of WT cells observed in *iMOS*^{WT} mosaics, indicating that apoptosis inhibition significantly, although not totally, preserved WT cells from elimination when confronted with Myc-overexpressing cells (figure 10 G).

We also tested generating *iMOS*$^{T1\text{-}Myc/T2p35}$ mosaics using *Islet1-Cre* to analyze the behaviour of second heart field progenitors (figure 13 C, G, G'). We found, accordingly with the observations with *Nkx2.5-Cre* recombination, that the ECFP population is partially protected from elimination (figure 13H).

We found, however, that the expansion of the EYFP-Myc population was similar to that observed in *iMOS*$^{T1\text{-}Myc}$ mosaics (figure 11D), indicating that the expansion of Myc-overexpressing cardiomyocytes takes place also by eliminating non-recombined WT cardiomyocytes, being not affected by the presence of a low proportion of ECFP-p35 cardiomyocytes.

These results indicate that cell death is a predominant mechanism in the population shift observed in *iMOS*$^{T1\text{-}Myc}$ mosaics.

To further assess this, we performed TUNEL assays to score apoptotic rates in E10.5 mosaic hearts recombined using *Nkx2.5-Cre*. We decided to focus mainly on the outflow tract region (OFT) since it was the one showing higher apoptotic rates in the *iMOS*^{WT} mosaics (figure 16 A, B).

While the proportion of TUNEL-positive cardiomyocytes was in general extremely low in *iMOS*^{WT} mosaics, we observed a 5-fold increase in the overall apoptotic rate in *iMOS*$^{T1\text{-}Myc}$ mosaics (figure 16 C). Moreover, in *iMOS*$^{T1\text{-}Myc}$ mosaics, the apoptotic rate in the ECFP-WT population was remarkably higher than that seen in the EYFP Myc population (figure 16 D-F).

Interestingly, the apoptosis rate varied between heart regions: whereas the ECFP/EYFP TUNEL ratio was 4 to 5-fold above baseline in the ventricles, in the OFT it was over 10-fold higher, indicating that ECFP-WT

Figure 16. Myc-overexpressing cardiomyocytes expand by inducing apoptosis of neighbouring WT cardiomyocytes

A, B. Maximal projections of confocal stacks (30 µm deep) from the OFT region of *Nkx2.5-Cre* recombined *iMOS*^{WT} (WT) (**A**) and *iMOS*$^{T1\text{-}Myc}$ (MYC) (**B**) whole-mount TUNEL-stained E10.5 hearts. Bar, 50 µm. **C**. TUNEL staining frequency in cardiomyocytes from the mosaics shown in **A**, **B** (N = 4 WT and 7 MYC mosaics). **D**, **E**. Confocal sections from the LV of *Nkx2.5-Cre* recombined *iMOS*^{WT} (WT) (**D**) and *iMOS*$^{T1\text{-}Myc}$ (MYC) (**E**) Whole-mount TUNEL-stained E10.5 hearts, showing overlaid EYFP, ECFP and TUNEL signals. Filled arrowheads point to EYFP+ TUNEL+ cells and empty arrowheads to ECFP+ TUNEL+ cells. Bar, 50 µm. **F.** ECFP/EYFP TUNEL frequency ratios in different regions of *Nkx2.5-Cre* recombined *iMOS*^{WT} (WT) and *iMOS*$^{T1\text{-}Myc}$ (MYC) whole-mount E10.5 hearts (N = 4 WT and 7 MYC mosaics). LV, left ventricle; RV, right ventricle; OFT, outflow tract. Arrowhead marks the unbiased ECFP/EYFP TUNEL frequency ratio = 1. **G.** Maximal projection of the OFT from an *Islet1-Cre* recombined *iMOS*$^{T1\text{-}Myc}$ E10.5 heart (MYC), showing overlaid EYFP, DAPI and TUNEL signals. Bar, 70 µm. **H.** Computer 3D reconstruction of the stack shown in **G**. **H'.** Magnification of the boxed region in **H**, showing TUNEL+ WT cells contacting (red) and not contacting (light blue, arrowhead) MYC-overexpressing cells. Bar, 20 µm. I TUNEL frequency in WT cells contacting and not contacting EYFP cells in Islet1Cre- recombined iMOST1-Myc E10.5 hearts (MYC) (N=3 and ≥ 2815 cells). Data in **C**, **F**, **I** are means ±SEM. *p<0.05; **p<0.01; ***p<0.001.

cardiomyocytes in this region are especially sensitive to mosaic Myc overexpression (figure 16 F).

Competition induced apoptosis relies on short range interactions

Since ECFP-WT cells are normal viable cells, our results suggested that a cell-non autonomous mechanism was involved in their increased death rates.

We therefore studied the spatial range of these interactions of these interactions. To do so, we took advantage of the low-rate, interspersed recombination generated in the OFT region by the *Islet1-Cre* driver. This way, we generated a mosaic in which a few EYFP cells would lie within an excess of WT cells, allowing us to score apoptosis separately in WT cells in direct contact with EYFP-Myc cells and in those not in contact (figure 16 G-H').

Apoptotic rate was found to be highly increased only in those WT cardiomyocytes that were in direct contact with Myc-overexpressing EYFP cardiomyocytes. Specifically, we found a 17-fold increase in apoptosis in WT contacting cardiomyocytes compared to WT non-contacting cardiomyocytes (figure 16 I).

Therefore, these results indicate that the expansion of Myc-overexpressing cardiomyocytes is dependent on the elimination of neighbouring WT cardiomyocytes through apoptosis triggered by direct cell-cell contact or short-range signalling.

Our characterization thus establishes that the replacement of the WT cardiomyocyte population by the Myc-overexpressing population is due to apoptosis-driven cell competition.

Flower is not involved in Myc induced cell competition in the developing heart

Flower protein has been previously proposed to be implicated in cell competition in *Drosophila* through the expression of different protein isoforms that allow cells to communicate each others' fitness.

To determine whether *Flower* plays a role in induced cell competition in the developing heart, we generated *iMOST1-Myc* mosaics using *Nkx2.5-Cre* recombination in a *Flower* knockout background (*Flower* knock-outs have been described to be fertile, viable and to display a reduced indicence of papilloma formation) (Petrova et al., 2012).

Analysis of confocal sections showed that ECFP-WT cell elimination in $iMOS^{T1\text{-}Myc}$ mosaics was similar in WT, heterozygous and homozygous *Flower* knockout backgrounds (figure 17 A-D).

This indicates that, in this cell competition model, Flower activity is dispensable for the elimination of WT cells. Moreover we were unable to detect *Flower* expression in the heart by ISH (figure 17 E).

Endogenous cell competition does not play a role in the developing heart

Our results indicate that cardiac cells, including cardiomyocytes, are sensitive to induced cell competition.

These results however do not address whether endogenous cell competition could play a substantial physiological role in cardiac development. To test this, we generated a mouse mosaic strain in which EYFP labelled cells were WT (EYFP-WT) and ECFP labelled cells expressed p35 (ECFP-p35) cells.

This line, $iMOS^{t2\text{-}p35}$, was recombined using *Mef2C-AHF-Cre*, which recombines the anterior region of the second heart field, since

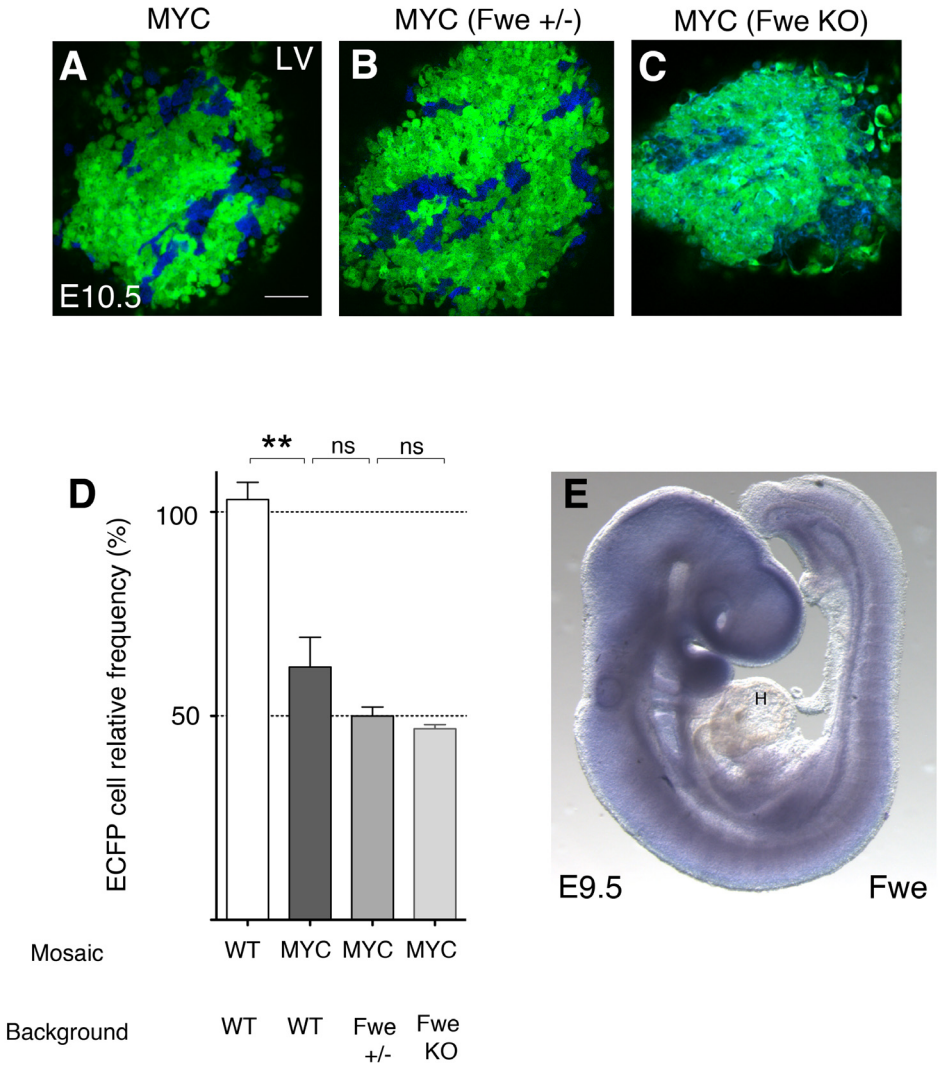

Figure 17. *Flower* is dispensable for induced cell competition in the developing heart

A, B, C. Confocal sections showing the left ventricle of an *iMOS*$^{T1\text{-}Myc}$ mosaic induced with *Nkx2.5-Cre* in a WT (MYC) (A), *Fwe* +/- (B) and *Fwe* KO (C) background. Bar 50 µm. **D.** Percentage of ECFP+ cells in whole hearts of the *iMOS*$^{T1\text{-}Myc}$ (MYC) mosaics in the different *Flower* backgrounds relative to that observed in the iMOSWT (WT) mosaics, which was normalized to 100%. (N>4 embryos) **E.** *Flower* mRNA detection by ISH hybridization on whole mount at E 9.5. Data in **D** are means ±SEM; * p<0,05; **p<0,01; ***p<0,001. H: Heart

this is the population that we have found to be more sensitive to cell competition.

In case endogenous cell death would be eliminating a substantial number of cardiac precursors, we would expect a significant enrichment in the proportion of ECFP-p35 cells.

In addition, in the case that these cells would have been eliminated by Myc-regulated cell competition, we would expect the ECFP-p35 cell population to express lower Myc levels than the EYFP-WT population. We then measured Myc protein levels in the ECFP-p35 population, in which apoptosis had been blocked (figure 18 A-D).

Analysis of Myc levels by immunodetection showed no differences between the EYFP-WT population and the ECFP-p35 population (protected from elimination), indicating that a mechanism for endogenous cell competition dependent on Myc levels is not present in the developing heart; since rescued cells

do not show differences in Myc levels (figure 18 D).

Mycn and Myc levels interplay in cell competition in the developing heart

We then explored whether modifying the relative differences in Myc dose between neighbouring cells affected the competition process.

To study this question, we manipulated Mycn levels in the myocardium by conditional elimination and combined this elimination with recombined *iMOS*$^{T1\text{-}Myc}$ mosaics (figure 19 A-C). We found that when EYFP-Myc cells were generated in a *Mycn* heterozygous

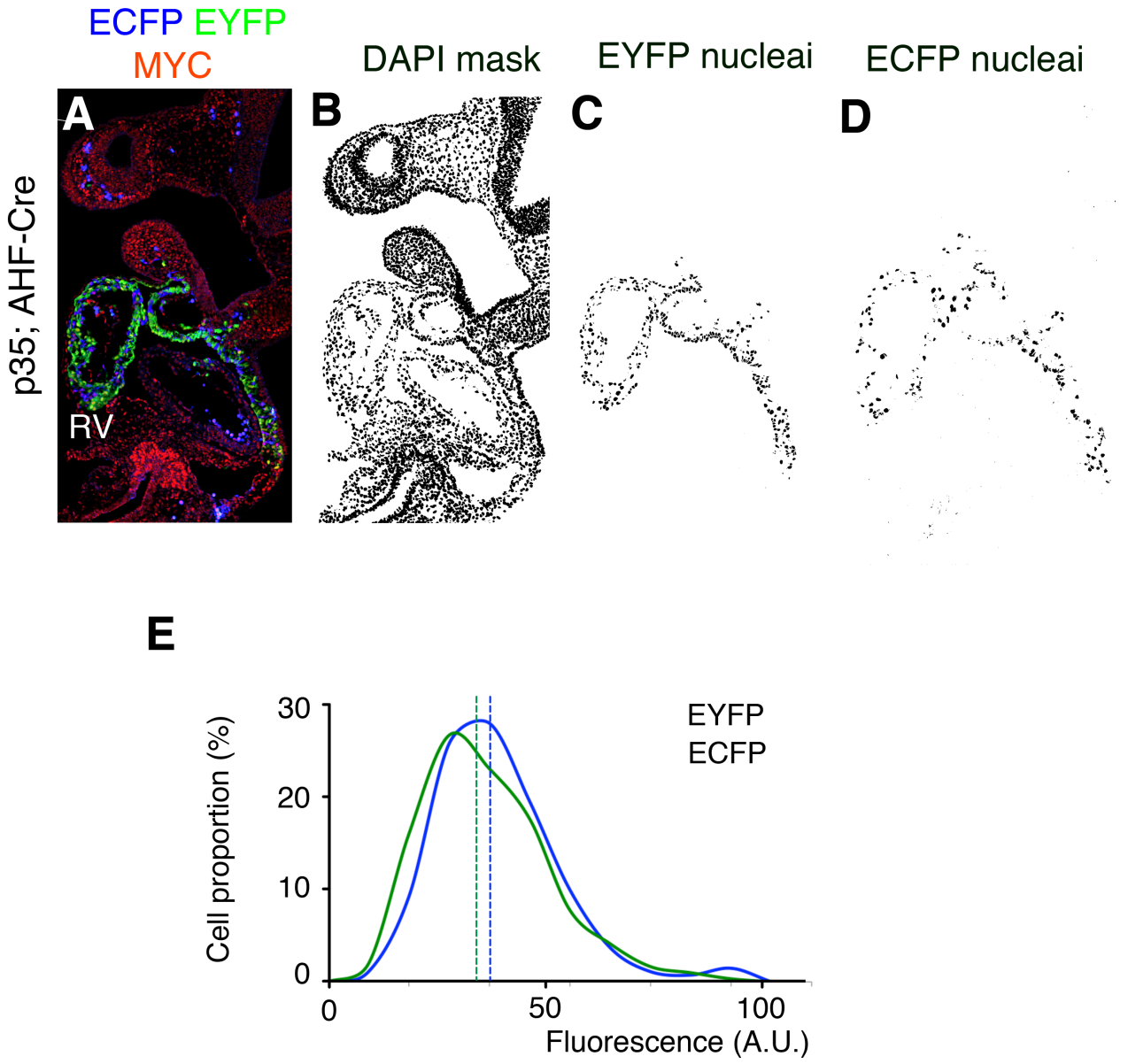

Figure 18. p35 rescued cells do not show a decrease in their Myc levels

A. Confocal image showing a histological section from a E9.5 *iMOS*$^{T2\text{-}p35}$*; AHF-Mef2C* (p35; AHF-Cre) embryo, showing EYFP, ECFP and Myc immunostaining. **B.** Binary mask of DAPI staining corresponding to **A**. **C.** Binary mask of the nucleai corresponding to EYFP cells. **D.** Binary mask of the nucleai corresponding to ECFP cells. **D.** Distribution of Myc protein levels in the EYFP-WT and ECFP-p35 cell populations of *iMOS*$^{T2\text{-}p35.}$
Myc protein levels were quantified from the immunofluorescence images similar to those in A. (N=4). Dashed vertical lines indicate the mean for each distribution.

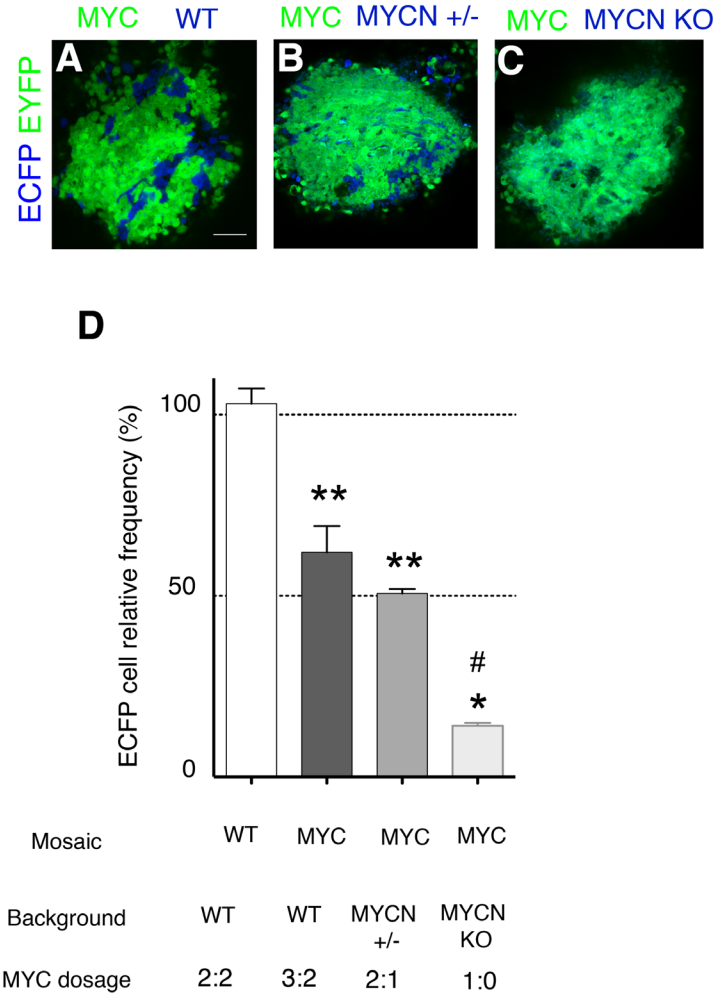

Figure 19. *Mycn* KO shows enhanced Myc induced cell competition in the developing heart

A-C Confocal sections from E10.5 hearts' left ventricles from *iMOS*$^{T1\text{-}Myc}$ mosaics induced with *Nkx2.5-Cre* in WT (**A**), *Mycn* (+/-) (**B**) and *Mycn* KO (**C**) showing an overlay of EYFP and ECFP. Bar 50 µm **D**. Percentage of ECFP+ cells in whole hearts of the *iMOS*$^{T1\text{-}Myc}$ (MYC) mosaics in the three different *Mycn* backgrounds relative to that observed in the *iMOS*^{WT} (WT) mosaics, which was normalized to 100%. Data in **D** are means ±SEM; * p<0,05; **p<0,01; ***p<0,001, when comparing with *iMOS*^{WT} and #p<0,05; ##p<0,01; ###p<0,001 when comparing with *iMOS*$^{T1\text{-}Myc}$ mosaic. (N>4)

background, ECFP-*Mycn* +/- cells were depleted to a similar extent than that found in a WT background (figure19 B, D).

Hence, confronting cells with the equivalent to two doses of Myc function with cells with one dose also eliminates those with lower relative Myc levels.

Moreover, ECFP-Mycn null cells were drastically reduced to 15% of the initial ECPF proportion when confronted with EYFP cells expressing a single Myc dose at stage E10.5 (Figure 19 C, D).

These results show that it is not the absolute level of Myc expression but the relative differences between cell populations, what triggers the elimination of those with relative low Myc levels.

Myc induced competition during adult heart homeostasis

Myc-overexpression in the adult heart causes no pathological alteration neither in homeostatic conditions nor in intense exercise conditions

Once we had determined that cell competition could be induced in embryonic cardiomyocytes during heart development, we then explored if an organ such as the adult heart could also be sensitive to Myc-induced cell competition.

To test this, we generated mosaic mouse lines in the adult heart taking advantage of the tamoxifen-inducible *My6-merCremer* strain (Sohal et al., 2001) (figure 20 A). We followed the protocol of induction shown in figure 20 A; in which induction was achieved through the diet, feeding the animals a tamoxifen diet for 1 month, starting right after weaning.

This protocol yields an initial EYFP recombination rate slightly above 50% (figure 21A). Since previous studies have reported that high Myc overexpression in cardiomyocytes of adult mice induces cardiomyocyte hypertrophy (Xiao et al., 2001), we performed a series of assays to address if this could be the case when we overexpress Myc moderately through the *iMOS* system in a long-term fashion.

Hearts from animals generated using the protocol previously described (figure 20 A) were tested for hypertrophic response. Firstly, we analyzed heart function and anatomy in $iMOS^{WT}$ and $iMOS^{T1\text{-}Myc}$ mosaics through echocardiographic study in basal conditions.

This study did not detect any differences between the mosaics studied (figure 20 B, C, D) in any parameter analyzed, neither anatomical nor functional; including ejection fraction and left ventricular mass.

We then studied whether challenging heart function following a protocol of intense exercise could trigger differences between $iMOS^{WT}$ and $iMOS^{T1\text{-}Myc}$ animals. We set up a swimming protocol that lasted for two months and that got the animals to swim for up to 90 minutes everyday (see methods: table 2).

Echocardiographic assays performed right after the protocol and one month after finishing showed again no differences in any of the parameters analyzed, regarding heart anatomy or function (figure 20 C, D right panels).

Even though hearts were not altered macroscopically (figure 20 E), we analyzed cardiomyocyte size to determine the consequences of long-term Myc overexpression. Measurement of average cardiomyocyte 2D-size, both in histological sections and incultures of disaggregated cardiac cells (fi-

Figure 20. Mosaic Myc overexpression in adult cardiomyocytes is phenotypically silent

A. *My6-merCremer* recombined $iMOS^{T1\text{-}Myc}$ mosaics and control littermates were treated as schematized for experiments in **B**. **B.** Long axis M-mode echocardiography image from an $iMOS^{T1\text{-}Myc}$ (MYC) mosaic WT littermate at t2. Graphs (**C**) show ejection fraction (EF) and left ventricle (LV) mass from the echocardiographic study, and heart/body weight ratios (**E**) in the $iMOS^{T1\text{-}Myc}$ mosaics (MYC) and in WT littermates (WT) at t3 (N≥3). **D.** Shows EF and LV mass at t2 after a protocol of intense exercise from t0 to t2 (see experimental procedures). **F**, **G**. Confocal sections showing wheat germ agglutinin (WGA) staining to highlight cell perimeters in $iMOS^{WT}$ (WT) (**F**) and $iMOS^{T1\text{-}Myc}$ (MYC) (**G**) mosaics at t3. Bar, 50 µm. **H**, **I**. Brightfield confocal section of cardiomyocytes isolated from $iMOS^{WT}$ (WT) (**H**) and $iMOS^{T1\text{-}Myc}$ (MYC) (**I**) mosaic hearts at t3. Bar, 50 µm. **J.** Size (2D area) of cardiomyocytes shown in **H**, **I**. (N≥4 hearts and 236 cells).*p<0.1; **p<0.05; *** p<0.001. Horizontal bars represent mean values. **K**, **L.** EYFP fluorescence intensity plotted against cell size for cardiomyocytes isolated from $iMOS^{WT}$(WT) (**K**) and $iMOS^{T1\text{-}Myc}$ (MYC) (**L**) mosaics. Lines in **K** and **L** represent the regression line (R-square = 2.040e-5 and 0.007204, respectively).

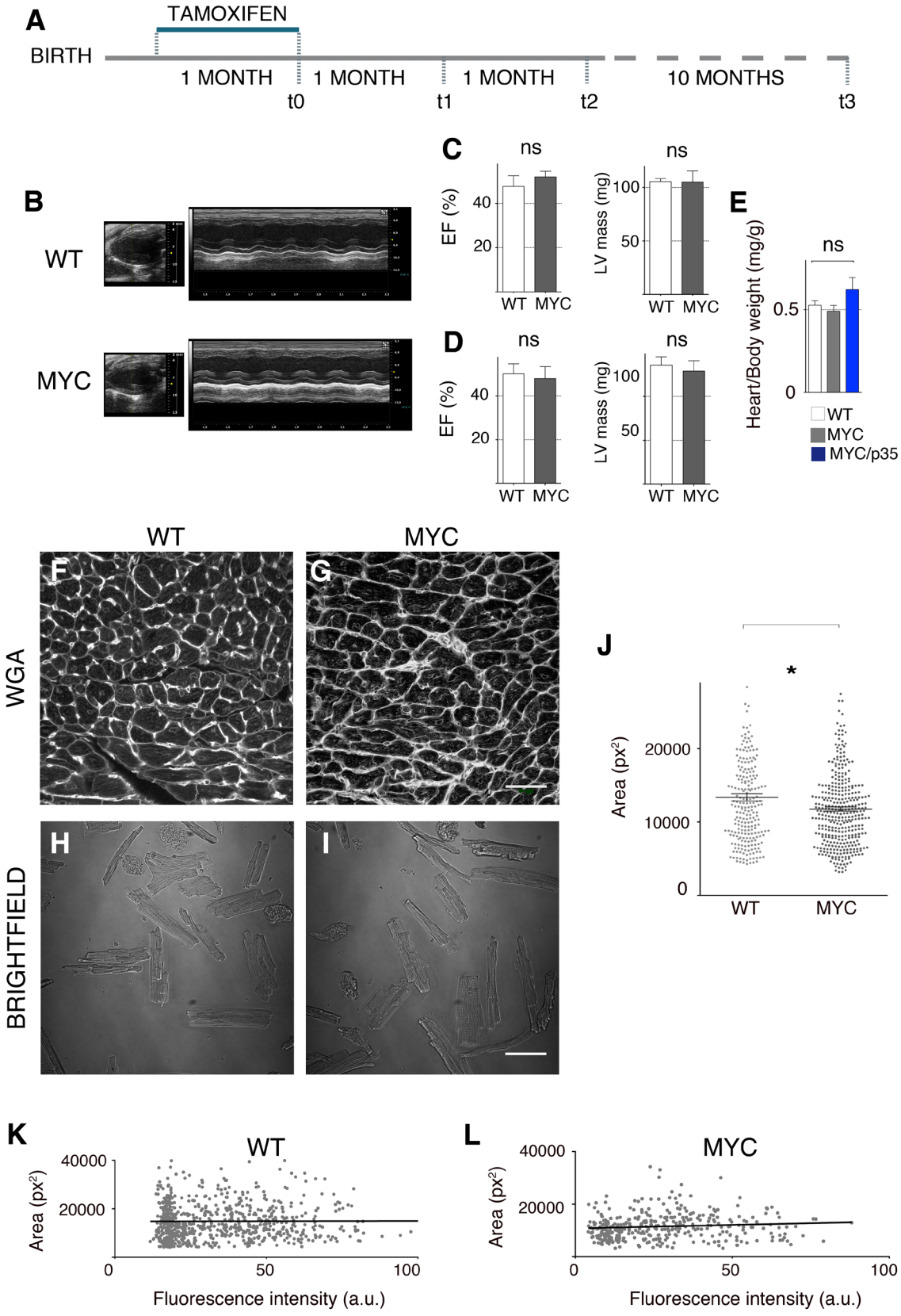
A
TAMOXIFEN
BIRTH
1 MONTH
1 MONTH
1 MONTH
10 MONTHS
t0
t1
t2
t3
B
WT
MYC
C
ns
EF (%)
40
20
WT MYC
ns
LV mass (mg)
100
50
WT MYC
D
ns
EF (%)
40
20
WT MYC
ns
LV mass (mg)
100
50
WT MYC
E
ns
Heart/Body weight (mg/g)
0.5
0
WT
MYC
MYC/p35
WT
MYC
WGA
BRIGHTFIELD
F
G
H
I
J
*
Area (px²)
20000
10000
0
WT
MYC
K
WT
Area (px²)
40000
20000
0
50
100
Fluorescence intensity (a.u.)
L
MYC
Area (px²)
40000
20000
0
50
100
Fluorescence intensity (a.u.)

gure 20 F-I), showed that cardiomyocytes in *iMOS*$^{T1\text{-}Myc}$ hearts were not only not bigger than those in *iMOS*^{WT} hearts, but were in fact slightly smaller (figure 20 J).

Moreover, we also measured the correlation between Myc levels and cell size: since recombination occurs after binucleation, adult cardiomyocytes could contain more than one recombined EYFP-Myc copy and therefore are predicted to express variable levels of extra Myc in correlation with EYFP levels.

In *iMOS*$^{T1\text{-}Myc}$ mosaics EYFP levels correlate with the Myc dose. Analysis of per-cell cardiomyocyte size and EYFP level showed no correlation between these two parameters in either *iMOS*^{WT} or *iMOS*$^{T1\text{-}Myc}$ mosaic hearts (figure 20 K, L), indicating that Myc expression in our system has no direct effect over cell size.

These results show that sustained Myc overexpression from the *iMOS*$^{T1\text{-}Myc}$ allele during adult life does not provoke cardiomyocyte hypertrophy.

Heart size and heart/body weight ratios were moreover similar in both mosaics, indicating that overall cardiac cellular and organ anatomy are preserved (figure 20 E).

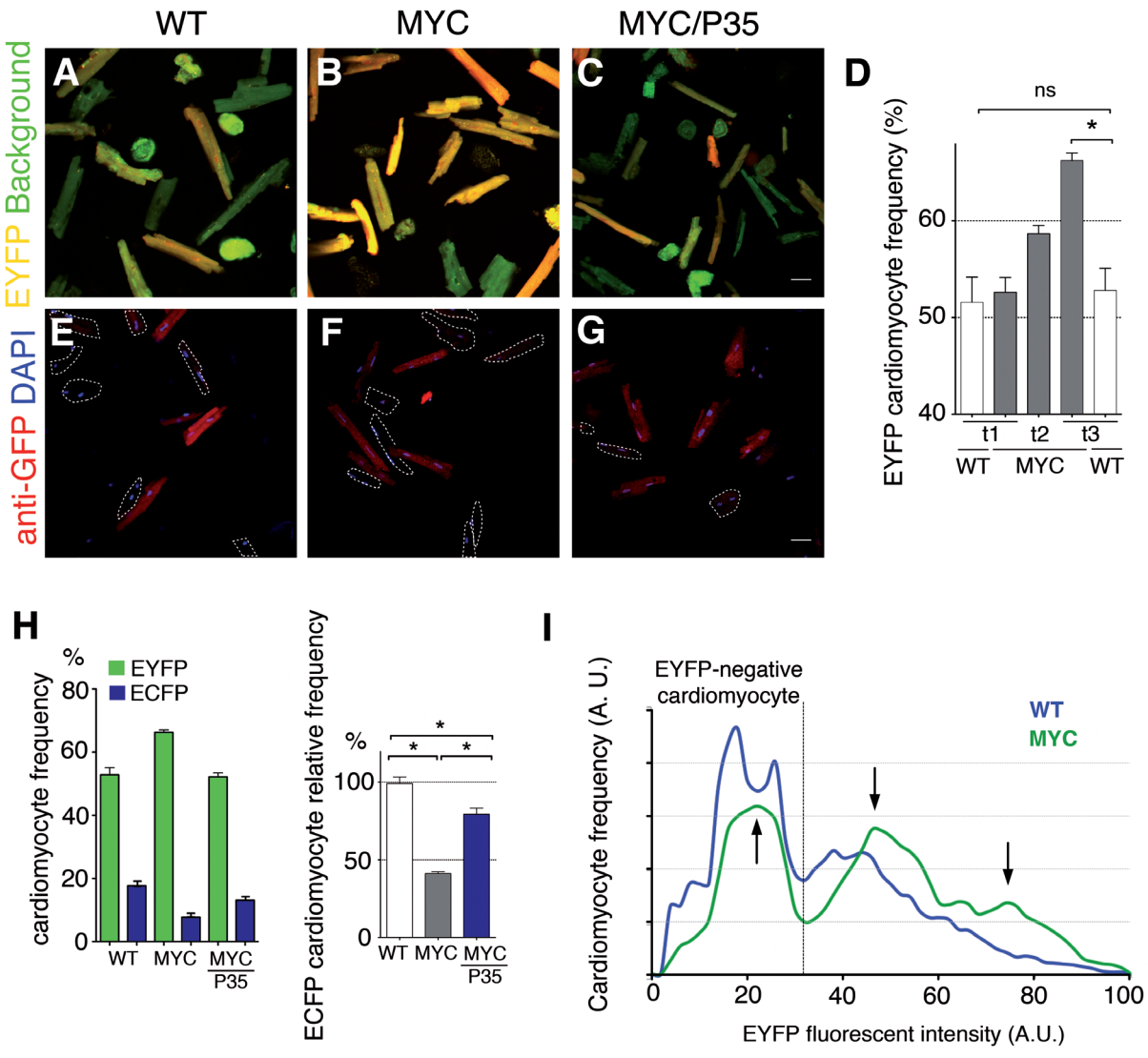

Myc overexpression induces cardiomyocyte population expansion in the adult heart

Once we had established the lack of pathological response due to Myc mild overexpression, we proceeded to determine the proportions of cardiomyocyte populations at different times after mosaic induction.

While in *iMOS^{WT}* hearts the proportion of EYFP cardiomyocytes did not increase during aging and was 53% at 1 year of age (figure 21A, D), in the *iMOS$^{T1\text{-}Myc}$* mosaics the proportion increased progressively from a frequency similar to that found in *iMOS^{WT}* hearts to 66% at 1 year of age (figure 21 B, D).

Interestingly, half of this enrichment took place during the first month of observation. Since there were no major changes in heart mass or cardiomyocyte size (figure 21 E, J), these observations suggest that Myc-overexpressing cardiomyocytes expand at the expense of WT cardiomyocytes during adult life.

To directly test this, we determined the relative frequency of ECFP cardiomyocytes with respect to all fluorescent (ECFP+EYFP) cardiomyocytes in 1-year-old *iMOS$^{T1\text{-}Myc}$* and *iMOS^{WT}* mosaics (figure 21 E-H).

The ECFP cell frequency was ~60% lower in the *iMOS$^{T1\text{-}Myc}$* mosaics, confirming that the expansion of the Myc- overexpressing cardiomyocyte population is concomitant with a reduction in the WT population.

Since we had detected differences in Myc levels due to ploidy and nucleation of cardiomyocytes (most adult cardiomyocytes in the mouse are tetraploid and contain two nuclei (Soonpaa et al., 1996); together with the partial recombination achieved by tamoxifen treatment, we had generated heterogeneous levels of EYFP-Myc content in cardiomyocytes, with a predicted predominance of cardiomyocytes with one or two active EYFP-Myc copies.

We therefore refined our study to determine whether cardiomyocyte population expansion correlated with EYFP-Myc levels.

Fluorescence was measured in isolated cardiomyocytes and the frequency of cells according to fluorescence intensity was determined (figure 21 I). This analysis showed that the enrichment in EYFP+ cardiomyocytes in iMOST1-Myc mosaics mostly affects the populations with higher EYFP levels at the expense of EYFP-negative cardiomyo-

Figure 21. Myc overexpression induces replacement of adult cardiomyocytes.

A-C. Confocal images of plated cardiomyocytes isolated at t3 (12 months after tamoxifen administration; see scheme in figure 20) from *My6-merCremer* recombined *iMOS^{WT}* (WT) (**A**), *iMOS$^{T1\text{-}Myc}$* (MYC) (**B**) and *iMOS$^{T1\text{-}Myc/T2\text{-}p35}$* (MYC/P35) (**C**) mosaics, showing native EYFP expression and background autofluorescence. **D.** Percentage of EYFP+ cardiomyocytes in cultures obtained from *My6-merCremer* recombined *iMOS^{WT}* (WT) hearts at t1 and t3 and from *iMOS$^{T1\text{-}Myc}$* (MYC) hearts at t1-t3 (N≥3 and 300 cells). Data are means ± SEM. **E-G.** Confocal images of plated cardiomyocytes obtained as in **A-C**, showing anti-GFP immunofluorescence, which identifies EYFP+ and ECFP+ cardiomyocytes. Bar, 50 µm. **H.** Quantification of data represented in **A-G** at t3. **H.** The graph on the left shows the absolute frequencies of EYFP-Myc and ECFP-WT cardiomyocytes in *iMOS^{WT}* (WT), *iMOS$^{T1\text{-}Myc}$* (MYC) and *iMOS$^{T1\text{-}Myc/T2\text{-}p35}$* (MYC/P35) mosaics. In the graph on the right, the same data were expressed as relative ECFP+/EYFP+ cardiomyocyte proportions relative to that observed in *iMOS^{WT}* (WT) mosaics, which was normalized to 100%. **I.** Graph represents the frequency of cardiomyocytes according to EYFP intensity in tamoxifen-induced *My6-merCremer* recombined *iMOS^{WT}* (WT) and *iMOS$^{T1\text{-}Myc}$* (MYC) mosaics, measured in cardiomyocytes isolated at t3, as in **A-C**. The vertical dotted line marks the limit between background-fluorescent and EYFP-positive cardiomyocytes. Arrows indicate regions in which the frequencies overtly differ between the two mosaics studied. Data in bar graphs are means ± SEM. *p<0.05 **p<0.01 ***p<0.001.

cytes, whose frequency decreased (figure 19 I). These observations indicate a correlation between Myc dose levels and cardiomyocyte population prevalence in the adult myocardium.

Analysis of the pathways involved in adult cardiomyocyte competition

To identify the pathways altered in the *iMOS*$^{T1\text{-}Myc}$ adult mosaic heart, we performed a transcriptomic analysis by RNA-seq, com-

A

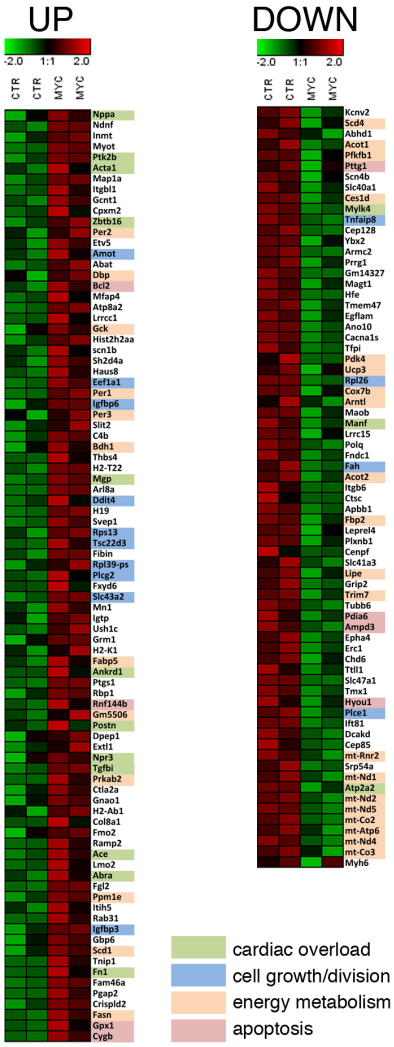

B

Enriched Functional Gene Classes (all genes)	
Upregulated	**Downregulated**
Inflammation	
BIOCARTA_MONOCYTE_PATHWAY	
BIOCARTA_COMP_PATHWAY (complement pathway)	
Response to Cardiac Overload	
BIOCARTA_ALK_PATHWAY (Fetal cardiomyocyte program)	BIOCARTA_EGF_PATHWAY (Involved in Cardiac Hypetrophy Progression)
BIOCARTA_MET_PATHWAY (Signaling of Hepatocyte Growth Factor Receptor)	
BIOCARTA_RHO_PATHWAY (Rho cell motility signaling pathway)	
GOBP_TISSUE_REMODELING	
KEGG_TGF_BETA_SIGNALING_PATHWAY	
Metabolic Pathways	
KEGG_CIRCADIAN_RHYTHM_MAMMAL (Circadian Rythm Regulation)	KEGG_PEROXISOME (Peroxisome biogenesis and function)
GOBP_RRNA_METABOLIC_PROCESS (Ribosome Biosynthesis)	GOBP_PEROXISOME_ORGANIZATION_AND_BIOGENESIS
KEGG_LYSOSOME (Lysosome assembly and function)	GOMF_LIPASE_ACTIVITY (Lipid catalysis)
Other	
GOBP_APOPTOTIC_PROGRAM	

Ingenuity Pathway Analysis (UP and Down genes)	
Upregulated	**Downregulated**
Top Canonical Pathways	
	OXIDATIVE PHOSPHORYLATION
OXIDATIVE PHOSPHORYLATION	
Top Diseases and Biofunctions	
CARDIOVASCULAR DISEASE	CARDIOVASCULAR DISEASE
CARDIOVASCULAR SYSTEM DEVELOPMENT AND FUNCTION	CARDIOVASCULAR SYSTEM DEVELOPMENT AND FUNCTION
CARDIOVASCULAR DISEASE	
LIPID METABOLISM	
CARDIOVASCULAR SYSTEM DEVELOPMENT AND FUNCTION	
Top Networks	
CARDIOVASCULAR DISEASE, CARDIAC HYPERTROPHY, DEVELOPMENTAL DISORDER	CARDIOVASCULAR DISEASE, CARDIAC HYPERTROPHY, DEVELOPMENTAL DISORDER

Figure 22. Transcriptomic analysis of the changes induced by Myc mosaic overexpression in the adult heart. Ingenuity pathway analysis

A representation of the list of genes up- or down-regulated in *iMOS*$^{T1\text{-}Myc}$ mosaics with respect to controls and their expression levels. Criteria for inclusion were adjusted p-value≤0.05 and expression levels ≥10 counts/million reads in at least one condition. Genes are colour-coded for involvement in predominant known functional classes for this gene set (see legend). **B.** top table; significant (p≤0.05) gene sets enriched in up- or down-regulated genes, including all genes in the analysis. Lower table; Top Ingenuity pathways and networks detected in the gene set shown in **A** (p≤0.01). Pathways include those detected in the independent analysis of the upregulated and downregulated genes and in their joint analysis.

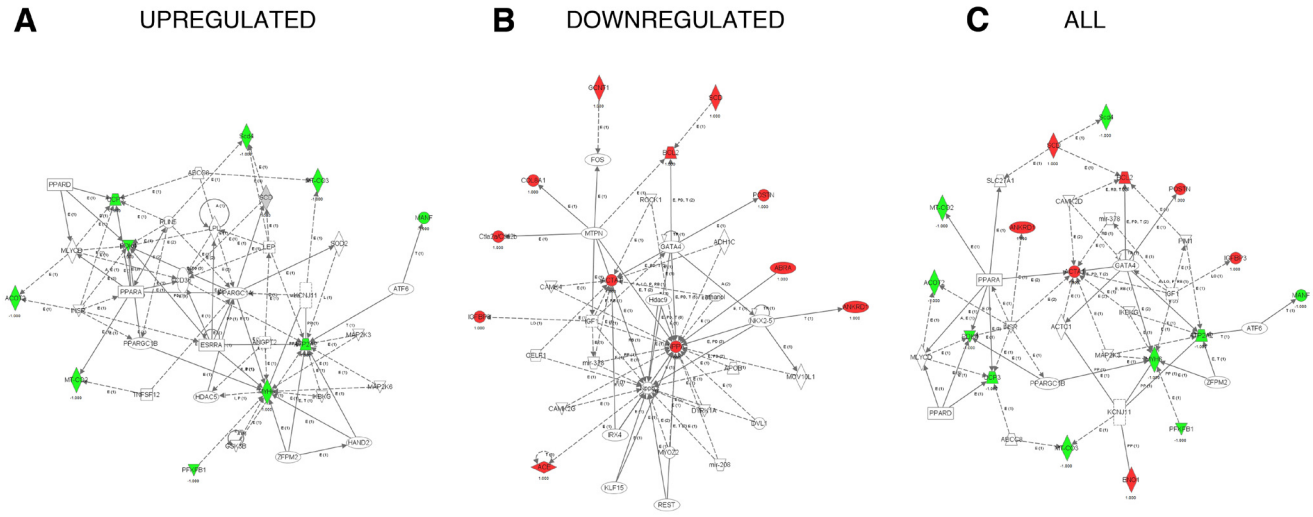

Figure 23. Transcriptomic analysis of the changes induced by Myc mosaic overexpression in the adult heart. Top networks differentially expressed

A-C Representation of the Top Networks found regulated in the Ingenuity analysis of the downregulated (**A**), upregulated (**B**) and joint list of genes (**C**).

paring 8-week old *iMOS*$^{T1\text{-}Myc}$ and control hearts (figure 22).

Among the genes more significantly up or downregulated in *iMOST*$^{1\text{-}Myc}$ hearts there is a strong representation of genes involved in the response to cardiac overload, in cell growth/division, in energy metabolism and in apoptosis (figure 22 A).

Gene set enrichment analysis on all genes present in the RNAseq experiment again detected the protective response to cardiac overload in *iMOS*$^{T1\text{-}Myc}$ hearts, including the activation of the atrial natriuretic peptide and fetal cardiomyocyte programs (Kishimoto et al., 2001) (Kuhn et al., 2002) and the HGF/Rho/Tissue remodeling pathways (Madonna et al., 2012).

In contrast, the EGF pathway, involved in the development of pathological hypertrophy (Shah and Catt, 2003) was found repressed in *iMOS*$^{T1\text{-}Myc}$ hearts.

Regarding metabolic processes, activation of the ribosome biosynthesis, a typical response to Myc overexpression, was also detected. In parallel, activation of the lysosomal pathway was as well present, indicating that metabolic activity was globally increased including both anabolic and catabolic processes.

With regard to the metabolic processes, *iMOS*$^{T1\text{-}Myc}$ hearts showed a reduction in lipid catabolism and in assembly of the peroxisome, the main organelle for lipid catabolism, suggesting a modification in the fuel usage by Myc-overexpressing cardiomyocytes.

A remarkable alteration was found in various regulators of the circadian rhythm; *Dbp* and *Per1*, *2* and *3* were upregulated and *Arntl* (*Bmal1*) was downregulated. Circadian rhythm transcription factors are essential regulators of cardiac metabolism, regulate the balance between lipid and glucose usage in the heart and display a feedback regulation with the oxidative phosphorylation pathway (Durgan and Parker, 2010).

A major regulator of cardiac metabolism, AMPK, has also been described to undergo circadian regulation (Tsai et al., 2010) its

regulatory subunit is overexpressed in the *iMOS*$^{T1\text{-}Myc}$ hearts, and it can be activated by Myc overexpression (Nieminen et al., 2013).

The results observed are therefore compatible with a modified metabolic status of the *iMOS*$^{T1\text{-}Myc}$ with either a direct or indirect impact of Myc overexpression on the circadian metabolic regulation.

In agreement with this view, the Ingenuity Pathway analysis on the selected up- and down-regulated genes (figure 22 B) indicates a modification of the Lipid metabolism and a reduction of the Oxidative Phosphorylation activity in *iMOS*$^{T1\text{-}Myc}$ hearts.

The top networks identified by this analysis for the upregulated, the downregulated and the joint gene sets are again the networks activated in response to cardiac overload (figure 22 B, 23A-C). In agreement with these results we found that the expression of the atrial natriuretic peptide was clearly activated in a patchy pattern in the ventricles of the *iMOS*$^{T1\text{-}Myc}$ mosaic hearts (figure 24A-B').

Given the known functions of Myc in cardiomyocytes, the pathways detected likely result from cell-autonomous Myc functions and may relate to the ability of Myc-overexpressing cardiomyocytes to replace the WT cardiomyocyte population.

In addition, the Gene Set Enrichment study identified the activation of the apoptosis regulation and inflammation pathways in *iMOS*$^{T1\text{-}Myc}$ hearts, which could be related to the death and removal of WT cardiomyocytes. We therefore used the *iMOS*$^{T1\text{-}Myc/T2p35}$ mosaics to undertake a functional study of the involvement of cell death.

This analysis showed that p35 expression largely rescues the ECFP cell population (figure 21 C, G, H).

These results indicate that adult cardiomyocytes undergo Myc-induced cell competition, which progresses by elimination of WT cardiomyocytes and their replacement by cardiomyocytes with high Myc levels.

We then analyzed whether increased proliferation of the Myc-overexpressing population is contributing to this phenomenon. We found that BrdU incorporation was 4-fold more frequent in the EYFP-Myc cardio-

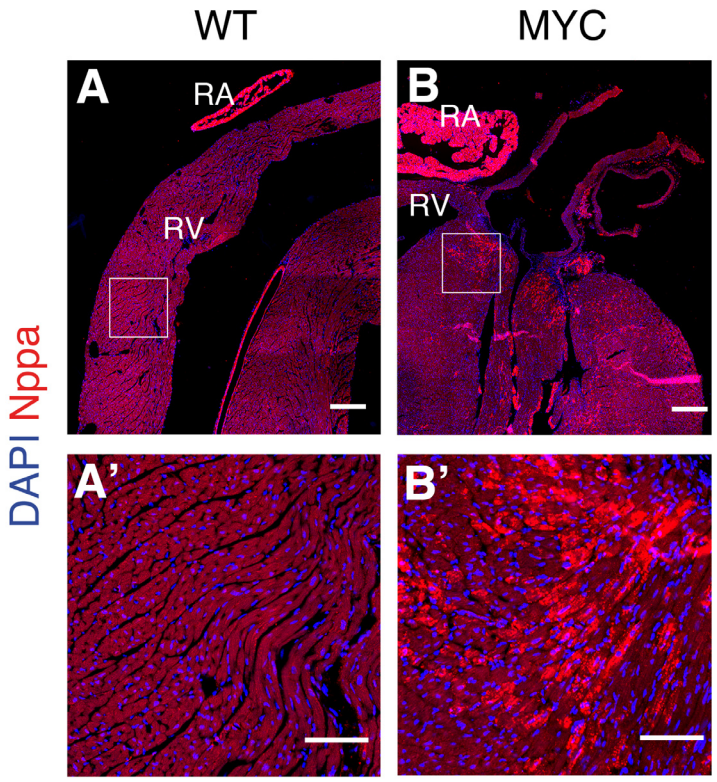

Figure 24. Nppa is upregulated in *iMOS*$^{T1\text{-}Myc}$ mosaic

A. Expression analysis of Nppa protein in adult *iMOS*^{WT} (WT) **B.** *iMOS*$^{T1\text{-}Myc}$ (MYC) mosaics. **A** and **B** panels show low magnification images of immunofluorescence detection of Nppa and boxed areas are magnified in the bottom **A'** and **B'** panels. RA, right atrium, RV, right ventricle. Bars, 100µm top; 50µm bottom.

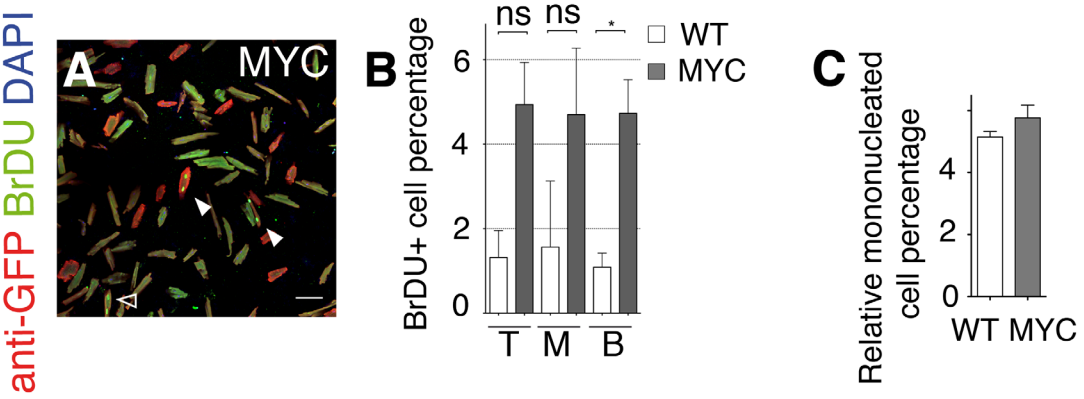

Figure 25. Analysis of BrDU incorporation in postnatal hearts

A. Confocal image of cardiomyocytes isolated from an iMOST1-Myc adult heart showing GFP and BrDU staining. Arrowheads show BrDU+/GFP+ mononucleated (empty arroheads) and binucleated (filled arroheads) cardiomyocytes. Bar,50 µm. B, Graph showing the frequency of of BrDU+ cardiomyocytes in the the WT (WT) and EYFP Myc (MYC) populations of the iMOST1-Myc adult hearts. Bi, binucleated; Mo, mononucleated. C, Graph showing the proportion of mononucleated cardiomyocytes within the WT (WT) and EYFP Myc (MYC) populations of the iMOST1-Myc adult hearts. (N=4 hearts and >300 cells/heart). Graphs in C, F, G show means ± SEM.*p<0.1; **p<0.05; ***p<0.001. Statistical analysis in B was done using the #-square test. ns, not sig-

myocytes than in the WT cardiomyocytes of *iMOS*$^{T1\text{-}Myc}$ mosaic hearts (figure 25 A, B).

This increase did not alter the proportion of mononucleated cardiomyocytes (figure 25 C), suggesting that the balance between mononucleated cardiomyocyte division and binucleation is preserved.

To directly assess the involvement of apoptosis in the cardiomyocyte population shift, we analyzed the TUNEL pattern in adult *iMOS*$^{T1\text{-}Myc}$ mosaics, however, we found no significant differences in TUNEL frequency between the EYFP-Myc and ECFP-WT cell populations.

These results suggested that, unlike the situation during development, apoptosis might not be involved in the elimination of WT cardiomyocytes in adults, despite the activation of apoptotic pathways detected by RNAseq.

We then explored whether alternative cell death pathways could be operating in postnatal cardiomyocytes.

Given that p35, in addition to inhibiting apoptotic cell death, can also inhibit autophagic cell death (Martin and Baehrecke, 2004) and that many apoptosis regulators are also involved in autophagic cell death, we tested whether this pathway could be involved in postnatal cardiomyocyte cell competition.

Analysis of the autophagic death-specific marker Beclin (Liang et al., 1999) showed rare positive cells in *iMOS*^{WT} hearts (figure 26 A, A', A''), however the frequency of Beclin-positive cells increased by 5-fold in *iMOS*$^{T1\text{-}Myc}$ mosaic hearts (figure 26 B, B', B'', C).

Moreover, the frequency of Beclin-positive cells within the *iMOS*$^{T1\text{-}Myc}$ mosaics was 9-fold higher in ECFP-WT cells than in EYFP-Myc

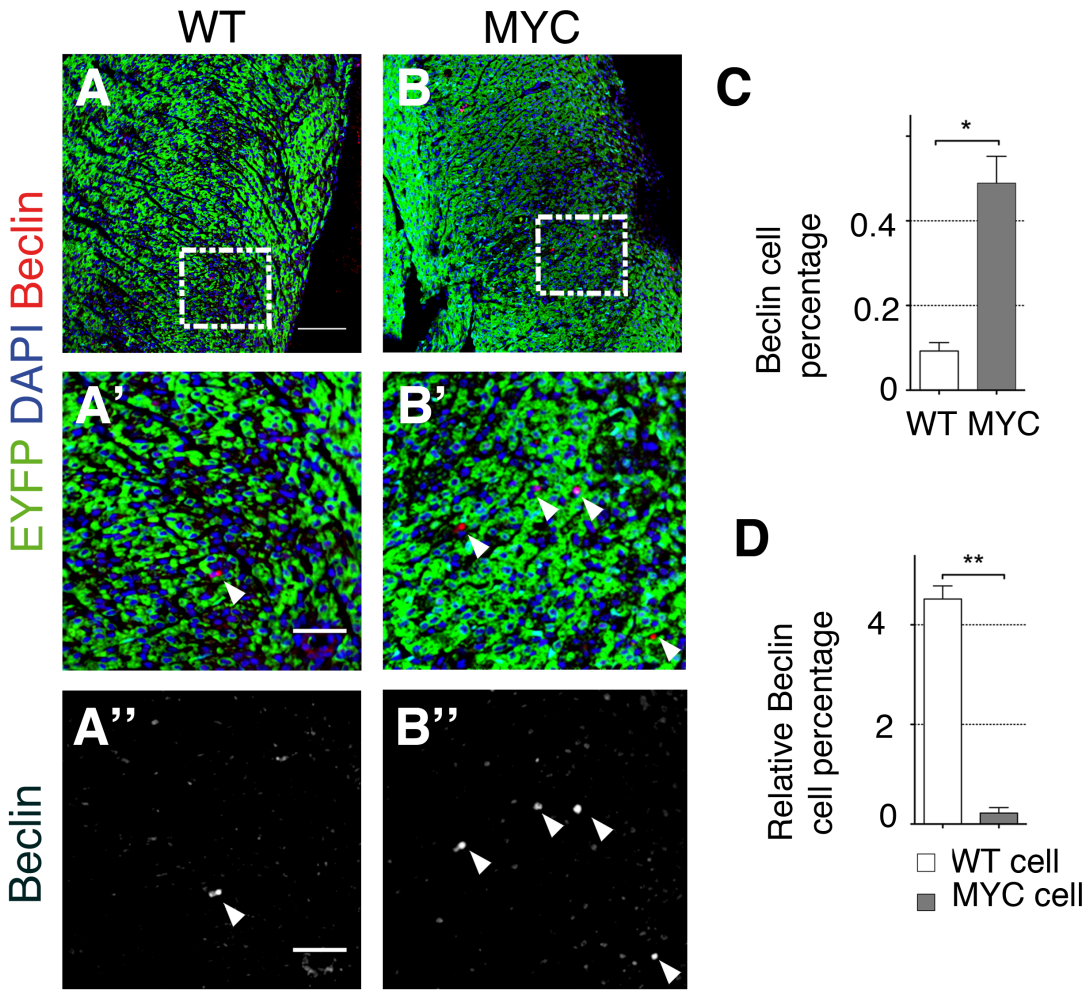

Figure 26. Analysis of autophagy in postnatal hearts

A-C. Confocal sections showing posnatal hearts from *iMOS*^{WT} (WT) (**A**) and *iMOS*$^{T1\text{-}Myc}$ (MYC) mosaics (**B**) showing Beclin-1 antibody staining together with *iMOS* cell populations mapping. Bar, 50 µm. **A', B'.** Higher magnification of boxed areas in **D** and **E**. Arrowheads point to Beclin+ cells. **A'', B''** show the Beclin signal from **A', B'** in isolation. Bar, 20 µm. **C.** Total Beclin+ cell frequency in *iMOS*^{WT} (WT) and *iMOS*$^{T1\text{-}Myc}$ (MYC) mosaics (N=3 WT and 5 MYC). **D.** Beclin+ cell frequency within the ECFP-WT (ECFP) and EYFP-Myc cell populations (MYC) of the *iMOS*$^{T1\text{-}Myc}$ mosaics. Graphs in **C**, **F**, **G** show means ± SEM.*p<0.1; **p<0.05; ***p<0.001.

cells (figure 26 D).

These results indicate that autophagic cell death instead of apoptotic cell death is a major contributor to postnatal cardiomyocyte cell competition.

Cell competition in the developing epicardium

Myc overexpression increases the contribution of Wt1 lineage to the heart during development

Having induced cell competition in the cardiomyocyte lineage during heart development, we decided to test the potential of cell competition in the developing epicardium.

The epicardium gives rise to different cell types during heart development (Wessels and Perez-Pomares, 2004) and has risen a lot of attention as a possible source of progenitors to replenish smooth muscle cells and myocardium, both during development and in the adult heart upon injury (Smart et al., 2011, Smart et al., 2007, Zhou et al., 2008).

To explore the roles of Cell Competition in epicardium, we recombined either *iMOS*^{WT} or *iMOS*$^{T1\text{-}Myc}$ transgenes using *Wt1-Cre*.

Analysis of histological sections at E14.5 in the *iMOS*^{WT} heart showed the described contribution of the Wt1 lineage to the myocardium. We found contribution to the epicardial layer and to epicardial derived cells (EPDCs) as well as to a few cardiomyocytes that appear scattered in the inter-ventricular septum (Wessels et al., 2012)(figure 27 A, A').

In contrast, histological sections from E14.5 *iMOS*$^{T1\text{-}Myc}$ hearts showed a remarkable contribution to both ventricles and the inter-ventricular septum (IVS) of the *Wt1-Cre* lineage (figure 27 B, B').

Quantification of the recombined area showed a four to five- fold increase in the contribution of Wt1 lineage to the ventricles and the IVS at E14.5 (figure 25 E-G).

This contribution progressed until birth when the proportion of the *Wt1-Cre* lineage to the ventricles raised to 50% of the total ventricle area (figure 27 C-D' and E,G), whereas the increase in the area of contribution to the IVS was lower (figure 27 G).

Myc overexpression in the *Wt1-Cre* lineage promotes preferential colonization of epicardium, EPDCs and Ventricular Cardiomyocyte populations.

To determine the contribution of EYFP-Myc cells from the *Wt1-Cre* lineage at E14.5, we performed flow cytometry analysis of whole E14.5 *iMOS*^{WT} and *iMOS*$^{T1\text{-}Myc}$ hearts.

Quantification of these assays showed a doubling in the EYFP population proportion in *iMOS*$^{T1\text{-}Myc}$ hearts compared with that observed in *iMOS*^{WT} hearts (figure 28 A-C).

We detected that the increase in the area of contribution of *Wt1-Cre* lineage was mostly due to a contribution to the cardiomyocyte population (figure 29 A-B').

To further determine the effect of Myc overexpression on the *Wt1-Cre* lineage in the different cell populations, we quantified the relative proportion of EYFP cells with respect to the total recombination (EYFP+ECFP) in histological sections in non-cardiomyocyte (mostly EPDCs and epicardial cells) and in cardiomyocyte cell populations from the free walls of both ventricles (VFW) and the IVS.

In both left and right VFWs and in the IVS, we detected a homogeneous enrichment (as an increase in the EYFP/ECFP ratio) in EYFP-Myc cells in the non-cardiomyocyte fraction of around 10-15% in *iMOS*$^{T1\text{-}Myc}$ versus *iMOS*^{WT} hearts (figure 29 C-E). Moreover, in histological sections we detected that the coronary perivascular cell population was composed 100% of EYFP-Myc cells in *iMOS*$^{T1\text{-}Myc}$ hearts (figure 30 A-C), indicating a competitive advantage of Myc-overexpressing EPDCs in colonizing the perivascular niche and differentiating to smooth

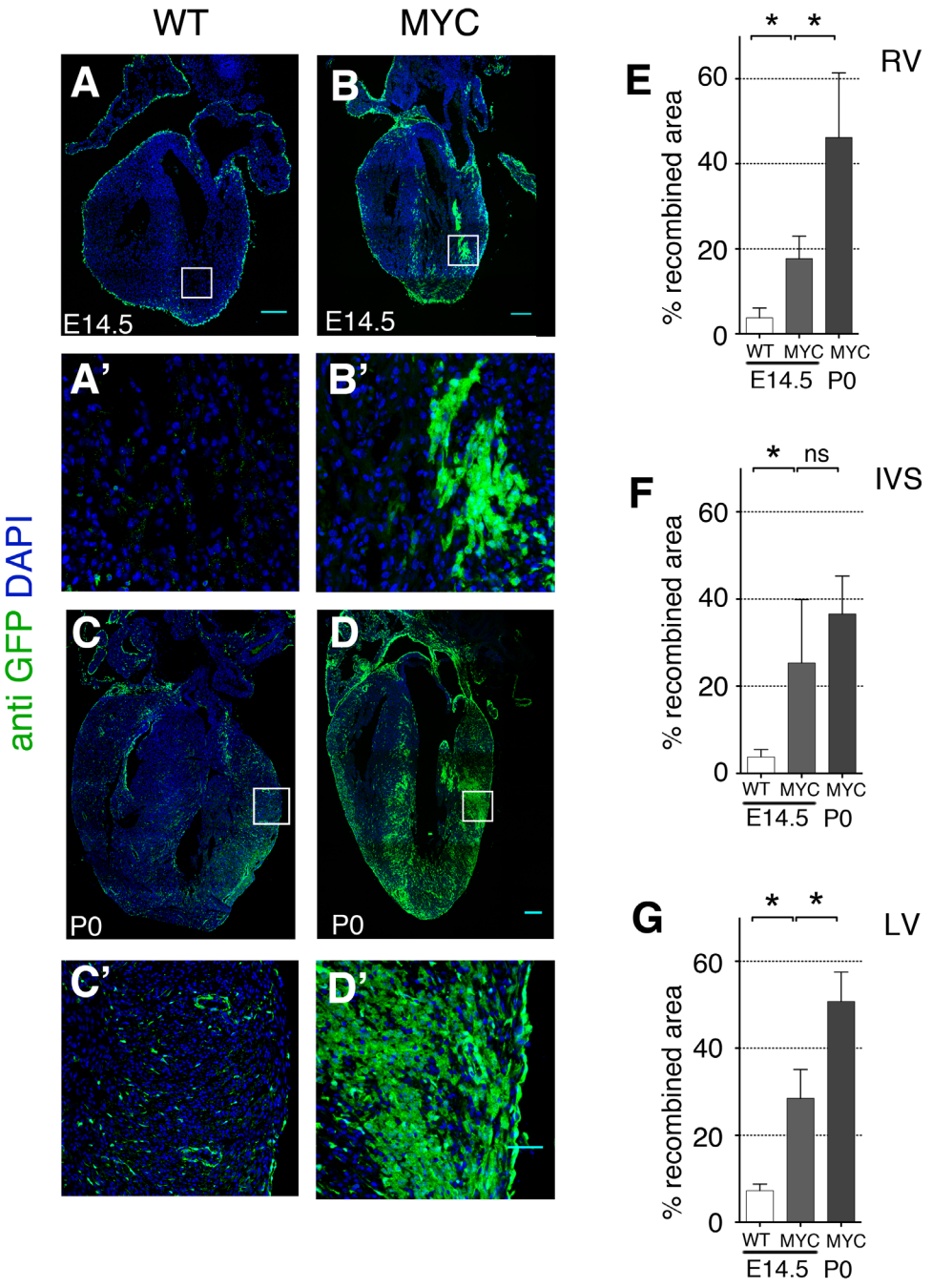

Figure 27. Myc overexpression enhances Wt1 lineage contribution to the developing heart

A-B'. Confocal images from histological sections of *iMOS*^{WT} (WT) (**A**) and *iMOS*$^{T1\text{-}Myc}$ (MYC) (**B**) hearts at E14.5 induced with *Wt1-Cre*. **A'** and **B'** show magnification of the boxed areas shown in **A** and **B**. **C-D'**. Confocal images from histological sections of P0 *iMOS*^{WT} (WT) (**C**) and *iMOS*$^{T1\text{-}Myc}$ (MYC) (**D**) recombined with *Wt1-Cre*. **C'** and **D'** show magnification of the boxed areas shown in **C** and **D**. **E-F.** Quantification of the percentage of recombined area detected in *iMOS*^{WT} (WT) and *iMOS*$^{T1\text{-}Myc}$ (MYC) at E14.5 and P0 in the RV (**E**), IVS (**F**) and LV (**G**). Graphs in **E, F, G** show means ± SEM.*p<0.1; **p<0.05; ***p<0.001. Bar, 200 µm in **A,B,C,D** and 50 in **A',B', C', D'** n≥ 5 hearts.

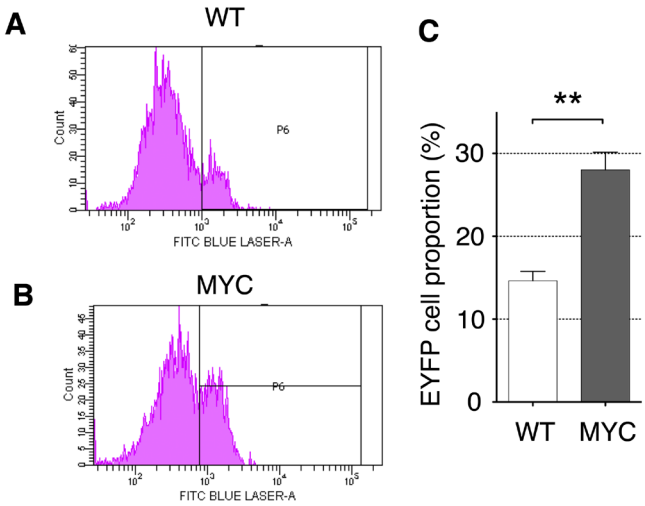

Figure 28. Increased contribution of EYFP-Myc cells from Wt1 lineage at E14.5

A.Cytometer histogram plot showing Counts (X axis) versus FITC laser (EYFP detection) in *iMOS*^{WT} (WT) E14.5 whole digested hearts. **B.** Cytometer histogram plot showing Counts (X axis) versus FITC laser (EYFP detection) in *iMOS*$^{T1\text{-}Myc}$ (MYC) E14.5 whole digested hearts. **C.** Quantification on EYFP+ population related to the total amount of live cells detected on the cytometer for *iMOS*^{WT} (WT) and *iMOS*$^{T1\text{-}Myc}$ (MYC) E14.5 hearts. Graphs show means ± SEM.*p<0.1; **p<0.05; ***p<0.001. n≥ 7 hearts

muscle cells.

As mentioned before, we detected no EYFP or ECFP cells in the *iMOS*^{WT} in either of the VFWs (ventricular free walls) (figure 29 C-E).

In agreement, all contribution of the *Wt1-Cre* lineage to the VFW cardiomyocyte population in *iMOS*$^{T1\text{-}Myc}$ hearts was 100% from EYFP+ Myc-overexpressing cells. (figure 29 C, E). An important enrichment in the EYFP/ECFP ratio was also detected in the IVS cardiomyocite fraction in *iMOST*$^{1\text{-}Myc}$ (figure 29 D).

These results indicate that Myc overexpression promotes preferential expansion cells derived from the epicardium and EPDCs, both known derivatives of the *Wt1-Cre* lineage. In addition, we found thatMyc overexpression drives a strong contribution of the *WT1-Cre* lineage to the cardiomyocyte population, especially that of the VFWs.

Myc overexpression promotes the invasive behaviour of epicardial cells

To further understand the effect of Myc overexpression in epicardial cells, we set up a new ex-vivo system of epicardium-myocardium co-explants. This system allows us to understand epicardial behaviour when in presence of myocardium and myocardial signals, and represents an ex-vivo way of understanding epicardium-myocardium cross-talk.

We performed co-explant assays of E10.5 left ventricles (covered by epicardium) from *iMOS*^{WT} and *iMOS*$^{T1\text{-}Myc}$ mosaics confronting them with E9.5 WT left ventricles (not yet covered by epicardium), and cultured them for 24 hours.

We detected that epicardial cells form both *iMOS*^{WT} and *iMOS*$^{T1\text{-}Myc}$ E10.5 LVs were able to expand, migrate and reach the surface of the E9.5 WT myocardium. While *iMOS*^{WT} epicardial cells remained on the myocardial surface (figure 31 A), in contrast, *iMOS*$^{T1\text{-}Myc}$ epicardial cells invaded the WT myocardium

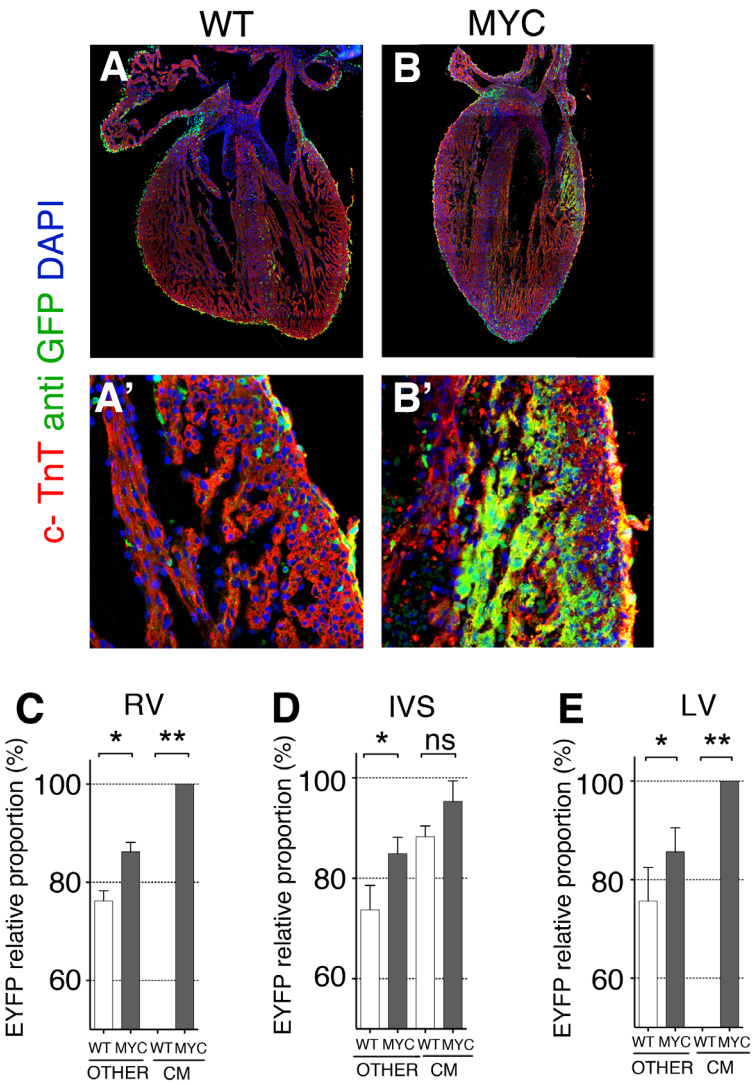

Figure 29. Myc-induced Cell Competition takes place in epicardium and Epicardium derived cells. Myc overexpression promotes contribution of Wt1 lineage to the developing myocardium

A-B'. Confocal images from histological sections of *iMOS*^{WT} (WT) (**A**) and *iMOS*$^{T1\text{-}Myc}$ (MYC) (**B**) hearts at E14.5 induced with *Wt1-Cre*. **A'** and **B'** show amplified regions from boxed areas in **A** and **B**. **C-E** Percentage of EYFP+ cells observed at E14.5 in whole hearts of the *iMOS*$^{T1\text{-}Myc}$ (MYC) and *iMOS*^{WT} (WT) mosaics in the non cardiomyocytic fraction and in the cardiomyocyte fraction in the RV (**C**), IVS (**D**) and LV (**E**). Data are means ±SEM; * p<0,05; **p<0,01; ***p<0,001. n≥ 5 hearts. Bar, 200 µm in A,B and 50 in A',B'

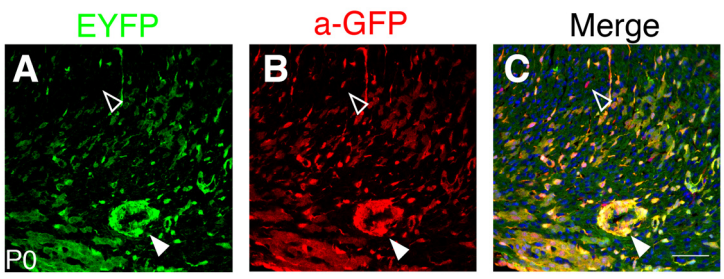

Figure 30. Contribution of EYFP-Myc cells to Smooth muscle lineage is enhanced

A-C. Confocal image from histological sections of P0 *iMOS*$^{T1\text{-}Myc}$ hearts; showing EYFP (**A**), anti-GFP staining (**B**) and a merged image showing both channels (**C**). Bar, 50 µm. Filled arrowhead points to smooth muscle layer contribution to coronaries. Empty arrowhead points to a ECFP EPDC.

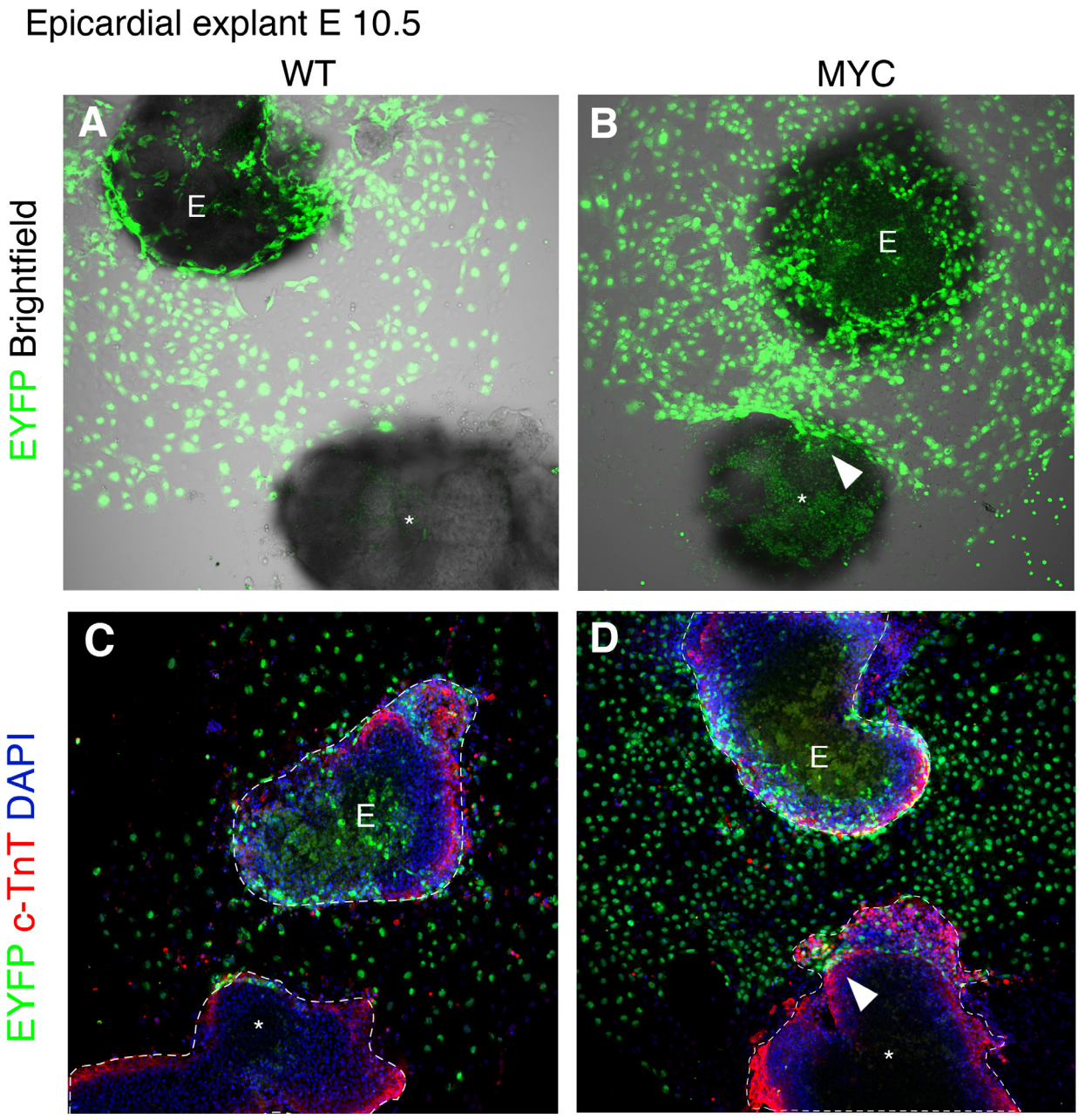

Figure 31. Coculture assays show enhanced invasiveness in *iMOS$^{T1\text{-}Myc}$; Wt1-Cre* epicardium

A. Coculture from *iMOS^{WT}* (WT) (**A**) and *iMOS$^{T1\text{-}Myc}$* (MYC) (**B**) E 10.5 epicardium and a WT E9.0 heart, image showing EYFP and Brightfield. **C.** Maximum intensity projection of a Coculture of *iMOS^{WT}* (WT) E10.5 epicardium and a WT E9.0 heart stained for c-TnT (Z=36 µm). **D.** Coculture of *iMOS$^{T1\text{-}Myc}$* (MYC) E10.5 epicardium and a WT E9.0 heart stained for c-TnT (Z=36 µm). Dashed lines mark the outline of both explants, where (*) marks the WT heart and (E) is the epicardial explant. Filled arrowhead shows invading EYFP-Myc epicardial cells.

(figure 31 B), intermingling with the cardiomyocytes and showing a mesenchymal morphology (figure 31 C-C').

Contribution of *Wt1-Cre* lineage to cardiomyocytes in the VFW can not be explained by expansion of interventricular septum cardiomyocytes or transdifferentiation from blood or endocardial cells.

We then addressed the source of the newly found contribution of *Wt1-Cre* lineage to the cardiomyocyte fraction. Since *Wt1-Cre* is also reported to give rise to cardiomyocytes scattered in the IVS (Wessels et al., 2012), we addressed whether these cardiomyocytes could be expanding by cell competition.

Since there is no Cre line available that allows for a specific recombination in the IVS, we took advantage of *Mef2C-AHF-Cre* (Verzi et al., 2005), that recombines the anterior part of the second heart field, labelling cardiomyocytes in the right ventricle and in the vast majority of the interventricular septum, excluding the left outermost region.

We found that in *iMOS*$^{T1\text{-}Myc}$ mosaics, even though the majority of the IVS cardiomyocytes overexpress Myc, there is no colonization of the LV; indicating Myc overexpression is unable to induce cardiomyocytes colonization of remote regions (figure 32 A, B).

Wt1-Cre has also been shown to recombine cells from the endocardial/endothelial lineage, as well as haematopoietic progenitors (Alberta et al., 2003).

To study whether either of these cell types could be transdifferentiating upon Myc overexpression and giving rise to cardiomyocytes, we took advantage of the *Tie2-Cre* mouse line that recombines both endocardial/endothelial lineage and haematopoietic progenitors. *iMOS*$^{T1\text{-}Myc}$ activation in blood and endothelium didn't show any contribution to cardiomyocytes in the E14.5 embryonic heart (figure 32 C, C'), indicating that Myc overexpression in the *Tie2-Cre* lineage is unable to induce transdifferentiation to cardiomyocytes.

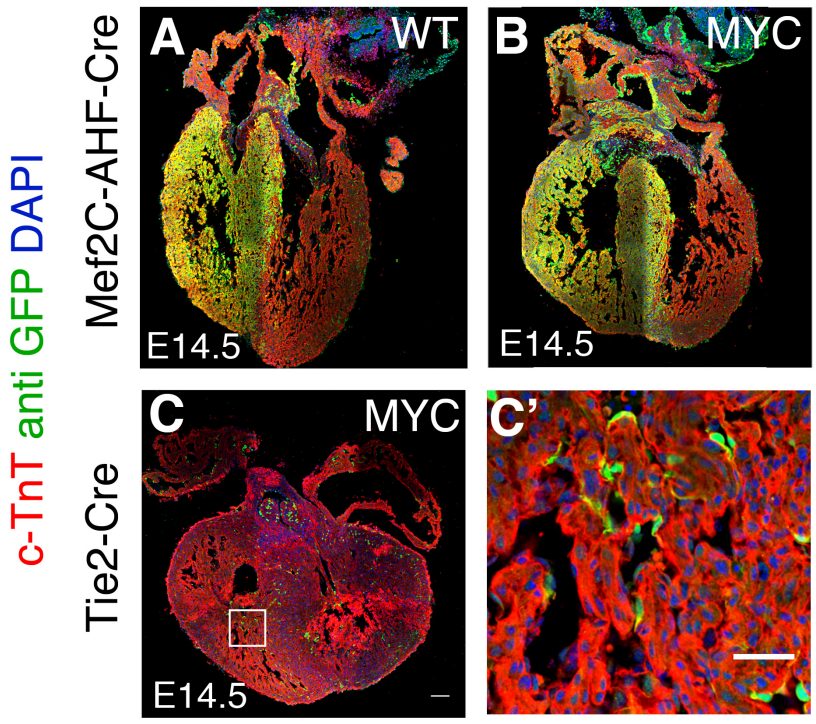

Figure 32. Myc expression does not induce differentiation to cardiomyocytes from IVS region or endocardial/endothelial lineage

A, B. Confocal images from histological sections of *iMOS*^{WT} (WT) (**A**) and *iMOS*$^{T1\text{-}Myc}$ (MYC) (**B**) mosaic hearts at E14.5 recombined with *Mef2C-AHF-Cre*. **C, C'** Confocal images from histological sections of *iMOS*$^{T1\text{-}Myc}$ (MYC) E14.5 heart induced with *Tie2-Cre*. **C'** shows a magnification from the boxed area in C. Bar, 100 µm in A,B,C and 50 in C'.

Ex-vivo epicardial assays do not show a differentiation of the epicardium to cardiomyocytes

We then decided to address if Myc overexpression was able drive the epicardial cells towards the cardiomyocyte lineage in an epicardial explant culture system.

We performed explant assays from *iMOS*^{WT} and *iMOS*$^{T1\text{-}Myc}$ mosaics at E10.5. After 6 days of culture, *iMOS*^{WT} and *iMOS*$^{T1\text{-}Myc}$ explants showed an epicardial layer of cells typically cobble-stone shaped with some differentiation to mesenchymal cells mostly at the edges of the culture (figure 33 A-B').

However, we were unable to detect cardiomyocytes by c-TnT staining or beating after scoring around 30.000 cells from different explants. Moreover, in the previously mentioned co-explant assays, invading epicardial cells from *iMOS*$^{T1\text{-}Myc}$ didn't show myocardial differentiation (figure 29 C,C').

It has been reported that proepicardial explants (Garriock et al., 2014) spontaneously give rise to cardiomyocytes, so we decided to assess if Myc overexpression could promote cardiomyocyte differentiation from proepicardium.

We performed proepicardial explants from E9.0 hearts of *iMOS*^{WT} and *iMOS*$^{T1\text{-}Myc}$ and after 24 hours beating cells could be scored. We detected contribution to beating cells from *Wt1-Cre* lineage in *iMOS*^{WT} explants but we couldn't detect any increase in the contribution to cardiomyocytes upon Myc overexpression.

These results show that assays do not support a role of Myc in driving the cardiomyocyte fate from epicardial cells.

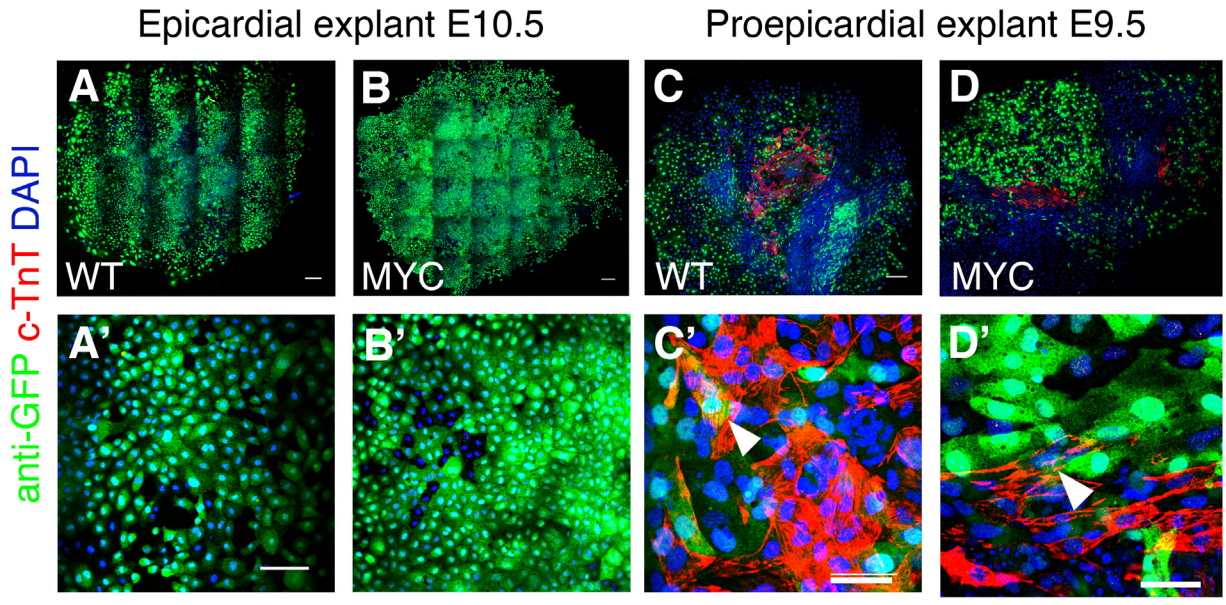

Figure 33. Proepicardium explants give rise to cardiomyocytes spontaneously as opposed to epicardial explants regardless of Myc expression

A-B' Proepicardial explants performed at E10.5 after 6 days in culture from *iMOS*^{WT} (WT) (A) and *iMOS*$^{T1\text{-}Myc}$ (MYC) (B). Bar 200µm A' and B' show magnification of cultures shown in A and B where cells display a typical "cobble-stone" morphology. Bar 100µm. **C-D'** Proepicardial explants cultured for 48h from *iMOS*^{WT} (WT) (**C**) and i*MOS*$^{T1\text{-}Myc}$ (MYC) (**D**) where big clusters of beating cells were detected to be positive for cadiac TnT stainig. Bar 200µm C' and **D'** show a magnified area from **C** and **D** where EYFP+ cardiomyocytes are detected. Bar 50µm.

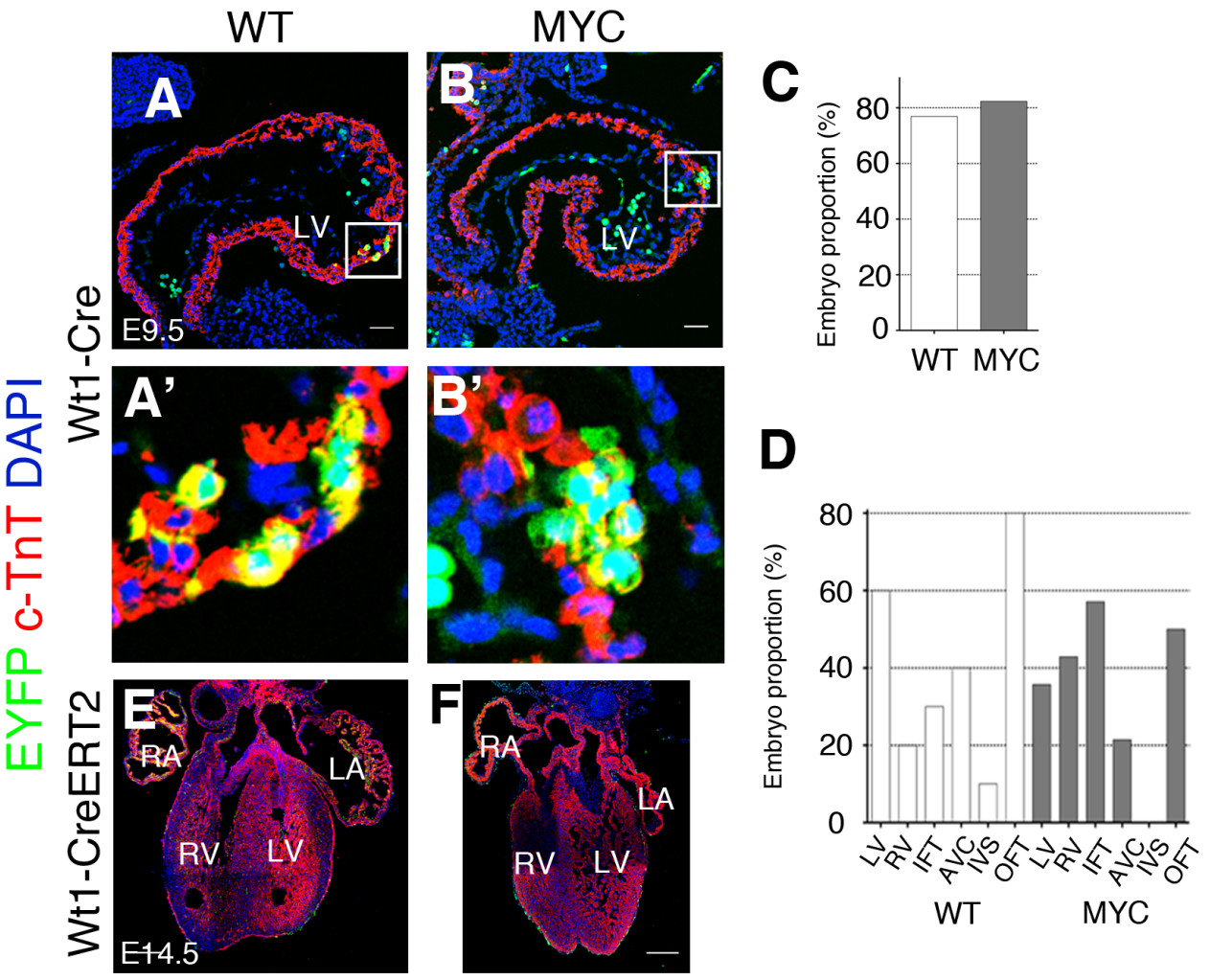

RESULTS

Contribution of Wt1 lineage to cardiomyocytes upon Myc overexpression takes place before establishment of the epicardial layer

To pin down the origin of cardiomyocytes from *Wt1-Cre* lineage, we decided to explore the origin of *Wt1-Cre* lineage derived cardiomyocytes in earlier developmental stages.

We analysed the contribution to cardiomyocytes in stages ranging from E9 to E9.5. Surprisingly, we found a small contribution to cardiomyocytes in both *iMOS*^{WT} and *iMOS*$^{T1\text{-}Myc}$ at a similar proportion (around 75% of the embryos); at various locations of the embryonic hearts, with no reproducible pattern (figure 34 A-D).

These observations suggest that the contribution of the *Wt1-Cre* lineage to cardiomyocytes upon Myc overexpression takes place before establishment of the epicardial layer

We then decided to directly test the contribution of the epicardial layer to the cardiomyocyte population at later stages, which would avoid the confounding effect of the early contribution of the *Wt1-Cre* lineage. For this, we used again a *Wt1* driver but this time controlling a tamoxifen-inducible Cre.

We induced recombination injecting between E9-E9.5 and we found that even with the highest tolerable tamoxifen dose, although we detected recombination in the epicardium at E14.5, we were unable to detect any recombined cardiomyocyte (figure 34 E-F).

Taken together, these results indicate that in most likelihood, Myc overexpression in the epicardial layer does not drive epicardium or EPDC differentiation towards the cardiomyo-

Figure 34. Cardiomyocyte contribution of Wt1 lineage appears previous to epicardial colonization

A-B'. Confocal images of histological sections from E9.5 hearts *iMOS^{WT}* (WT) (**A**) and *iMOS$^{T1\text{-}Myc}$* (MYC) (**B**) stained for c-TnT. **A'** and **B'** show magnification of boxed areas in **A** and **B**. **C.** Graph showing the proportion of embryos showing *Wt1* lineage contribution to cardiomyocytes in *iMOS^{WT}* (WT) and *iMOS$^{T1\text{-}Myc}$* at stage E9.5. **D.** Graph showing the distribution of *Wt1* contribution to different areas of the heart in *iMOS^{WT}* (WT) and i*MOS$^{T1\text{-}Myc}$* (MYC) at stage E9.5. **E,F.** Confocal images of histological sections from E14.5 hearts *iMOS^{WT}* (WT) (**E**) and *iMOS$^{T1\text{-}Myc}$* (MYC) (**F**);*Wt1-Cre ERT2*.
Bar is 50µm in A and B and 100µm in **E** and **F**. RA.Right atrium, RV Right ventricle, LA left atrium, LV left ventricle.

Most likely, it is the contribution of the *Wt1-Cre* lineage to the early cardiomyocyte lineage what explains the presence cardiomyocytes in these experiments.

These cardiomyocytes would then expand by cell competition colonizing large portions of the ventricles. Whether this early contribution of the *Wt1-Cre* lineage reflects an early expression of endogenous *Wt1* in the cardiomyocyte lineage or a failure of the Cre line to recapitulate Wt1 expression at early developmental stages remains to be determined.

DISCUSSION

Something good will come of all things yet
(Jack Kerouac)

In this thesis we have demonstrated the ability of Myc mild overexpression in a mosaic fashion to trigger a response in the heart that eliminates cells with relative lower Myc levels, preserving organ size and function.

Previous studies have pointed to Myc as an inducer of pathological responses in the heart, both during development, when it triggers cardiomyocyte overproliferation and heart hyperplasia (Jackson et al., 1990); and in an adult context, where Myc overexpression induces cell hypertrophy which eventually leads to cardiac failure and death (Xiao et al., 2001).

These studies, however, rely on strong cardiac promoters to drive Myc homogeneous overexpression and thus, cannot be used as a reference for milder Myc overexpressions; such as the one used in this thesis.

Myc overexpression through the *iMOS* system in the heart is mild and has not rendered any pathological effects neither during development; nor in adulthood, at anatomical or functional level. This goes in agreement to what has been previously described for Myc levels through the *Rosa 26* promoter; which do not induce cardiac hypertrophy even with two extra *Myc* alleles.

Upon Myc overexpression in adult hearts we have detected, through differential expression analysis, a pattern that resembles cardiac overload response. The activated pathways (Nppa, HGF), are a consequence of reactivation of fetal programs. This reactivation has been described upon higher demands in cardiac function and is cardioprotective and benign (Kishimoto et al., 2001, Kuhn et al., 2002, Madonna et al., 2012).

HGF in particular has been described not only to play a protective role but also to be implicated in heart regeneration (Madonna et al., 2012). Moreover, a specific hypertrophy-upregulated pathway (EGF), usually present in maladaptative hypertrophic responses (Lee et al., 2011) was downregulted in our experimental context. At the light of the transcriptomic analysis and the lack of pathological effect, neither anatomical nor functional, it is clear that Myc levels used to study cell competition in the heart are within homeostatic values, and do not induce any functional impairment or defect in the developing or adult heart.

Myc overexpression in the developing heart is able to induce cell competition, eliminating those cardiomyocytes with relative lower Myc levels, and it promotes these changes in cell composition without exerting alterations in the function or size of the heart.

The fact that cardiomyocytes are eliminated during heart development goes in agreement with previous studies which have highlighted its enormous plasticity, (Drenckhahn et al., 2008) being able to compensate for defective cell loss during morphogenesis whilst preserving organ size and function and give rise to a phenotypically normal heart. Our results indicate that even WT cells can be eliminated by cell competition when confronted with more active cells. This suggests that the replacement ability observed by Drenckhahn et al. could be boosted by cell competition, although this aspect was not explored in this model.

Moreover, we have shown that this plasticity is different if we induce cell competition in the second heart field population of the heart, suggesting that inducing cell competition at different differentiation stages (in this case, prior to the addition of precursors to the heart tube) (Cai et al., 2003) could have an effect on the replacement of WT cardiomyocytes; although it could also be the case that second heart field progenitors are highly sensitive to heterogeneity in Myc levels *per se* and thus

the competitive response is exacerbated. In the light of these data, and because we had detected Myc endogenous expression also in second heart field precursors, endogenous cell competition could also be taking place in this particular population.

However, rescuing this cell population from death by mosaic p35 overexpression did not result in a cell population with lower Myc levels, suggesting that programmed endogenous cell competition does not take place during cardiac development.

The results obtained with the induced cell competition however show that cardiomyocytes remain sensitive to fitness heterogeneity and do activate cell competition in response to it. These observations suggest cell competition could be used contingently to eliminate accidentally defective cardiomyocytes.

Whereas the mechanisms underlying cell competition remain elusive (not only in mammals but also in *Drosophila*), a common feature is the elimination of "loser" cells by apoptosis (Claveria et al., 2013). This also holds true in heart development induced cell competition, where it has also been shown to rely on short-range signals to be induced; in a similar fashion to what has been described both in mammals (Claveria et al., 2013) and in *Drosophila* (Moreno and Basler, 2004, Moreno et al., 2002).

We have not detected, however, a compensatory overproliferation of winner cells or an increase in their size as a compensatory mechanism to ensure organ size, as it had been reported in *Drosophila* in postmitotic tissues (Tamori and Deng, 2013).

Moreover, these results agree with previously reported effect of Myc overexpression through *Rosa 26* promoter in the heart (Murphy et al., 2008) and the described cell competition in the mammalian epiblast (Claveria et al., 2013). Maintenance of cell numbers and organ size could be due to the fact that cell competition is a rather lo cal phenomenon; since apoptosis is scarce during heart development (Poelmann et al., 2000) and probably because a subtle increase in the proliferation rate of both populations compensates for the loss of wild-type cells; thus preserving organ size and cell number but not being detected through our experimental approach.

Further attempts to gain insight in cell competition mechanisms have been negative; *Flower* elimination did not show any alteration of the Myc-induced competition in the heart, suggesting alternative mechanisms for sensing cellular fitness in mammalian cardiomyocytes must be present.

We have tested competition by confronting cell populations with different doses of overexpressed Myc and endogenous Mycn. Mycn has been previously shown to functionally replace Myc (Malynn et al., 2000) and by depleting *Mycn* we have shown that competition and its intensity depend on the comparison of relative Myc functional doses between neighbouring cardiomyocytes, rather the absolute Myc levels.

Moreover, we have shown that Myc-expressing cardiomyocytes are able to promote a very strong elimination of *Mycn* KO cardiomyocytes from the developing heart, rescuing the otherwise embryonic lethal phenotype of *Mycn* mutants (Harmelink et al., 2013).

Elimination of *Mycn* KO cardiomyocytes, however, is not due to a cell autonomous deleterious effect of the mutation since it has been shown that *Mycn* deficiency doesn't increase apoptotic rates in cardiomyocytes during development (Harmelink et al., 2013).

Therefore, the strong depletion in *Mycn* KO cells is attributable to an active elimination by cell competition. These results indicate that cell competition underlies the plastic capacity of the developing heart to eliminate flawed

cells and restore myocardial function.

Interestingly, this ability is maintained in adult life, albeit at a lower rate. Despite cardiomyocytes being mostly a postmitotic cell population, cell competition appears to be able to displace the WT population without altering cardiac function. In contrast, in an example of postmitotic cell competition in *Drosophila*, lost cells are replaced by hypertrophy of the winners (Tyler et al., 2007).

In adult heart competition there are, however, notable differences with that observed in the developmental context. Wild-type cardiomyocytes are eliminated by a mechanism prevented by p35 expression, and even though apoptosis wasn't directly detected, a role for autophagy-driven cell death was found.

Autophagy is a catabolic process by lysosomal degradation of cytoplasmic content. Homeostatic autophagy is usually protective and needed to maintain healthy cardiomyocytes, but exacerbated autophagy levels can be deleterious and lead to cell death. In several studies it is autophagy and not apoptosis what leads to cell death in cardiomyocytes (Zhu et al., 2007, Knaapen et al., 2001).

Apoptosis and autophagy pathways have been shown to be tightly linked and their crosstalk has been largely reported (Reviewed in Rubinstein and Kimchi, 2012) and (Jain et al., 2013). Moreover, a master regulator of deleterious autophagy, Beclin1, is inhibited by *Bcl2*-family of antiapoptotic proteins (Pattingre et al., 2005).

The activation of autophagy in loser cells upon cell competition in the adult heart is most likely related to the specific characteristics of adult cardiomyocytes. Since their size is several times bigger than that of macrophages, in order for corpses to be cleared, presumably they need to be downsized, which would be achieved by increasing their autophagy levels. It has been described that autophagy can facilitate events leading to cell death (Qu et al., 2007) and the classic elimination of giant cells of the salivary gland in *Drosophila* involves caspase-dependent autophagic cell death (Martin and Baehrecke, 2004).

Interestingly, the observed replacement of cardiomyocytes in the adult context is relevant to a long-debated question as to whether the heart is able to turn-over its cardiomyocyte population and the putative source of new cardiomyocytes. Since there's an increase in the relative EYFP-Myc cell population and due to experimental design it seems likely that the new cardiomyocytes generate from pre-existing ones. Some authors argue that *Myh6* is expressed in certain postnatal cardiac stem cells (Kwon et al., 2007, Bailey et al., 2009), which could be a confounding factor as of the source of the newly formed

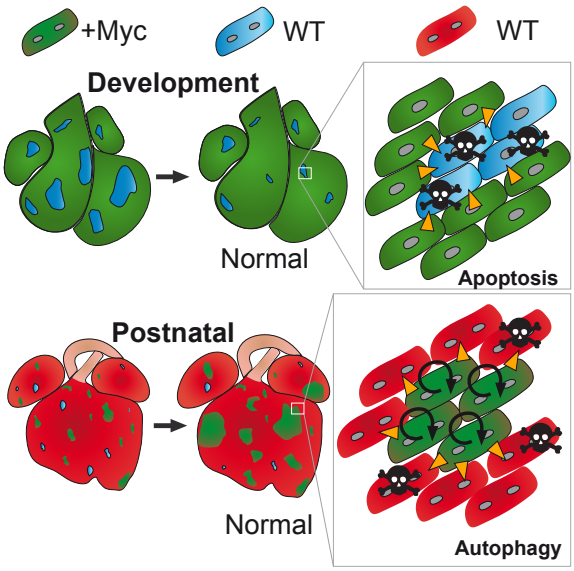

Figure 35. Schematic model on the results obtained in this thesis in cell competition in the developing and adult heart

During development, Myc overexpressing cardiomyocytes expand at the expense of WT, which are eliminated by apoptosis. In the adult heart, Myc overexpressing cardiomyocytes expand and autophagy is induced in WT cardiomyocytes prior to their elimination.

cardiomyocytes. Other studies, however, state the contrary (Ali et al., 2014); so even though this remains a controversial issue, it is highly likely that newly formed EYFP Myc cardiomyocytes arise from pre-existing ones; which would also be in agreement with previous reports on cardiomyocyte turnover (Ali et al., 2014, Senyo et al., 2013, Bergmann et al., 2009, Bersell et al., 2009).

Moreover, there is an increase in the BrDU incorporation in EYFP Myc cardiomyocytes that would support this hypothesis, accounting for the relative increase in this population. (Assuming of course that DNA synthesis results in cytokinesis). In fact, the ratio between mono and multinucleated cardiomyocytes was maintained, suggesting that increased bi-nucleation events were balanced with proliferation of mononucleated cardiomyocytes (Bersell et al., 2009).

This proliferation cannot be attributed to a cell-autonomous effect, since homogeneous overexpression of up to two copies of *Rosa26-MycER* do not lead to cardiomyocyte overproliferation (Murphy et al., 2008), and thus, most likely, corresponds to a mechanism that compensates for the loss of WT cells.

The compensatory nature of this proliferation is supported by the observation that in *iMOS*$^{T1\text{-}Myc/T2\text{-}p35}$ mosaics, heart size and shape is maintained. Therefore, our results suggest that local cell competition and compensatory proliferation balance each other preserving heart size.

Results from differential expression analysis showed activation of fetal programs that are typical hallmarks of cardiac overload and hypertrophy. This activation did not lead to phenotypic or functional cardiac alterations, suggesting they are directly activated by Myc in the absence of any cardiac stress.

Disruption of these pathways has been shown to lead to cardiac pathologies and death (Oliver et al., 1997, Kuhn et al., 2002) and they have been shown to be protective in induced hypertrophy models (Kishimoto et al., 2001).

Overall, these changes can be attributable to an autonomous effect of Myc overexpression and further transcriptomic and proteomic assays must be performed in detail in both winner and loser populations to shed light in mechanisms regulating cell competition.

However, it is still to be explored whether *Myc* mild activation in cardiomyocytes triggers by itself a protective response in hypertrophic or ischemic models.

Epicardium

Given the limited regenerative capacity of the mammalian adult heart, the search for cells that can stimulate cardiac repair is intense, and the epicardium has arisen as a potential source of cardiac progenitors (Wessels and Perez-Pomares, 2004).

The understanding of the full potential of epicardial cells to constitute a source of progenitors with regenerative ability is of key importance. Therefore, the quest to understand the full potential of this population during development has been a focal point in cardiac developmental and regenerative studies.

In this thesis we obtained results apparently pointing to Myc's ability to induce differentiation of epicardial or epicardial-derived cells to the cardiomyocyte lineage. Initial results showed a very strong contribution to the cardiomyocyte lineage, which would be in agreement with previous reports on the potential of epicardial cells to contribute to the developing myocardium (Zhou et al., 2008, Cai et al., 2008).

However, studies of epicardial fate are confusing because of unreliability of the tools used in the fate-mapping experiments (Rudat and Kispert, 2012, Zhou et al., 2008, Zhou and Pu, 2012).

Genetic fate mapping studies strongly rely on Cre expression in the precursor tissue without any leakiness in the target tissue. Regarding *Tbx18-Cre*, for example, contribution of EPDCs to myocardium has been debated (Christoffels et al., 2009) and direct Tbx18 expression in cardiomyocytes has been reported (Zeng et al., 2011). It has been shown that *Wt1-Cre* lines are not completely reliable recapitulating Wt1 expression and suggested not to be useful to assign an epicardial origin of the traced cells (Rudat and Kispert, 2012).

Moreover, use of the inducible *Wt1-CreERT2* line yields a very inefficient recombination and studies on its contribution to the cardiomyocyte pool are also contradictory (Zhou and Pu, 2012, Rudat and Kispert, 2012, Zhou et al., 2008). Despite all of these data regarding the reliability of the tools used; the specific Cre line used for this study has not been reported to label cardiomyocytes (Wessels et al., 2012, Wilm et al., 2005) besides those found sparsely in the IVS. The reason for a putative sporadic Cre activation in cardiomyocytes in this line (*Wt1-CreEGFP*) (Wessels et al., 2012) remains unknown but has also been reported elsewhere (Zhou and Pu, 2012).

Some studies discard the expression of Wt1 in cardiomyocytes during development (Zeng et al., 2011); but only addressed developmental stages from E10.5 onwards. However, expression of Wt1 in cardiomyocytes has been detected at stage E9.5, albeit weak (Rudat and Kispert, 2012), and could underlie our observation.

All of these studies highlight that results obtained using these tools need to be carefully assessed.

In our experiments, despite the initial appearance, we could not relate the contribution of the *Wt1-Cre* lineage to cardiomyocytes to an epicardial origin. Our fate-mapping performed at E14.5 showed a strong contribution to cardiomyocytes upon Myc overexpression, but we have been unable to induce that differentiation in vitro and this observation has not been reproduced inducing temporal conditional epicardial lineage tracing.

Moreover, we have detected the presence of cardiomyocytes from a *Wt1-Cre* lineage prior to the appearance of the epicardium. This contribution was poorly reproducible and not dependent on Myc activation since it was observed equally in $iMOS^{WT}$ and $iMOS^{T1\text{-}Myc}$ mosaics.

The fact that Myc overexpression provokes very efficient and fast competition in early heart precursors and cardiomyocytes and the undetectable differences between Myc and control mosaics as we have detected in Islet1 progenitors, suggests that this contribution of the *Wt1-Cre* lineage to cardiomyocytes is produced from de novo activation in cardiomyocytes shortly before the time of observation (E9-9.5) and does not result from an early recombination in earlier cardiac precursors.

The question on the origin and nature of the cardiomyocytes present at E14.5 and P0 upon Myc overexpression is therefore still unanswered, although it seems that early expression in cardiomyocytes at E9.5 and further expansion of these cardiomyocytes by cell competition is the most likely scenario.

The inability to detect this cardiomyocyte population in the free walls of the ventricles at late stages in the WT mosaics is intriguing.

One possibility is that this early *Wt1-Cre*-labeled cardiomyoytes represents a subset of cardiomyocytes with limited ability to contribute to the definitive myocardium except in the IVS, and upon Myc overexpression are rescued and promoted to contribute to the ventricular free wall through cell competition.

Further studies need to be performed to address this hypothesis and if this is the

case, on the implications of rescuing this subset of cardiomyocytes for development and homeostasis.

CONCLUSIONS

The beauty of things must be that they end
(Jack Kerouac)

Conclusions

1.- Myc mild overexpression in a mosaic fashion induces cell competition in the developing heart, eliminating cells with lower Myc levels.

2.- Elimination of WT cardiomyocytes is a phenotypically silent proces and heart morphology and function are preserved.

3.- Elimination of WT cardiomyocytes relies on short range interactions.

4.- Second heart field progenitors show a strong response to cell competition.

5.- Adult cardiomyocytes compete, eliminating those with relative lower Myc levels in homeostasis.

6.- Cell competition in the adult heart relies on proliferation of “winner cardiomyocytes” at the expense of those with relative lower Myc levels, which activate autophagic pathways prior to their elimination.

7.- Myc mosaic overexpression at moderate levels in the adult heart induces activation of fetal programs typical of a protective response to cardiac overload.

8.- Myc mosaic overexpression in Wt1 lineage induces cell competition in epicardium and epicardial derived lineages.

9.- Wt1-Myc overexpression promotes the contribution of Wt1 lineage to cardiomyocytes in the ventricular free walls, although epicardial contribution to this lineage is discarded.

Conclusiones

1.- La sobreexpresión moderada de Myc en mosaico induce competición celular en el corazón durante la gestación, eliminando aquéllas células con menor nivel relativo de Myc.

2.- La eliminación de los cardiomiocitos salvajes es un proceso fenotípicamente silencioso y la morfologíaa y función del corazón están inalteradas.

3.- La eliminación de los cardiomiocitos salvajes depende de interacciones a corta distacia.

4.- Los progenitores del campo cardiaco secundario tienen una respuesta más acusada a la competición celular.

5.- Los cardiomiocitos adultos también son sensibles a la competición celular inducida, eliminandose aquéllos con menos nivel de Myc.

6.- La competición celular en el corazón adulto depende de la proliferación de los cardiomiocitos “ganadores” a expensas de aquellos con menor nivel relativo de Myc, que activan vías de señalización de autofagia previamente a ser eliminados.

7.- La sobreexpresion moderada de Myc en el corazon adulto induce la activacion de programas de expresión fetales característicos de una respuesta cardioprotectora en respuesta a la sobrecarga cardiaca.

8.- La sobreexpresión de Myc en mosaico en progenitores Wt1 positivos induce competición en el epicardio y linajes derivados.

9.- La sobreexpresión de Myc en mosaico en progenitores Wt1 positivos promueve su contribución a cardiomiocitos de la pared libre del ventrículo, aunque se descarta la contribución directa del epicardio.

BIBLIOGRAPHY

The saddest aspect of life right now is that science gathers knowledge faster than society gathers wisdom
(Isaac Asimov)

A

ADACHI-YAMADA, T. & O'CONNOR, M. B. 2002. Morphogenetic apoptosis: a mechanism for correcting discontinuities in morphogen gradients. Dev Biol, 251, 74-90.

ALBERTA, J. A., SPRINGETT, G. M., RAYBURN, H., NATOLI, T. A., LORING, J., KREIDBERG, J. A. & HOUSMAN, D. 2003. Role of the WT1 tumor suppressor in murine hematopoiesis. Blood, 101, 2570-4.

ALI, S. R., HIPPENMEYER, S., SAADAT, L. V., LUO, L., WEISSMAN, I. L. & ARDEHALI, R. 2014. Existing cardiomyocytes generate cardiomyocytes at a low rate after birth in mice. Proc Natl Acad Sci U S A, 111, 8850-5.

B

BAILEY, B., IZARRA, A., ALVAREZ, R., FISCHER, K. M., COTTAGE, C. T., QUIJADA, P., DIEZ-JUAN, A. & SUSSMAN, M. A. 2009. Cardiac stem cell genetic engineering using the alphaMHC promoter. Regen Med, 4, 823-33.

BAKER, N. E. & LI, W. 2008. Cell competition and its possible relation to cancer. Cancer Res, 68, 5505-7.

BALLESTEROS-ARIAS, L., SAAVEDRA, V. & MORATA, G. Cell competition may function either as tumour-suppressing or as tumour-stimulating factor in Drosophila. Oncogene.

BELLOSTA, P. & GALLANT, P. 2010. Myc Function in Drosophila. Genes Cancer, 1, 542-546.

BERGMANN, O., BHARDWAJ, R. D., BERNARD, S., ZDUNEK, S., BARNABE-HEIDER, F., WALSH, S., ZUPICICH, J., ALKASS, K., BUCHHOLZ, B. A., DRUID, H., JOVINGE, S. & FRISEN, J. 2009. Evidence for cardiomyocyte renewal in humans. Science, 324, 98-102.

BERSELL, K., ARAB, S., HARING, B. & KUHN, B. 2009. Neuregulin1/ErbB4 signaling induces cardiomyocyte proliferation and repair of heart injury. Cell, 138, 257-70.

BONDAR, T. & MEDZHITOV, R. 2010. p53-mediated hematopoietic stem and progenitor cell competition. Cell Stem Cell, 6, 309-22.

BROWER, G. L., GARDNER, J. D., FORMAN, M. F., MURRAY, D. B., VOLOSHENYUK, T., LEVICK, S. P. & JANICKI, J. S. 2006. The relationship between myocardial extracellular matrix remodeling and ventricular function. Eur J Cardiothorac Surg, 30, 604-10.

C

CAI, C. L., LIANG, X., SHI, Y., CHU, P. H., PFAFF, S. L., CHEN, J. & EVANS, S. 2003. Isl1 identifies a cardiac progenitor population that proliferates prior to diffe-

rentiation and contributes a majority of cells to the heart. Dev Cell, 5, 877-89.

CAI, C. L., MARTIN, J. C., SUN, Y., CUI, L., WANG, L., OUYANG, K., YANG, L., BU, L., LIANG, X., ZHANG, X., STALLCUP, W. B., DENTON, C. P., MCCULLOCH, A., CHEN, J. & EVANS, S. M. 2008. A myocardial lineage derives from Tbx18 epicardial cells. Nature, 454, 104-8.

CHEN, C. L., SCHROEDER, M. C., KANGO-SINGH, M., TAO, C. & HALDER, G. 2012. Tumor suppression by cell competition through regulation of the Hippo pathway. Proc Natl Acad Sci U S A, 109, 484-9.

CHEN, T., CHANG, T. C., KANG, J. O., CHOUDHARY, B., MAKITA, T., TRAN, C. M., BURCH, J. B., EID, H. & SUCOV, H. M. 2002. Epicardial induction of fetal cardiomyocyte proliferation via a retinoic acid-inducible trophic factor. Dev Biol, 250, 198-207.

CHONG, J. J., CHANDRAKANTHAN, V., XAYMARDAN, M., ASLI, N. S., LI, J., AHMED, I., HEFFERNAN, C., MENON, M. K., SCARLETT, C. J., RASHIDIANFAR, A., BIBEN, C., ZOELLNER, H., COLVIN, E. K., PIMANDA, J. E., BIANKIN, A. V., ZHOU, B., PU, W. T., PRALL, O. W. & HARVEY, R. P. 2011. Adult cardiac-resident MSC-like stem cells with a proepicardial origin. Cell Stem Cell, 9, 527-40.

CHRISTOFFELS, V. M., GRIESKAMP, T., NORDEN, J., MOMMERSTEEG, M. T., RUDAT, C. & KISPERT, A. 2009. Tbx18 and the fate of epicardial progenitors. Nature, 458, E8-9; discussion E9-10.

CLAVERIA, C., GIOVINAZZO, G., SIERRA, R. & TORRES, M. 2013. Myc-driven endogenous cell competition in the early mammalian embryo. Nature, 500, 39-44.

CRUZ-ADALIA, A., JIMENEZ-BORREGUERO, L. J., RAMIREZ-HUESCA, M., CHICO-CALERO, I., BARREIRO, O., LOPEZ-CONESA, E., FRESNO, M., SANCHEZ-MADRID, F. & MARTIN, P. 2010. CD69 limits the severity of cardiomyopathy after autoimmune myocarditis. Circulation, 122, 1396-404.

D

DAVIS, A. C., WIMS, M., SPOTTS, G. D., HANN, S. R. & BRADLEY, A. 1993. A null c-myc mutation causes lethality before 10.5 days of gestation in homozygotes and reduced fertility in heterozygous female mice. Genes Dev, 7, 671-82.

DE BECO, S., ZIOSI, M. & JOHNSTON, L. A. 2012. New frontiers in cell competition. Dev Dyn, 241, 831-41.

DE BOER, B. A., VAN DEN BERG, G., DE BOER, P. A., MOORMAN, A. F. & RUIJTER, J. M. 2012. Growth of the developing mouse heart: an interactive qualitative and quantitative 3D atlas. Dev Biol, 368, 203-13.

DE LA COVA, C., ABRIL, M., BELLOSTA, P., GALLANT, P. & JOHNSTON, L. A. 2004. Drosophila myc regulates organ size by inducing cell competition. Cell,

117, 107-16.

DE LA COVA, C. & JOHNSTON, L. A. 2006. Myc in model organisms: a view from the flyroom. Semin Cancer Biol, 16, 303-12.

DE LA COVA, C., SENOO-MATSUDA, N., ZIOSI, M., WU, D. C., BELLOSTA, P., QUINZII, C. M. & JOHNSTON, L. A. 2014. Supercompetitor status of Drosophila Myc cells requires p53 as a fitness sensor to reprogram metabolism and promote viability. Cell Metab, 19, 470-83.

DIAZ, B. & MORENO, E. 2005. The competitive nature of cells. Exp Cell Res, 306, 317-22.

DRENCKHAHN, J. D., SCHWARZ, Q. P., GRAY, S., LASKOWSKI, A., KIRIAZIS, H., MING, Z., HARVEY, R. P., DU, X. J., THORBURN, D. R. & COX, T. C. 2008. Compensatory growth of healthy cardiac cells in the presence of diseased cells restores tissue homeostasis during heart development. Dev Cell, 15, 521-33.

DURGAN, J. & PARKER, P. J. 2010. Regulation of the tumour suppressor Fbw7alpha by PKC-dependent phosphorylation and cancer-associated mutations. Biochem J, 432, 77-87.

F

FAGARD, R. H. 1997. Effect of training on left ventricular structure and functioning of the normotensive and the hypertensive subject. Blood Press Monit, 2, 241-245.

FROLDI, F., ZIOSI, M., GAROIA, F., PESSION, A., GRZESCHIK, N. A., BELLOSTA, P., STRAND, D., RICHARDSON, H. E., PESSION, A. & GRIFONI, D. 2010. The lethal giant larvae tumour suppressor mutation requires dMyc oncoprotein to promote clonal malignancy. BMC Biol, 8, 33.

G

GALLANT, P. 2005. Myc, cell competition, and compensatory proliferation. Cancer Res, 65, 6485-7.

GARRIOCK, R. J., MIKAWA, T. & YAMAGUCHI, T. P. 2014. Isolation and culture of mouse proepicardium using serum-free conditions. Methods, 66, 365-9.

GIBSON, M. C. & PERRIMON, N. 2005. Extrusion and death of DPP/BMP-compromised epithelial cells in the developing Drosophila wing. Science, 307, 1785-9

GITTENBERGER-DE GROOT, A. C., VRANCKEN PEETERS, M. P., MENTINK, M. M., GOURDIE, R. G. & POELMANN, R. E. 1998. Epicardium-derived cells contribute a novel population to the myocardial wall and the atrioventricular cushions. Circ Res, 82, 1043-52..

H

HARMELINK, C., PENG, Y., DEBENEDITTIS, P., CHEN, H., SHOU, W. & JIAO, K. 2013. Myocardial Mycn is essential for mouse ventricular wall morphogenesis.

Dev Biol, 373, 53-63.

HAY, B. A., WOLFF, T. & RUBIN, G. M. 1994. Expression of baculovirus P35 prevents cell death in Drosophila. Development, 120, 2121-9.

I

IEMITSU, M., MIYAUCHI, T., MAEDA, S., SAKAI, S., KOBAYASHI, T., FUJII, N., MIYAZAKI, H., MATSUDA, M. & YAMAGUCHI, I. 2001. Physiological and pathological cardiac hypertrophy induce different molecular phenotypes in the rat. Am J Physiol Regul Integr Comp Physiol, 281, R2029-36.

IGAKI, T., PAGLIARINI, R. A. & XU, T. 2006. Loss of cell polarity drives tumor growth and invasion through JNK activation in Drosophila. Curr Biol, 16, 1139-46.

J

JACKSON, T., ALLARD, M. F., SREENAN, C. M., DOSS, L. K., BISHOP, S. P. & SWAIN, J. L. 1990. The c-myc proto-oncogene regulates cardiac development in transgenic mice. Mol Cell Biol, 10, 3709-16.

JAIN, M. V., PACZULLA, A. M., KLONISCH, T., DIMGBA, F. N., RAO, S. B., ROBERG, K., SCHWEIZER, F., LENGERKE, C., DAVOODPOUR, P., PALICHARLA, V. R., MADDIKA, S. & LOS, M. 2013. Interconnections between apoptotic, autophagic and necrotic pathways: implications for cancer therapy development. J Cell Mol Med, 17, 12-29.

K

KAJSTURA, J., GURUSAMY, N., OGOREK, B., GOICHBERG, P., CLAVO-RONDON, C., HOSODA, T., D'AMARIO, D., BARDELLI, S., BELTRAMI, A. P., CESSELLI, D., BUSSANI, R., DEL MONTE, F., QUAINI, F., ROTA, M., BELTRAMI, C. A., BUCHHOLZ, B. A., LERI, A. & ANVERSA, P. 2010. Myocyte turnover in the aging human heart. Circ Res, 107, 1374-86.

KELLY, R. G., BROWN, N. A. & BUCKINGHAM, M. E. 2001. The arterial pole of the mouse heart forms from Fgf10-expressing cells in pharyngeal mesoderm. Dev Cell, 1, 435-40.

KIRBY, M. L. & HUTSON, M. R. 2010. Factors controlling cardiac neural crest cell migration. Cell Adh Migr, 4, 609-21.

KISANUKI, Y. Y., HAMMER, R. E., MIYAZAKI, J., WILLIAMS, S. C., RICHARDSON, J. A. & YANAGISAWA, M. 2001. Tie2-Cre transgenic mice: a new model for endothelial cell-lineage analysis in vivo. Dev Biol, 230, 230-42.

KISHIMOTO, I., ROSSI, K. & GARBERS, D. L. 2001. A genetic model provides evidence that the receptor for atrial natriuretic peptide (guanylyl cyclase-A) inhibits cardiac ventricular myocyte hypertrophy. Proc Natl Acad Sci U S A, 98, 2703-6.

KNAAPEN, M. W., DAVIES, M. J., DE BIE, M., HAVEN, A. J., MARTINET, W. & KOCKX, M. M. 2001. Apoptotic versus autophagic cell death in heart failure. Cardiovasc Res, 51, 304-12.

KNOEPFLER, P. S., CHENG, P. F. & EISENMAN, R. N. 2002. N-myc is essential during neurogenesis for the rapid expansion of progenitor cell populations and the inhibition of neuronal differentiation. Genes Dev, 16, 2699-712.

KUHN, M., HOLTWICK, R., BABA, H. A., PERRIARD, J. C., SCHMITZ, W. & EHLER, E. 2002. Progressive cardiac hypertrophy and dysfunction in atrial natriuretic peptide receptor (GC-A) deficient mice. Heart, 87, 368-74.

KWON, C., ARNOLD, J., HSIAO, E. C., TAKETO, M. M., CONKLIN, B. R. & SRIVASTAVA, D. 2007. Canonical Wnt signaling is a positive regulator of mammalian cardiac progenitors. Proc Natl Acad Sci U S A, 104, 10894-9.

L

LEE, K. S., PARK, J. H., LIM, H. J. & PARK, H. Y. 2011. HB-EGF induces cardiomyocyte hypertrophy via an ERK5-MEF2A-COX2 signaling pathway. Cell Signal, 23, 1100-9.

LI, F., WANG, X., CAPASSO, J. M. & GERDES, A. M. 1996. Rapid transition of cardiac myocytes from hyperplasia to hypertrophy during postnatal development. J Mol Cell Cardiol, 28, 1737-46.

LI, W. & BAKER, N. E. 2007. Engulfment is required for cell competition. Cell, 129, 1215-25.

LIANG, X. H., JACKSON, S., SEAMAN, M., BROWN, K., KEMPKES, B., HIBSHOOSH, H. & LEVINE, B. 1999. Induction of autophagy and inhibition of tumorigenesis by beclin 1. Nature, 402, 672-6.

LOLO, F. N., CASAS TINTO, S. & MORENO, E. 2013. How winner cells cause the demise of loser cells: cell competition causes apoptosis of suboptimal cells: their dregs are removed by hemocytes, thus preserving tissue homeostasis. Bioessays, 35, 348-53.

LOLO, F. N., CASAS-TINTO, S. & MORENO, E. 2012. Cell competition time line: winners kill losers, which are extruded and engulfed by hemocytes. Cell Rep, 2, 526-39.

LOPASCHUK, G. D., USSHER, J. R., FOLMES, C. D., JASWAL, J. S. & STANLEY, W. C. 2010. Myocardial fatty acid metabolism in health and disease. Physiol Rev, 90, 207-58

M

MADONNA, R., CEVIK, C., NASSER, M. & DE CATERINA, R. 2012. Hepatocyte growth factor: molecular biomarker and player in cardioprotection and cardiovascular regeneration. Thromb Haemost, 107, 656-61.

MALYNN, B. A., DE ALBORAN, I. M., O'HAGAN, R. C., BRONSON, R., DAVIDSON, L., DEPINHO, R. A. & ALT, F. W. 2000. N-myc can functionally replace c-myc in murine development, cellular growth, and differentiation. Genes Dev, 14, 1390-9.

MARTIN, D. N. & BAEHRECKE, E. H. 2004. Caspases function in autophagic programmed cell death in Drosophila. Development, 131, 275-84.

MARTIN, F. A., HERRERA, S. C. & MORATA, G. 2009. Cell competition, growth and size control in the Drosophila wing imaginal disc. Development, 136, 3747-56.

MARTINS, V. C., BUSCH, K., JURAEVA, D., BLUM, C., LUDWIG, C., RASCHE, V., LASITSCHKA, F., MASTITSKY, S. E., BRORS, B., HIELSCHER, T., FEHLING, H. J. & RODEWALD, H. R. 2014. Cell competition is a tumour suppressor mechanism in the thymus. Nature, 509, 465-70.

MARUSYK, A., PORTER, C. C., ZABEREZHNYY, V. & DEGREGORI, J. 2010. Irradiation selects for p53-deficient hematopoietic progenitors. PLoS Biol, 8, e1000324.

MCMULLEN, J. R. & JENNINGS, G. L. 2007. Differences between pathological and physiological cardiac hypertrophy: novel therapeutic strategies to treat heart failure. Clin Exp Pharmacol Physiol, 34, 255-62.

MERINO, M. M., RHINER, C., PORTELA, M. & MORENO, E. 2013. "Fitness fingerprints" mediate physiological culling of unwanted neurons in Drosophila. Curr Biol, 23, 1300-9.

MIKAWA, T. & GOURDIE, R. G. 1996. Pericardial mesoderm generates a population of coronary smooth muscle cells migrating into the heart along with ingrowth of the epicardial organ. Dev Biol, 174, 221-32.

MILAN, M. 2002. Survival of the fittest. Cell competition in the Drosophila wing. EMBO Rep, 3, 724-5.

MOENS, C. B., STANTON, B. R., PARADA, L. F. & ROSSANT, J. 1993. Defects in heart and lung development in compound heterozygotes for two different targeted mutations at the N-myc locus. Development, 119, 485-99.

MORATA, G. & RIPOLL, P. 1975. Minutes: mutants of drosophila autonomously affecting cell division rate. Dev Biol, 42, 211-21.

MORENO, E. & BASLER, K. 2004. dMyc transforms cells into super-competitors. Cell, 117, 117-29.

MORENO, E., BASLER, K. & MORATA, G. 2002. Cells compete for decapentaplegic survival factor to prevent apoptosis in Drosophila wing development. Nature, 416, 755-9.

MURPHY, D. J., JUNTTILA, M. R., POUYET, L., KARNEZIS, A., SHCHORS, K., BUI, D. A., BROWN-SWIGART, L.,

JOHNSON, L. & EVAN, G. I. 2008. Distinct thresholds govern Myc's biological output in vivo. Cancer Cell, 14, 447-57.

N

NIEMINEN, A. I., ESKELINEN, V. M., HAIKALA, H. M., TERVONEN, T. A., YAN, Y., PARTANEN, J. I. & KLEFSTROM, J. 2013. Myc-induced AMPK-phospho p53 pathway activates Bak to sensitize mitochondrial apoptosis. Proc Natl Acad Sci U S A, 110, E1839-48.

NORMAN, M., WISNIEWSKA, K. A., LAWRENSON, K., GARCIA-MIRANDA, P., TADA, M., KAJITA, M., MANO, H., ISHIKAWA, S., IKEGAWA, M., SHIMADA, T. & FUJITA, Y. 2012. Loss of Scribble causes cell competition in mammalian cells. J Cell Sci, 125, 59-66.

O

OBERPRILLER, J. O. & OBERPRILLER, J. C. 1974. Response of the adult newt ventricle to injury. J Exp Zool, 187, 249-53.

OERTEL, M., MENTHENA, A., DABEVA, M. D. & SHAFRITZ, D. A. 2006. Cell competition leads to a high level of normal liver reconstitution by transplanted fetal liver stem/progenitor cells. Gastroenterology, 130, 507-20; quiz 590.

OLIVER, E. R., SAUNDERS, T. L., TARLE, S. A. & GLASER, T. 2004. Ribosomal protein L24 defect in belly spot and tail (Bst), a mouse Minute. Development, 131, 3907-20.

OLIVER, P. M., FOX, J. E., KIM, R., ROCKMAN, H. A., KIM, H. S., REDDICK, R. L., PANDEY, K. N., MILGRAM, S. L., SMITHIES, O. & MAEDA, N. 1997. Hypertension, cardiac hypertrophy, and sudden death in mice lacking natriuretic peptide receptor A. Proc Natl Acad Sci U S A, 94, 14730-5.

P

PASUMARTHI, K. B., NAKAJIMA, H., NAKAJIMA, H. O., SOONPAA, M. H. & FIELD, L. J. 2005. Targeted expression of cyclin D2 results in cardiomyocyte DNA synthesis and infarct regression in transgenic mice. Circ Res, 96, 110-8.

PATTINGRE, S., TASSA, A., QU, X., GARUTI, R., LIANG, X. H., MIZUSHIMA, N., PACKER, M., SCHNEIDER, M. D. & LEVINE, B. 2005. Bcl-2 antiapoptotic proteins inhibit Beclin 1-dependent autophagy. Cell, 122, 927-39.

PEREZ-POMARES, J. M., CARMONA, R., GONZALEZ-IRIARTE, M., ATENCIA, G., WESSELS, A. & MUNOZ-CHAPULI, R. 2002. Origin of coronary endothelial cells from epicardial mesothelium in avian embryos. Int J Dev Biol, 46, 1005-13.

PEREZ-POMARES, J. M. & DE LA POMPA, J. L. 2011. Signaling during epicardium and coronary vessel development. Circ Res, 109, 1429-42.

PETROVA, E., LOPEZ-GAY, J. M., RHINER, C. & MORENO, E. 2012. Flower-deficient mice have reduced susceptibility to skin papilloma formation. Dis Model Mech, 5, 553-61.

POELMANN, R. E., MOLIN, D., WISSE, L. J. & GITTENBERGER-DE GROOT, A. C. 2000. Apoptosis in cardiac development. Cell Tissue Res, 301, 43-52.

POSS, K. D., WILSON, L. G. & KEATING, M. T. 2002. Heart regeneration in zebrafish. Science, 298, 2188-90.

Q

QU, X., ZOU, Z., SUN, Q., LUBY-PHELPS, K., CHENG, P., HOGAN, R. N., GILPIN, C. & LEVINE, B. 2007. Autophagy gene-dependent clearance of apoptotic cells during embryonic development. Cell, 128, 931-46.

R

PETROVA, E., LOPEZ-GAY, J. M., RHINER, C. & MORENO, E. 2012. Flower-deficient mice have reduced susceptibility to skin papilloma formation. Dis Model Mech, 5, 553-61.

RAFF, M. C. 1992. Social controls on cell survival and cell death. Nature, 356, 397-400.

RANA, M. S., CHRISTOFFELS, V. M. & MOORMAN, A. F. 2013. A molecular and genetic outline of cardiac morphogenesis. Acta Physiol (Oxf), 207, 588-615.

RAYA, A., KOTH, C. M., BUSCHER, D., KAWAKAMI, Y., ITOH, T., RAYA, R. M., STERNIK, G., TSAI, H. J., RODRIGUEZ-ESTEBAN, C. & IZPISUA-BELMONTE, J. C. 2003. Activation of Notch signaling pathway precedes heart regeneration in zebrafish. Proc Natl Acad Sci U S A, 100 Suppl 1, 11889-95.

RHINER, C., LOPEZ-GAY, J. M., SOLDINI, D., CASAS-TINTO, S., MARTIN, F. A., LOMBARDIA, L. & MORENO, E. 2010. Flower forms an extracellular code that reveals the fitness of a cell to its neighbors in Drosophila. Dev Cell, 18, 985-98.

RHINER, C. & MORENO, E. 2009. Super competition as a possible mechanism to pioneer precancerous fields. Carcinogenesis, 30, 723-8.

ROBINSON, M. D., MCCARTHY, D. J. & SMYTH, G. K. 2010. edgeR: a Bioconductor package for differential expression analysis of digital gene expression data. Bioinformatics, 26, 139-40.

RODRIGUES, A. B., ZORANOVIC, T., AYALA-CAMARGO, A., GREWAL, S., REYES-ROBLES, T., KRASNY, M., WU, D. C., JOHNSTON, L. A. & BACH, E. A. 2012. Activated STAT regulates growth and induces competitive interactions independently of Myc, Yorkie, Wingless and ribosome biogenesis. Development, 139, 4051-61.

RUBINSTEIN, A. D. & KIMCHI, A. 2012. Life in the balance - a mechanistic view of the crosstalk between autophagy and apoptosis. J Cell Sci, 125, 5259-68.

RUDAT, C. & KISPERT, A. 2012. Wt1 and epicardial fate mapping. Circ Res, 111, 165-9.

S

PETROVA, E., LOPEZ-GAY, J. M., RHINER, C. & MORENO, E. 2012. Flower-deficient mice have reduced susceptibility to skin papilloma formation. Dis Model Mech, 5, 553-61.

SAITO, Y., NAKAO, K., ARAI, H., SUGAWARA, A., MORII, N., YAMADA, T., ITOH, H., SHIONO, S., MUKOYAMA, M., OBATA, K. & ET AL. 1987. Atrial natriuretic polypeptide (ANP) in human ventricle. Increased gene expression of ANP in dilated cardiomyopathy. Biochem Biophys Res Commun, 148, 211-7.

SAMSA, L. A., YANG, B. & LIU, J. 2013. Embryonic cardiac chamber maturation: Trabeculation, conduction, and cardiomyocyte proliferation. Am J Med Genet C Semin Med Genet, 163C, 157-68.

SANCHO, M., DI-GREGORIO, A., GEORGE, N., POZZI, S., SANCHEZ, J. M., PERNAUTE, B. & RODRIGUEZ, T. A. 2013. Competitive interactions eliminate unfit embryonic stem cells at the onset of differentiation. Dev Cell, 26, 19-30.

SATOH, M., OGITA, H., TAKESHITA, K., MUKAI, Y., KWIATKOWSKI, D. J. & LIAO, J. K. 2006. Requirement of Rac1 in the development of cardiac hypertrophy. Proc Natl Acad Sci U S A, 103, 7432-7.

SENOO-MATSUDA, N. & JOHNSTON, L. A. 2007. Soluble factors mediate competitive and cooperative interactions between cells expressing different levels of Drosophila Myc. Proc Natl Acad Sci U S A, 104, 18543-8.

SENYO, S. E., STEINHAUSER, M. L., PIZZIMENTI, C. L., YANG, V. K., CAI, L., WANG, M., WU, T. D., GUERQUIN-KERN, J. L., LECHENE, C. P. & LEE, R. T. 2013. Mammalian heart renewal by pre-existing cardiomyocytes. Nature, 493, 433-6.

SHAH, B. H. & CATT, K. J. 2003. A central role of EGF receptor transactivation in angiotensin II -induced cardiac hypertrophy. Trends Pharmacol Sci, 24, 239-44.

SHEN, J. & DAHMANN, C. 2005. Extrusion of cells with inappropriate Dpp signaling from Drosophila wing disc epithelia. Science, 307, 1789-90.

SIMPSON, P. 1979. Parameters of cell competition in the compartments of the wing disc of Drosophila. Dev Biol, 69, 182-93.

SIMPSON, P. & MORATA, G. 1981. Differential mitotic rates and patterns of growth in compartments in the Drosophila wing. Dev Biol, 85, 299-308.

SMART, N., BOLLINI, S., DUBE, K. N., VIEIRA, J. M., ZHOU, B., DAVIDSON, S., YELLON, D., RIEGLER, J., PRICE, A. N., LYTHGOE, M. F., PU, W. T. & RI LEY, P. R. 2011. De novo cardiomyocytes from within the activated adult heart after injury. Nature, 474, 640-4.

SMART, N., RISEBRO, C. A., MELVILLE, A. A., MOSES, K., SCHWARTZ, R. J., CHIEN, K. R. & RILEY, P. R. 2007. Thymosin beta4 induces adult epicardial progenitor mobilization and neovascularization. Nature, 445, 177-82.

SNARR, B. S., KERN, C. B. & WESSELS, A. 2008. Origin and fate of cardiac mesenchyme. Dev Dyn, 237, 2804-19.

SOHAL, D. S., NGHIEM, M., CRACKOWER, M. A., WITT, S. A., KIMBALL, T. R., TYMITZ, K. M., PENNINGER, J. M. & MOLKENTIN, J. D. 2001. Temporally regulated and tissue-specific gene manipulations in the adult and embryonic heart using a tamoxifen-inducible Cre protein. Circ Res, 89, 20-5.

SOONPAA, M. H. & FIELD, L. J. 1994. Assessment of cardiomyocyte DNA synthesis during hypertrophy in adult mice. Am J Physiol, 266, H1439-45.

SOONPAA, M. H. & FIELD, L. J. 1997. Assessment of cardiomyocyte DNA synthesis in normal and injured adult mouse hearts. Am J Physiol, 272, H220-6.

SOONPAA, M. H., KIM, K. K., PAJAK, L., FRANKLIN, M. & FIELD, L. J. 1996. Cardiomyocyte DNA synthesis and binucleation during murine development. Am J Physiol, 271, H2183-9.

STANLEY, E. G., BIBEN, C., ELEFANTY, A., BARNETT, L., KOENTGEN, F., ROBB, L. & HARVEY, R. P. 2002. Efficient Cre-mediated deletion in cardiac progenitor cells conferred by a 3'UTR-ires-Cre allele of the homeobox gene Nkx2-5. Int J Dev Biol, 46, 431-9.

T

TAMORI, Y., BIALUCHA, C. U., TIAN, A. G., KAJITA, M., HUANG, Y. C., NORMAN, M., HARRISON, N., POULTON, J., IVANOVITCH, K., DISCH, L., LIU, T., DENG, W. M. & FUJITA, Y. 2010. Involvement of Lgl and Mahjong/VprBP in cell competition. PLoS Biol, 8, e1000422.

TAMORI, Y. & DENG, W. M. 2013. Tissue repair through cell competition and compensatory cellular hypertrophy in postmitotic epithelia. Dev Cell, 25, 350-63.

TSAI, J. Y., KIENESBERGER, P. C., PULINILKUNNIL, T., SAILORS, M. H., DURGAN, D. J., VILLEGAS-MONTOYA, C., JAHOOR, A., GONZALEZ, R., GARVEY, M. E., BOLAND, B., BLASIER, Z., MCELFRESH, T. A., NANNEGARI, V., CHOW, C. W., HEIRD, W. C., CHANDLER, M. P., DYCK, J. R., BRAY, M. S. & YOUNG, M. E. 2010. Direct regulation of myocardial triglyceride metabolism by the cardiomyocyte circadian clock. J Biol Chem, 285, 2918-29.

TYLER, D. M., LI, W., ZHUO, N., PELLOCK, B. & BAKER, N. E. 2007. Genes affecting cell competition in Drosophila. Genetics, 175, 643-57.

V

VERZI, M. P., MCCULLEY, D. J., DE VAL, S., DODOU, E. & BLACK, B. L. 2005. The right ventricle, outflow tract, and ventricular septum comprise a restricted expression domain within the secondary/anterior heart field. Dev Biol, 287, 134-45.

VINCENT, S. D. & BUCKINGHAM, M. E. 2010. How to make a heart: the origin and regulation of cardiac progenitor cells. Curr Top Dev Biol, 90, 1-41.

W

WESSELS, A. & PEREZ-POMARES, J. M. 2004. The epicardium and epicardially derived cells (EPDCs) as cardiac stem cells. Anat Rec A Discov Mol Cell Evol Biol, 276, 43-57.

WESSELS, A., VAN DEN HOFF, M. J., ADAMO, R. F., PHELPS, A. L., LOCKHART, M. M., SAULS, K., BRIGGS, L. E., NORRIS, R. A., VAN WIJK, B., PEREZ-POMARES, J. M., DETTMAN, R. W. & BURCH, J. B. 2012. Epicardially derived fibroblasts preferentially contribute to the parietal leaflets of the atrioventricular valves in the murine heart. Dev Biol, 366, 111-24.

WILM, B., IPENBERG, A., HASTIE, N. D., BURCH, J. B. & BADER, D. M. 2005. The serosal mesothelium is a major source of smooth muscle cells of the gut vasculature. Development, 132, 5317-28.

X

XIAO, G., MAO, S., BAUMGARTEN, G., SERRANO, J., JORDAN, M. C., ROOS, K. P., FISHBEIN, M. C. & MACLELLAN, W. R. 2001. Inducible activation of c-Myc in adult myocardium in vivo provokes cardiac myocyte hypertrophy and reactivation of DNA synthesis. Circ Res, 89, 1122-9.

Y

YANG, L., CAI, C. L., LIN, L., QYANG, Y., CHUNG, C., MONTEIRO, R. M., MUMMERY, C. L., FISHMAN, G. I., COGEN, A. & EVANS, S. 2006. Isl1Cre reveals a common Bmp pathway in heart and limb development. Development, 133, 1575-85.

Z

ZAFFRAN, S., KELLY, R. G., MEILHAC, S. M., BUCKINGHAM, M. E. & BROWN, N. A. 2004. Right ventricular myocardium derives from the anterior heart field. Circ Res, 95, 261-8.

ZENG, B., REN, X. F., CAO, F., ZHOU, X. Y. & ZHANG, J. 2011. Developmental patterns and characteristics of epicardial cell markers Tbx18 and Wt1 in murine embryonic heart. J Biomed Sci, 18, 67.

ZHOU, B., MA, Q., RAJAGOPAL, S., WU, S. M., DOMIAN, I., RIVERA-FELICIANO, J., JIANG, D., VON GISE, A., IKEDA, S.,

CHIEN, K. R. & PU, W. T. 2008. Epicardial progenitors contribute to the cardiomyocyte lineage in the developing heart. Nature, 454, 109-13.

ZHOU, B. & PU, W. T. 2012. Genetic Cre-loxP assessment of epicardial cell fate using Wt1-driven Cre alleles. Circ Res, 111, e276-80.

ZHU, H., TANNOUS, P., JOHNSTONE, J. L., KONG, Y., SHELTON, J. M., RICHARDSON, J. A., LE, V., LEVINE, B., ROTHERMEL, B. A. & HILL, J. A. 2007. Cardiac autophagy is a maladaptive response to hemodynamic stress. J Clin Invest, 117, 1782-93.

ACKNOLEDGEMENTS

What separates privilege from entitlement is gratitude
(Brené Brown)

ACKNOLEDGEMENTS

APPENDIX

Article

Cell Reports

Cell Competition Promotes Phenotypically Silent Cardiomyocyte Replacement in the Mammalian Heart

Graphical Abstract

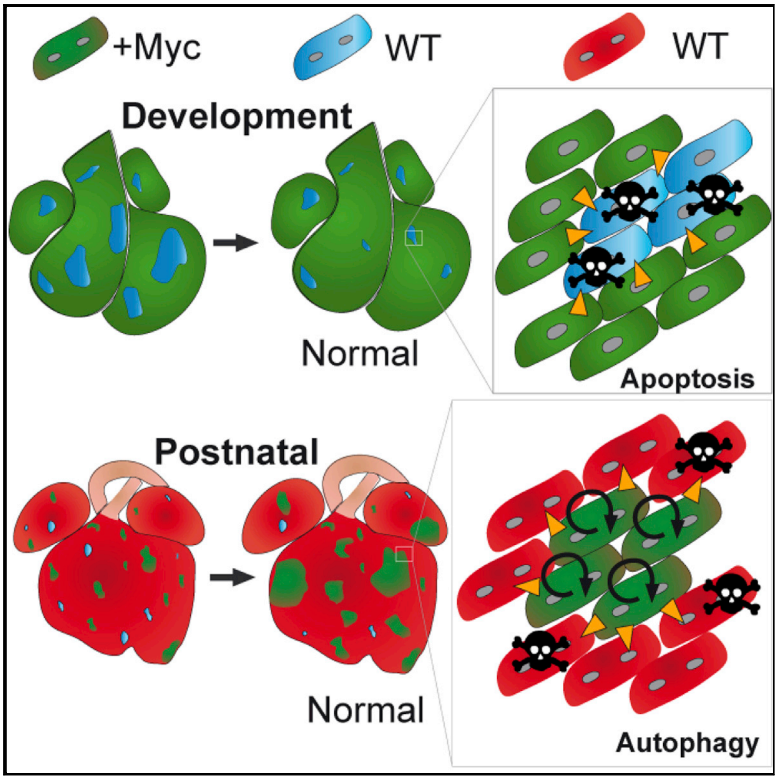

Highlights

Cardiomyocytes are sensitive to Myc-induced competition in development and adult life

Cardiomyocyte competition is driven by short-range interactions leading to cell death

Cardiomyocyte replacement by cell competition is phenotypically silent

Authors

Cristina Villa del Campo, Cristina Clavería, Rocío Sierra, Miguel Torres

Correspondence

mtorres@cnic.es

In Brief

Cardiomyocytes of the mammalian heart are generated during prenatal and early postnatal development and show very low turnover during adult life. Strategies for cardiomyocyte generation and replacement are therefore essential for repairing the diseased heart. Villa del Campo et al. show that mosaic Myc overexpression in cardiomyocytes leads to the phenotypically silent replacement of normal cardiomyocytes by the Myc-overexpressing ones, through a process known as cell competition. This work uncovers a mechanism potentially relevant to cardiac repair.

Accession Numbers

GSE58858

Villa del Campo et al., 2014, Cell Reports 8, 1741–1751
September 25, 2014 ©2014 The Authors
http://dx.doi.org/10.1016/j.celrep.2014.08.005

Cell Reports
Article

Cell Competition Promotes Phenotypically Silent Cardiomyocyte Replacement in the Mammalian Heart

Cristina Villa del Campo,[1] Cristina Clavería,[1] Rocío Sierra,[1] and Miguel Torres[1,*]
[1]Departamento de Desarrollo y Reparación Cardiovascular, Centro Nacional de Investigaciones Cardiovasculares (CNIC), c/ Melchor Fernández Almagro, 3, E-28029 Madrid, Spain
*Correspondence: mtorres@cnic.es
http://dx.doi.org/10.1016/j.celrep.2014.08.005

SUMMARY

Heterogeneous anabolic capacity in cell populations can trigger a phenomenon known as cell competition, through which less active cells are eliminated. Cell competition has been induced experimentally in stem/precursor cell populations in insects and mammals and takes place endogenously in early mouse embryonic cells. Here, we show that cell competition can be efficiently induced in mouse cardiomyocytes by mosaic overexpression of *Myc* during both gestation and adult life. The expansion of the *Myc*-overexpressing cardiomyocyte population is driven by the elimination of wild-type cardiomyocytes. Importantly, this cardiomyocyte replacement is phenotypically silent and does not affect heart anatomy or function. These results show that the capacity for cell competition in mammals is not restricted to stem cell populations and suggest that stimulated cell competition has potential as a cardiomyocyte-replacement strategy.

INTRODUCTION

Cell competition is a mechanism that eliminates suboptimal cells from tissues when "fitter" cells are present (reviewed in Baker, 2011; de Beco et al., 2012; Levayer and Moreno, 2013; Vincent et al., 2013). Cell-to-cell heterogeneity in anabolic capacity led to the first description of cell competition, during *Drosophila* development (Morata and Ripoll, 1975), and is currently the most frequent feature found associated with this phenomenon. The fluctuations in anabolic capacity that trigger cell competition are within a physiological range, and "loser" cells are viable and capable, in the absence of fitter cells, of sustaining tissue growth and performance. Cell competition can thus be envisioned as an optimization mechanism enabling tissues to achieve their best possible cellular composition by favoring the fitter cell population at the expense of less-fit cells. Cell competition can be experimentally induced by generating loser cells through the mosaic reduction of cell anabolism (Morata and Ripoll, 1975) or by generating "winner" cells through the mosaic increase of cell anabolism (supercompetition) (de la Cova et al., 2004; Moreno and Basler, 2004). The conserved cell anabolism regulator Myc is involved in cell growth and proliferation (reviewed in Dang, 2013; Gallant, 2013; Levens, 2013) and plays essential roles in mammalian development (Davis et al., 1993; reviewed in Hurlin, 2013). Moderate increase in Myc levels in a mosaic fashion in *Drosophila* imaginal discs (de la Cova et al., 2004; Moreno and Basler, 2004) and pregastrulation mammalian embryos (Clavería et al., 2013) induces supercompetition, leading to the phenotypically silent replacement of wild-type cells by Myc-overexpressing cells without overt phenotypic consequences. In addition, natural Myc fluctuations trigger cell competition in the mouse epiblast (Clavería et al., 2013), indicating an endogenous role for cell competition in optimization of the pool of precursor cells that generate the embryo. Mosaic Myc overexpression also induces cell supercompetition in embryonic stem cell cultures (Clavería et al., 2013; Sancho et al., 2013), and hematopoietic stem cells have been shown to undergo p53-dependent cell competition (Bondar and Medzhitov, 2010; Marusyk et al., 2010). These observations suggest that the capacity for cell competition might be associated with stemness, but this hypothesis has not been tested. Here, we explored this issue by asking whether cell competition could be induced in one of the first lineages to differentiate in the mammalian embryo, the cardiac lineage.

Cardiac precursors originate early in gastrulation within the anteriormost embryonic mesoderm (reviewed in Vincent and Buckingham, 2010). During mouse gastrulation, cardiac precursors migrate anteriorly and form a cardiac crescent, which by embryonic day 8.0 (E8.0) has folded into a primary tube containing still-proliferative but differentiated and functionally active cardiomyocytes (reviewed in Evans et al., 2010; Rana et al., 2013). A subset of cardiac precursors remain undifferentiated in the second heart field (Kelly et al., 2001) and are progressively added to the heart tube until cardiac chambers and outflow and inflow tracts are definitively laid down around E10. After birth, most cardiomyocytes stop dividing and undergo hypertrophy to establish the mature definitive myocardium (Soonpaa et al., 1996). Here, we show that mosaic Myc overexpression in cardiomyocytes at levels that do not alter heart anatomy or function promote the phenotypically silent replacement of wild-type (WT) cardiomyocytes in the mouse fetal and adult myocardium through cell competition. Our results show the widespread ability of mammalian cells to undergo Myc-driven cell competition and identify cell competition as an efficient mechanism for phenotypically silent substitution of cell populations while preserving organ function.

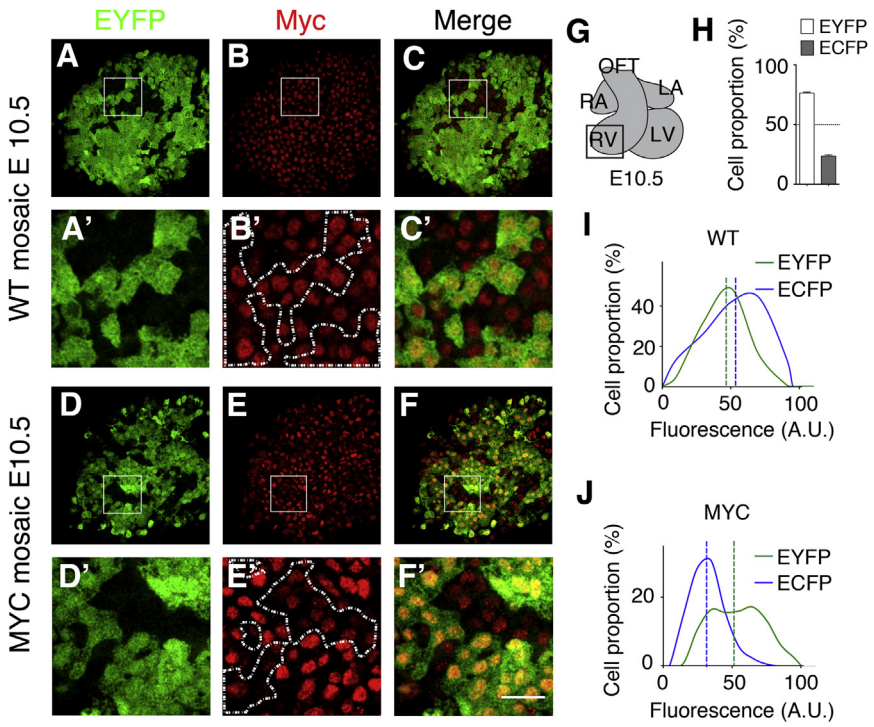

Figure 1. Mosaic Myc Overexpression Driven by Nkx2.5Cre in the Developing Heart

(A–C) Confocal sections showing EYFP$^+$ cardiomyocyte distribution and Myc expression by immunofluorescence in the right ventricle of a whole-mount *Nkx2.5Cre*-recombined *iMOS*^{WT} E10.5 heart (WT), as depicted in (G). (A′)–(C′) show magnified details of the boxed areas in (A)–(C).

(D–F′) Similar data for the *Nkx2.5Cre*-recombined *iMOS*$^{T1\text{-}Myc}$ E10.5 heart (MYC). Scale bar, 50 μm. Dashed lines in (B′) and (E′) outline the frontiers between EYFP$^+$ and EYFP$^-$ cells. ECFP fluorescence is lost upon Myc immunodetection; however, all EYFP$^-$ cells are ECFP$^+$ (see Figure 2).

(G) Schematic representation of an E10.5 heart identifying the area shown in A-F′. OFT, outflow tract; RA, right atrium; LA, left atrium; RV, right ventricle; LV, left ventricle.

(H) Graph showing the proportions observed of EYFP and ECFP cardiomyocytes in *Nkx2.5Cre*-recombined *iMOS*^{WT} E10.5 whole hearts (n = 7). Data are means ± SEM.

(I and J) Distribution of Myc protein levels in the EYFP and ECFP cell populations of *iMOS*^{WT} (I) and *iMOS*$^{T1\text{-}Myc}$ (J) mosaic whole hearts at E10.5; Myc protein levels were quantified from the immunofluorescence images similar to those in (A)–(F′). n = 425 cells in (I) and 449 in (J). Dashed vertical lines indicate the mean for each distribution.

RESULTS

Mosaic *Myc* Overexpression Induces Cardiomyocyte Population Expansion in the Developing Heart

To test the consequences of overexpressing *Myc* in the developing heart, we used the recently established *iMOS* system (Clavería et al., 2013), which allows the Cre-mediated conditional induction of random genetic mosaics. We first generated control random genetic mosaics in cardiac lineages using *Nkx2.5-Cre* (Stanley et al., 2002) to induce the *iMOS*^{WT} transgene, which produces a random mosaic of enhanced yellow fluorescent protein (EYFP) and enhanced cyan fluorescent protein (ECFP) WT cells. Quantitative confocal analysis of *iMOS*^{WT} recombination at E10.5 in *iMOS*^{WT}; *Nkx2.5-Cre* hearts confirmed the mosaic expression pattern of the two reporter proteins in embryonic cardiomyocytes at a reproducible cell population ratio, as previously described (EYFP:ECFP = 3:1) (Figures 1A–1C, 1G, and 1H). Again as described (Stanley et al., 2002), the fluorescent protein distribution pattern indicated *iMOS* activation throughout the embryonic heart (Figures 1A–1C′). We then generated *Nkx2.5-Cre*-induced *iMOS*$^{T1\text{-}Myc}$ mosaics, in which the EYFP cell population moderately overexpresses *Myc* (Clavería et al., 2013) (Figures 1D–1F′). Confocal analysis of EYFP simultaneously with MYC protein immunodetection showed the expected increase in MYC levels in the EYFP cell population of *iMOS*$^{T1\text{-}Myc}$ mosaics, but not *iMOS*^{WT} mosaics (Figures 1I and 1J). We then quantified the contribution of the mosaic cell populations by confocal analysis at different stages of heart development. In the *iMOS*$^{T1\text{-}Myc}$ mosaics we found a progressive reduction in the relative abundance of the ECFP-WT cell population —and a concomitantly increased relative abundance of the EYFP-Myc population— that was not observed in the *iMOS*^{WT} mosaics (Figures 2A–2G). The proportion of ECFP cardiomyocytes at E9.5 in *iMOS*$^{T1\text{-}Myc}$ mosaics was lower (but not significantly) than that observed in *iMOS*^{WT} mosaics. From then on, the relative abundance of the ECFP-WT population in *iMOS*$^{T1\text{-}Myc}$ mosaics showed a progressive decline to 60% of the *iMOS*^{WT} value at E10.5, 40% at E11.5, and 25% at postnatal day 0 (P0) (Figure 2G). The shift in cell populations thus takes place mostly in a narrow time window between E9.5 and E11.5.

Previous studies showed that Myc overexpression in cardiomyocytes during fetal life can lead to pathological cardiac hyperplasia (Jackson et al., 1990). However, in these studies, Myc expression was 20-fold above normal. To determine whether the overexpression levels used here could lead to cardiac hyperplasia we characterized adult heart anatomy and cardiomyocyte size. P0 hearts from *Nkx2.5-Cre*-recombined *iMOS*$^{T1\text{-}Myc}$ and *iMOS*^{WT} mice were of normal size and anatomy (Figures S1A and S1B and data not shown), and cardiomyocytes from the *iMOS*$^{T1\text{-}Myc}$ hearts were of a similar size to those from *iMOS*^{WT} hearts (Figure S1C).

The shift in the cell population proportion observed in *iMOS*^{WT} mosaics thus results from expansion of the EYFP *Myc*-overexpressing cardiomyocyte population and a concomitant reduction of the ECFP WT population relative contribution, without disruption of heart cell composition or anatomy. These results also indicate that the levels of *Myc* overexpression from the *iMOS*$^{T1\text{-}Myc}$ allele are within the limits that allow normal cardiomyocyte development and do not provoke hyperplasia.

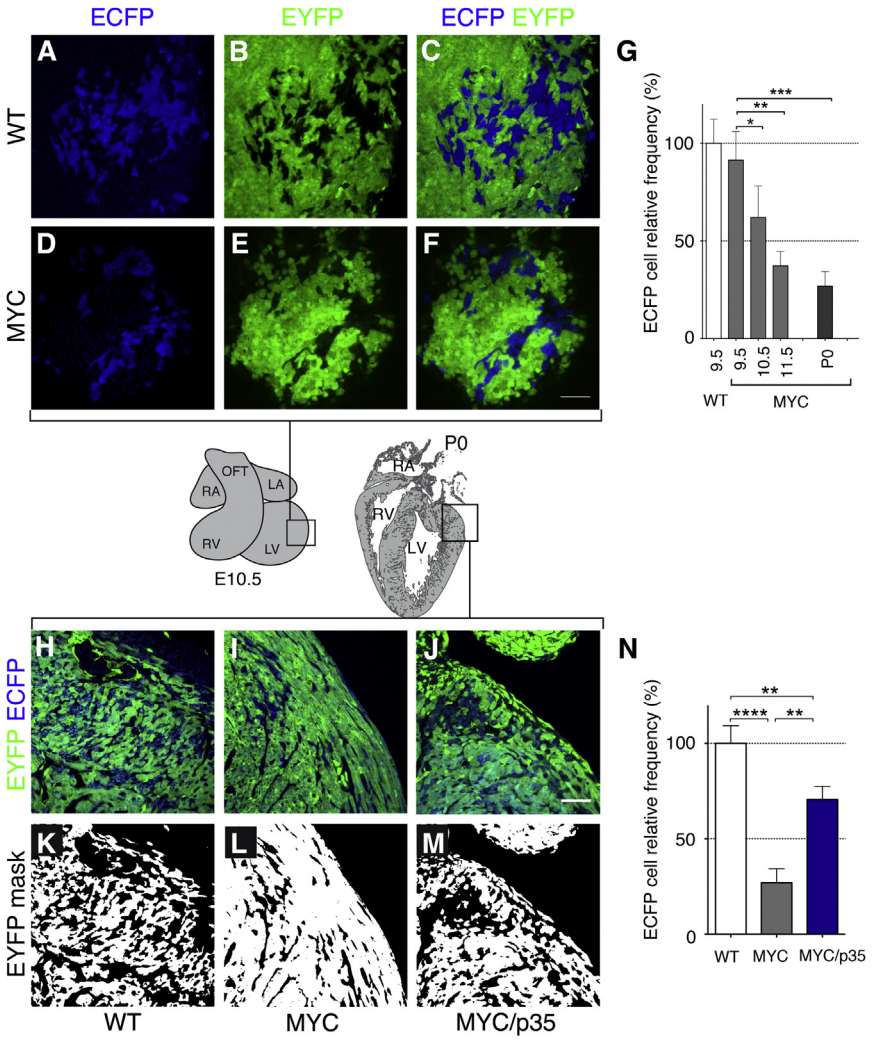

Figure 2. The Myc-Overexpressing Cardiomyocyte Population Expands in the Developing Heart

(A–F) Confocal sections showing EYFP$^+$ and ECFP$^+$ cardiomyocyte distributions in the left ventricle of whole-mount E10.5 hearts from *Nkx2.5Cre*-recombined *iMOS*^{WT} (WT) (A–C) and *iMOS*$^{T1\text{-}Myc}$ (MYC) (D–F) embryos. Scale bar, 50 μm.

(G) Percentage ECFP$^+$ area at different embryonic stages in whole hearts of the *iMOS*$^{T1\text{-}Myc}$ (MYC) mosaics relative to that observed in the *iMOS*^{WT} (WT) mosaics, which was normalized to 100%. Numbers on the x axis indicate the day of embryonic development; P0 indicates postnatal day 0 ($n \geq 5$ embryos).

(H–J) Confocal detection of EYFP$^+$ and ECFP$^+$ cardiomyocyte distributions in histological sections of the left ventricle of P0 hearts from *Nkx2.5Cre*-recombined *iMOS*^{WT} (WT) (H), *iMOS*$^{T1\text{-}Myc}$ (MYC) (I), and *iMOS*$^{T1\text{-}Myc/T2\text{-}p35}$ (MYC/p35) mice. Scale bar, 50 μm.

(K–M) show masks of the EYFP detection in (H) and (I).

(N) Percentage of ECFP$^+$ cells observed at P0 in whole hearts of the *iMOS*$^{T1\text{-}Myc}$ (MYC) and *iMOS*^{WT} (WT) mosaics relative to that observed in the *iMOS*^{WT} (WT) mosaics, which was normalized to 100%.

For ease of comparison, data for ECFP proportion in MYC mosaics at P0 is repeated in (G) and (N). $n \geq 4$). Data in (G) and (N) are means ± SEM; *$p < 0.05$; **$p < 0.01$; ***$p < 0.001$.

Islet-1 Progenitors Are Highly Sensitive to *Myc*-Induced Cell Competition

We next explored the impact of inducing *Myc* mosaicism in Islet1$^+$ cardiac progenitors. For this, we generated *iMOS*$^{T1\text{-}Myc}$ mosaics in second heart field (SHF) progenitors using *Islet1-Cre* (Yang et al., 2006). This Cre driver provides partial interspersed recombination of the SHF cell population, resulting in about 7% EYFP recombined cardiomyocytes in the right ventricle (RV) of *iMOS*^{WT} mosaics (Figures 3A, 3D, 3E, and 3E′). In contrast, the RV of *iMOS* $^{T1\text{-}Myc}$*; Islet1-Cre* hearts on average contained 40% EYFP cardiomyocytes at P0, representing a 5.7-fold expansion during gestation of the original EYFP cardiomyocyte population (Figures 3B, 3D, 3F, and 3F′). In addition, the ECFP cardiomyocyte population in the *Islet-Cre*-induced *iMOS*$^{T1\text{-}Myc}$ mosaic hearts was almost completely eliminated by P0 (Figures 3E′, 3F′, and 3H). These results indicate a more active elimination of the mosaic ECFP-WT cell population and a continued expansion of the *Myc*-overexpressing cardiomyocyte population during fetal life, in a context in which it is continuously confronted with WT cardiomyocytes. We then characterized the temporal progression of ECFP cardiomyocyte depletion in *iMOS*$^{T1\text{-}Myc}$ mosaics, finding that this population was already reduced to 40% of its original contribution by E9.5, with further progressive reduction until the final residual presence at birth (Figures 3I–3L). The enhanced early elimination of WT progenitors in the *Islet-Cre*-induced mosaics indicates that undifferentiated Islet1$^+$ cardiac progenitors are highly sensitive to *Myc* mosaicism.

The *Myc*-Overexpressing Cardiomyocyte Population Expands by Apoptosis-Driven Cell Competition

To study the mechanisms underlying the expansion of the *Myc*-overexpressing cardiomyocyte population during development, we first determined the abundance of PHH3$^+$ cells and bromodeoxyuridine (BrdU) incorporation in *iMOS* mosaics at E10.5, when the shift in the cell population proportion is taking place. Overall, PHH3$^+$ and BrdU$^+$ cell frequencies did not differ significantly between *iMOS*$^{T1\text{-}Myc}$ and *iMOS*^{WT} cardiomyocytes (Figure S2). Moreover, the PHH3$^+$ and BrdU$^+$ cell frequencies in the EYFP cell population of *iMOS*$^{T1\text{-}Myc}$ mosaics was not different from that in the ECFP population (Figures S2D and S2E). These results fit with previous studies showing that the *Myc* dosage induced by a single *Rosa26* allele does not increase proliferation rates in most tissues (Clavería et al., 2013; Murphy

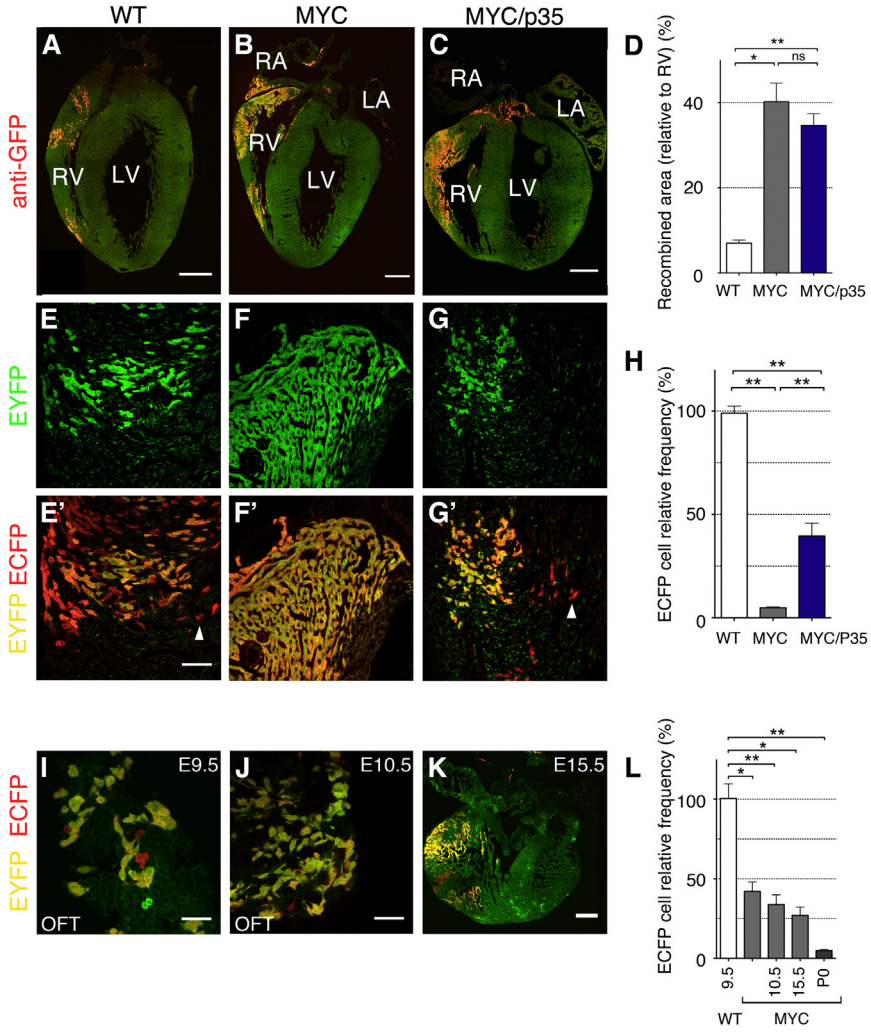

Figure 3. Enhanced Expansion of Myc-Overexpressing Cardiomyocytes upon Mosaic Induction in Islet-1^{+} Progenitors

(A–G′) Confocal detection of EYFP^{+} (A–C), anti-GFP immunofluorescence (detecting both EYFP and ECFP) (E–G) and colocalization of both signals (E′–G′) in histological sections from *Islet1Cre*-recombined *iMOS^{WT}* (WT) (A, E, and E′), *iMOS$^{T1\text{-}Myc}$* (MYC) (B, F, and F′), and *iMOS$^{T1\text{-}Myc/T2\text{-}p35}$* (MYC/p35) newborn mice. In (E′)–(G′), EYFP^{+} cells are yellow because they are positive for both EYFP and anti-GFP, and ECFP^{+} cells are detected in red, as they are only positive for anti-GFP. Scale bar, 100 μm for (A)–(C) and 50 μm for (E′). RA, right atrium; LA, left atrium; RV, right ventricle; LV, left ventricle. (D) Percentage of the RV area positive for anti-GFP immunofluorescence in *Islet1Cre*-recombined *iMOS^{WT}* (WT), *iMOS$^{T1\text{-}Myc}$* (MYC), and *iMOS$^{T1\text{-}Myc/T2\text{-}p35}$* (MYC/p35) newborn mice ($n \geq 4$).

(H) Percentage of ECFP^{+} recombined area with respect to the total EYFP+ECFP-recombined area observed at P0 in the *iMOS$^{T1\text{-}Myc}$* (MYC) and *iMOS$^{T1\text{-}Myc/T2\text{-}p35}$* (MYC/p35) mosaics relative to that observed in the *iMOS^{WT}* (WT) mosaics, which was normalized to 100% ($n \geq 4$).

(I–K) Confocal sections of the E9.5 (I) and E10.5 (J) OFT and the E15.5 RV (K) from *Islet1Cre*-recombined *iMOS$^{T1\text{-}Myc}$* hearts, showing overlays of EYFP and anti-GFP signals. Scale bar, 50 μm for I and J and 100 μm for (K).

(L) Percentage of ECFP^{+} area with respect to the total EYFP+ECFP-recombined area observed at different stages in the *iMOS$^{T1\text{-}Myc}$* (MYC) mosaics relative to that observed in the *iMOS^{WT}* (WT) mosaics, which was normalized to 100%. Numbers on the x axis indicate the day of embryonic development; P0 indicates postnatal day 0 ($n \geq 4$). For ease of comparison, data for ECFP proportion in MYC mosaics at P0 are repeated in (H) and (L). Data in (D), (H), and (L) are means ± SEM. *$p < 0.05$; **$p < 0.01$; ***$p > 0.001$.

et al., 2008) and suggest that the shift in cardiomyocyte populations is not produced by overt differences in cell proliferation between the two cell populations.

To evaluate the role of cell death in the depletion of WT cardiomyocytes, we generated mosaics of the *iMOS$^{T1\text{-}Myc/T2p35}$* strain, which produces a random mosaic of EYFP-*Myc* and ECFP-*p35* cells. p35 is a baculoviral caspase inhibitor able to prevent apoptosis in insects and mammals (Clavería et al., 1998; Hay et al., 1994). Quantitative confocal analysis of P0 hearts from *iMOS$^{T1\text{-}Myc/T2p35}$* mosaics induced with either *Nkx2.5-Cre* or *Islet1-Cre* showed that the p35-expressing ECFP population was substantially, although not completely, protected against elimination (Figures 2H–2N, 3C, and 3G–3H). This result indicates that cell death is a predominant mechanism in the population shift observed in *iMOS$^{T1\text{-}Myc}$* mosaics. However, expansion of the EYFP-Myc cell population did not differ significantly between *Islet1-Cre*-induced *iMOS$^{T1\text{-}Myc/T2p35}$* and *iMOS $^{T1\text{-}Myc}$* mosaics (Figure 3D), indicating that expansion of *Myc*-enriched cardiomyocytes can progress through elimination of nonrecombined WT cardiomyocytes even when small numbers of apoptosis-resistant ECFP-p35 cardiomyocytes are present.

We next scored apoptosis by TUNEL at E10.5 in the *Nkx2.5-Cre*-induced mosaics, concentrating on the outflow tract (OFT) because this region had higher rates of apoptosis in the *iMOS^{WT}* mosaics. The *iMOS$^{T1\text{-}Myc}$* mosaics had a 5-fold higher overall apoptosis rate than *iMOS^{WT}* mosaics (Figures 4A–4C). Furthermore, the apoptosis rate in ECFP-WT cells of the *iMOS$^{T1\text{-}Myc}$* mosaic was markedly higher than observed in the EYFP-*Myc* cells (Figures 4D–4F). Interestingly, the apoptosis rate varied between heart regions: whereas the ECFP/EYFP TUNEL ratio was 4- to 5-fold above baseline in the ventricles, in the OFT it was over 10-fold higher, indicating that ECFP-WT cardiomyocytes in this region are especially sensitive to mosaic *Myc* overexpression.

To study the range limit of the cellular interaction leading to ECFP-WT cardiomyocyte apoptosis in *iMOS$^{T1\text{-}Myc}$* mosaics, we took advantage of the *Islet-Cre* strain. The low-rate, interspersed recombination induced by this line allowed us to score apoptosis separately for WT cardiomyocytes in direct contact

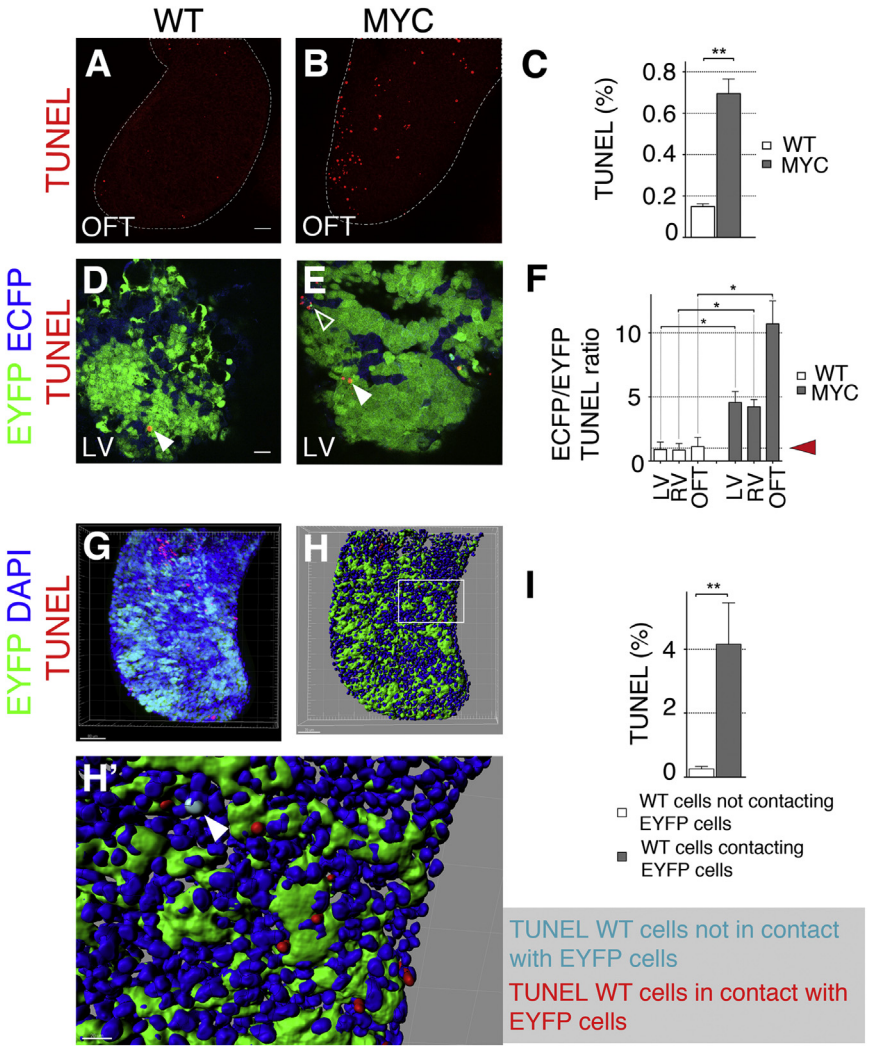

Figure 4. Myc-Overexpressing Cardiomyocytes Expand by Inducing Apoptosis of Neighboring WT Cardiomyocytes

(A and B) Maximal projections of confocal stacks (30 μm deep) from the OFT region of *Nkx2.5Cre*-recombined *iMOS*^{WT} (WT) (A) and *iMOS*$^{T1\text{-}Myc}$ (MYC) (B) whole-mount TUNEL-stained E10.5 hearts. Scale bar, 50 μm.

(C) TUNEL staining frequency in cardiomyocytes from the mosaics shown in (A) and (B) (n = 4 WT and 7 MYC mosaics).

(D and E) Confocal sections from the left ventricle (LV) of *Nkx2.5Cre*-recombined *iMOS*^{WT} (WT) (D) and *iMOS*$^{T1\text{-}Myc}$ (MYC) (E) whole-mount TUNEL-stained E10.5 hearts, showing overlaid EYFP, ECFP, and TUNEL signals. Filled arrowheads point to EYFP^{+} TUNEL^{+} cells and empty arrowheads to ECFP^{+} TUNEL^{+} cells. Scale bar, 50 μm.

(F) ECFP/EYFP TUNEL frequency ratios in different regions of *Nkx2.5Cre*-recombined *iMOS*^{WT} (WT) and *iMOS*$^{T1\text{-}Myc}$ (MYC) whole-mount E10.5 hearts (n = 4 WT and 7 MYC mosaics). LV, left ventricle; RV, right ventricle; OFT, outflow tract. Arrowhead marks the unbiased ECFP/EYFP TUNEL frequency ratio = 1.

(G) Maximal projection of the OFT from an *Islet1-MerCreMer*-recombined *iMOS*$^{T1\text{-}Myc}$ E10.5 heart (MYC), showing overlaid EYFP, DAPI and TUNEL signals. Scale bar, 70 μm.

(H) Computer 3D reconstruction of the stack shown in (G).

(H′) Magnification of the boxed region in (H), showing TUNEL+ WT cells contacting (red) and not contacting (light blue, arrowhead) MYC-overexpressing cells. Scale bar, 20 μm.

(I) TUNEL frequency in WT cells contacting and not contacting EYFP cells in *Islet1MerCreMer*-recombined *iMOS*$^{T1\text{-}Myc}$ E10.5 hearts (MYC) (N = 3 and ≥ 2,815 cells).

Data in (C), (F), and (I) are means ± SEM. *p < 0.05; **p < 0.01; ***p < 0.001.

with EYFP cells and those not in contact (Figures 4G–4H′). Apoptosis was 17-fold more frequent in WT cardiomyocytes in direct contact with *Myc*-overexpressing EYFP cardiomyocytes than in those not contacting EYFP cardiomyocytes (Figure 4I; Movie S1).

These results indicate that the expansion of *Myc*-overexpressing cardiomyocytes requires the elimination of neighboring WT cardiomyocytes through apoptosis triggered by direct cell-cell contact or short-range signaling. Our characterization thus establishes that the replacement of the WT cardiomyocyte population by the Myc-overexpressing population is due to apoptosis-driven cell competition.

Myc Overexpression Induces Cardiomyocyte Population Expansion in the Adult Heart

To determine whether increased *Myc* levels impact cardiomyocyte population homeostasis during adult life, we induced mosaicism in the adult cardiomyocyte population by using the tamoxifen-inducible *αMHC-merCremer* strain (Sohal et al., 2001) (Figure 5A). Mosaics were induced by feeding animals tamoxifen during the first month after weaning, and hearts were analyzed immediately after tamoxifen cessation and at subsequent intervals up to 1 year (Figure 5A). This protocol produced an initial EYFP recombination slightly above 50% (Figure 6D). Previous studies have shown that strong Myc overexpression in cardiomyocytes of adult mice induces cardiomyocyte hypertrophy (Xiao et al., 2001). We thus first analyzed whether hypertrophy also resulted from long-term moderate *Myc* overexpression. Tamoxifen-induced adult *iMOS*$^{T1\text{-}Myc}$ and *iMOS*^{WT} mice showed no spontaneous cardiac malfunction and their hearts were of normal size and anatomy even after 2 months of an intense exercise protocol (Figures 5B–5E). Measurement of average cardiomyocyte 2D size, both in histological sections and in cultures of disaggregated cardiac cells (Figures 5F–5I), showed that cardiomyocytes in *iMOS*$^{T1\text{-}Myc}$ hearts were not only not bigger than those in *iMOS*^{WT} hearts but also in fact slightly smaller (Figure 5J). Due to binucleation, adult cardiomyocytes could contain more that one *EYFP-Myc* copy, and the levels of EYFP are expected to correlate with the *Myc* dose in the *iMOS*$^{T1\text{-}Myc}$ mosaics. Analysis of per-cell cardiomyocyte size and EYFP level showed no

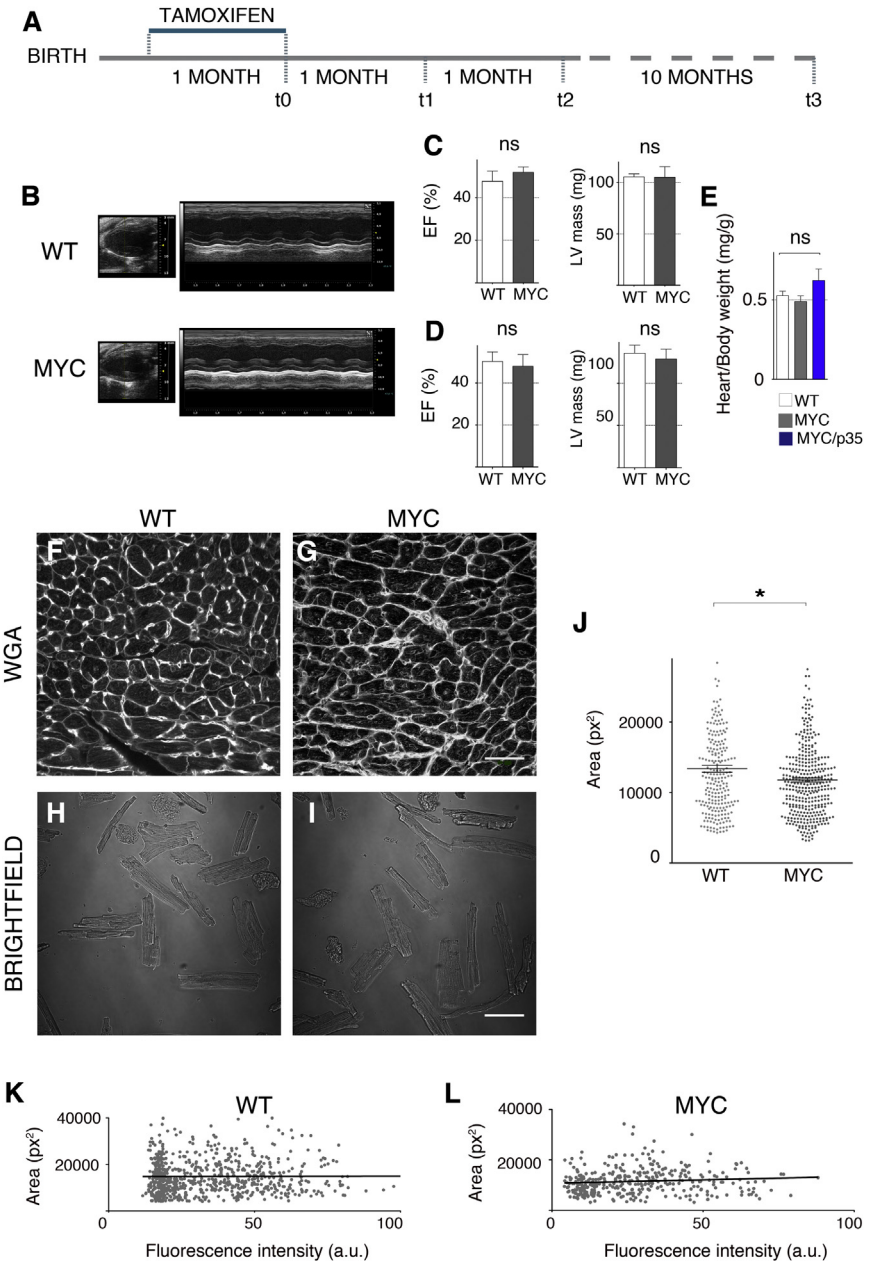

Figure 5. Mosaic MYC Overexpression in Adult Cardiomyocytes Is Phenotypically Silent

(A) αMHCmerCremer-recombined *iMOS*$^{T1\text{-}Myc}$ mosaics and control littermates were treated as schematized for experiments in (B)–(L) and in Figure 6.

(B) Long axis M-mode echocardiography image from an *iMOS*$^{T1\text{-}Myc}$ (MYC) mosaic WT littermate at t2.

(C) Graphs show ejection fraction (EF) and left ventricle (LV) mass from the echocardiographic study in the *iMOS*$^{T1\text{-}Myc}$ mosaics (MYC) and in WT littermates (WT) at t3 ($n \geq 3$).

(D) EF and LV mass at t2 after a protocol of intense exercise from t0 to t2 (see Experimental Procedures).

(E) Heart/body weight ratios in the *iMOS*$^{T1\text{-}Myc}$ mosaics (MYC) and in WT littermates (WT) at t3 ($n \geq 3$).

(F and G) Confocal sections showing wheat germ agglutinin (WGA) staining to highlight cell perimeters in *iMOS*^{WT} (WT) (F) and *iMOS*$^{T1\text{-}Myc}$ (MYC) (G) mosaics at t3. Scale bar, 50 μm.

(H and I) Bright-field confocal section of cardiomyocytes isolated from *iMOS*^{WT} (WT) (H) and *iMOS*$^{T1\text{-}Myc}$ (MYC) (I) mosaic hearts at t3. Scale bar, 50 μm.

(J) Size (2D area) of cardiomyocytes shown in (H) and (I). $n \geq 4$ hearts and 236 cells.*$p < 0.1$; **$p < 0.05$; ***$p < 0.001$. Horizontal bars represent mean values.

(K and L) EYFP fluorescence intensity plotted against cell size for cardiomyocytes isolated from *iMOS*^{WT} (WT) (K) and *iMOS*$^{T1\text{-}Myc}$ (MYC) (L) mosaics. Lines in (K) and (L) represent the regression line ($R^2 = 2.040 \times 10^{-5}$ and 0.007204, respectively).

Data in (C)–(E) are means ± SEM.

correlation between these two parameters in either *iMOS*^{WT} or *iMOS*$^{T1\text{-}Myc}$ mosaic hearts (Figures 5K and 5L). These results show that sustained *Myc* overexpression from the *iMOS*$^{T1\text{-}Myc}$ allele during adult life does not provoke cardiomyocyte hypertrophy. Heart size and heart/body weight ratios were moreover similar in both mosaics, indicating that overall cardiac cellular and organ anatomy are preserved.

We next determined the proportions of cardiomyocyte populations at different times after mosaic induction. While in *iMOS*^{WT} hearts the proportion of EYFP cardiomyocytes was 53% at 1 year of age (Figures 6A and 6D), in the *iMOS*$^{T1\text{-}Myc}$ mosaics, the proportion increased progressively from a frequency similar to that found in *iMOS*^{WT} hearts to 66% at 1 year of age (Figures 6B and 6D). Interestingly, half of this enrichment took place during the first month of observation. Since there were no major changes in heart mass or cardiomyocyte size (Figures 5E and 5J), these observations suggest that *Myc*-overexpressing cardiomyocytes expand at the expense of WT cardiomyocytes during adult life. To directly test this, we determined the relative frequency of ECFP cardiomyocytes with respect to all fluorescent (ECFP+EYFP) cardiomyocytes in 1-year-old *iMOS*$^{T1\text{-}Myc}$ and *iMOS*^{WT} mosaics (Figures 6E–6H). The ECFP cell frequency was ~60% lower in the *iMOS*$^{T1\text{-}Myc}$ mosaics, confirming that the expansion of the Myc-overexpressing cardiomyocyte population is concomitant with a reduction in the WT population. Most adult cardiomyocytes in the mouse are tetraploid and contain two nuclei (Soonpaa et al., 1996); this, together with the partial recombination achieved by tamoxifen treatment, generates heterogeneous levels of *EYFP-Myc* content in cardiomyocytes, with a predicted predominance of cardiomyocytes with one or two active *EYFP-Myc* copies. We therefore refined our study to

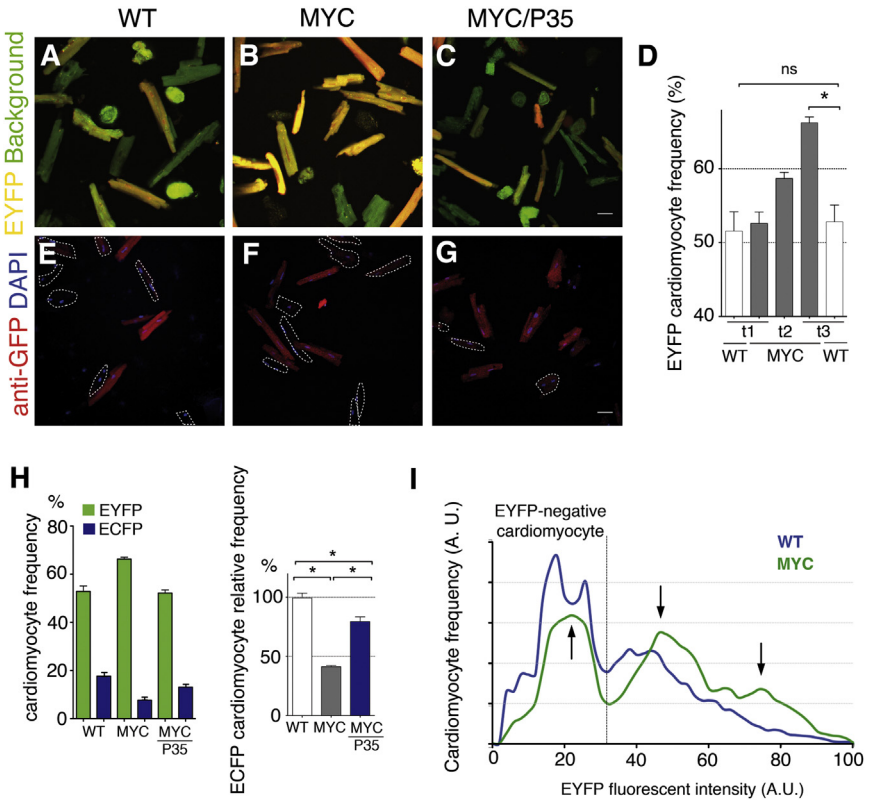

Figure 6. Myc Overexpression Induces Replacement of Adult Cardiomyocytes

(A–C) Confocal images of plated cardiomyocytes isolated at t3 (12 months after tamoxifen administration; see scheme in Figure 5) from *αMHCmerCremer*-recombined *iMOS*^{WT} (WT) (A), *iMOS*$^{T1\text{-}Myc}$ (MYC) (B), and *iMOS*$^{T1\text{-}Myc/T2\text{-}p35}$ (MYC/P35) (C) mosaics, showing native EYFP expression and background autofluorescence.

(D) Percentage of EYFP^{+} cardiomyocytes in cultures obtained from *αMHCmerCremer*-recombined *iMOS*^{WT} (WT) hearts at t1 and t3 and from *iMOS*$^{T1\text{-}Myc}$ (MYC) hearts at t1-t3 ($n \geq 3$ and 300 cells). Data are means ± SEM.

(E–G) Confocal images of plated cardiomyocytes obtained as in (A) –(C), showing anti-GFP immunofluorescence, which identifies EYFP^{+} and ECFP^{+} cardiomyocytes. Scale bar, 50 μm.

(H) Quantification of data represented in (A)–(G) at t3. The graph on the left shows the absolute frequencies of EYFP-Myc and ECFP-WT cardiomyocytes in *iMOS*^{WT} (WT), *iMOS*$^{T1\text{-}Myc}$ (MYC) and *iMOS*$^{T1\text{-}Myc/T2\text{-}p35}$ (MYC/P35) mosaics. In the graph on the right, the same data were expressed as relative ECFP^{+}/EYFP^{+} cardiomyocyte proportions relative to that observed in *iMOS*^{WT} (WT) mosaics, which was normalized to 100%.

(I) Graph represents the frequency of cardiomyocytes according to EYFP intensity in tamoxifen-induced *αMHCmerCremer*-recombined *iMOS*^{WT} (WT) and *iMOS*$^{T1\text{-}Myc}$ (MYC) mosaics, measured in cardiomyocytes isolated at t3, as in (A) –(C). The vertical dotted line marks the limit between background-fluorescent and EYFP-positive cardiomyocytes. Arrows indicate regions in which the frequencies overtly differ between the two mosaics studied. Data in bar graphs are means ± SEM. *$p < 0.05$ **$p < 0.01$ ***$p < 0.001$.

determine whether cardiomyocyte population expansion correlated with *EYFP-Myc* levels. Fluorescence was measured in isolated cardiomyocytes and the frequency of cells according to fluorescence intensity was determined (Figure 6I). This analysis showed that the enrichment in EYFP^{+} cardiomyocytes in *iMOS*$^{T1\text{-}Myc}$ mosaics mostly affects the populations with higher EYFP levels at the expense of EYFP-negative cardiomyocytes, whose frequency decreased (Figure 6I). These observations indicate a correlation between *Myc* dose levels and cardiomyocyte population prevalence in the adult myocardium.

Analysis of the Pathways Involved in Adult Cardiomyocyte Competition

To identify the pathways altered in the *iMOS*$^{T1\text{-}Myc}$ adult mosaic heart, we performed a transcriptomic analysis by RNA sequencing (RNA-seq), comparing 8-week old *iMOS*$^{T1\text{-}Myc}$ and control hearts (Figure S3). Among the genes more significantly up- or downregulated in *iMOS*$^{T1\text{-}Myc}$ hearts, there is a strong representation of genes involved in the response to cardiac overload, in cell growth/division, in energy metabolism, and in apoptosis (Figure S3A). Gene set enrichment analysis on all genes present in the RNA-seq experiment again detected the protective response to cardiac overload in *iMOS*$^{T1\text{-}Myc}$ hearts, including the activation of the atrial natriuretic peptide and fetal cardiomyocyte programs (Kishimoto et al., 2001; Kuhn et al., 2002) and the hepatocyte growth factor (HGF)/Rho/tissue remodeling pathways (Madonna et al., 2012). In contrast, the epidermal growth factor (EGF) pathway, involved in the development of pathological hypertrophy (Shah and Catt, 2003), was found repressed in *iMOS*$^{T1\text{-}Myc}$ hearts. Regarding metabolic processes, activation of the ribosome biosynthesis, a typical response to Myc overexpression, was also detected. In parallel, activation of the lysosomal pathway was as well present, indicating that metabolic activity was globally increased including both anabolic and catabolic processes. With regard to the metabolic processes, *iMOS*$^{T1\text{-}Myc}$ hearts showed a reduction in lipid catabolism and in assembly of the peroxisome, the main organelle for lipid catabolism, suggesting a modification in the fuel usage by Myc-overexpressing cardiomyocytes. A remarkable alteration was found in various regulators of the circadian rhythm; *Dbp* and *Per1*, *2*, and *3* were upregulated and *Arntl* (*Bmal1*) was downregulated. Circadian rhythm transcription factors are essential regulators of cardiac metabolism and regulate the balance between lipid and glucose usage in the heart and display a feedback regulation with the oxidative phosphorylation pathway in the heart (Durgan and Young, 2010). A major regulator of cardiac metabolism, AMP-activated protein kinase, has also been described to undergo circadian regulation (Tsai et al., 2010), its regulatory subunit is overexpressed in the *iMOS*$^{T1\text{-}Myc}$ hearts, and it can be activated by Myc overexpression (Nieminen et al., 2013). The results observed are therefore compatible with a modified metabolic status of the *iMOS*$^{T1\text{-}Myc}$

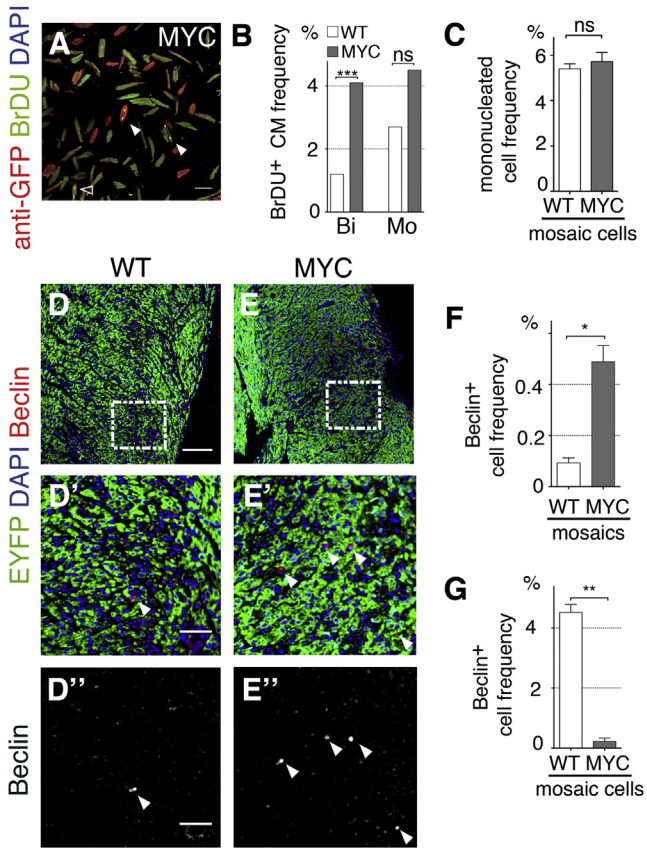

Figure 7. Analysis of Autophagy and BrdU Incorporation in Postnatal Hearts

(A) Confocal image of cardiomyocytes isolated from an *iMOS*$^{T1\text{-}Myc}$ adult heart showing GFP and BrdU staining. Arrowheads show BrdU^{+}/GFP^{+} mononucleated (empty arrowheads) and binucleated (filled arrowheads) cardiomyocytes. Scale bar, 50 μm.

(B) Graph showing the frequency of BrdU^{+} cardiomyocytes in the ECFP-WT (WT) and EYFP-Myc (MYC) populations of the *iMOS*$^{T1\text{-}Myc}$ adult hearts. Bi, binucleated; Mo, mononucleated.

(C) Graph showing the proportion of mononucleated cardiomyocytes within the ECFP-WT (WT) and EYFP-Myc (MYC) populations of the *iMOS*$^{T1\text{-}Myc}$ adult hearts. n = 4 hearts and >300 cells/heart.

(D and E) Confocal sections showing postnatal hearts from *iMOS*^{WT} (WT) (D) and *iMOS*$^{T1\text{-}Myc}$ (MYC) mosaics (E) showing Beclin-1 antibody staining together with iMOS cell populations mapping. Scale bar, 50 μm. (D′ and E′) Higher magnification of boxed areas in (D) and (E). Arrowheads point to Beclin^{+} cells. (D″ and E″) Beclin signal from (D′) and (E′) in isolation. Scale bar, 20 μm.

(F) Total Beclin^{+} cell frequency in *iMOS*^{WT} (WT) and *iMOS*$^{T1\text{-}Myc}$ (MYC) mosaics (n = 3 WT and 5 MYC).

(G) Beclin^{+} cell frequency within the ECFP-WT (ECFP) and EYFP-Myc cell populations (MYC) of the *iMOS*$^{T1\text{-}Myc}$ mosaics.

Graphs in (C), (F), and (G) show means ± SEM. *p < 0.1; **p < 0.05; ***p < 0.001. Statistical analysis in (B) was done using the χ^2 test. ns, not significant.

with either a direct or indirect impact of Myc overexpression on the circadian metabolic regulation. In agreement with this view, the Ingenuity Pathway analysis on the selected up- and downregulated genes (Figure S3B) indicates a modification of the lipid metabolism and a reduction of the oxidative phosphorylation activity in *iMOS*$^{T1\text{-}Myc}$ hearts. The top networks identified by this analysis for the upregulated, downregulated, and joint gene sets are again the networks activated in response to cardiac overload (Figures 3B and 3C). In agreement with these results, we found that the expression of the atrial natriuretic peptide was clearly activated in a patchy pattern in the ventricles of the *iMOS*$^{T1\text{-}Myc}$ mosaic hearts (Figure S3D).

Given the known functions of Myc in cardiomyocytes, the pathways detected likely result from cell-autonomous Myc functions and may relate to the ability of Myc-overexpressing cardiomyocytes to replace the WT cardiomyocyte population. In addition, the gene set enrichment study identified the activation of the apoptosis regulation and inflammation pathways in *iMOS*$^{T1\text{-}Myc}$ hearts, which could be related to the death and removal of WT cardiomyocytes. We therefore used the *iMOS*$^{T1\text{-}Myc/T2p35}$ mosaics to undertake a functional study of the involvement of cell death. This analysis showed that p35 expression largely rescues the ECFP cell population (Figures 6C, 6G, and 6H). These results indicate that adult cardiomyocytes undergo *Myc*-induced cell competition, which progresses by elimination of WT cardiomyocytes and their replacement by cardiomyocytes with high Myc levels. We then analyzed whether increased proliferation of the Myc-overexpressing population is contributing to this phenomenon. We found that BrdU incorporation was 4-fold more frequent in the EYFP-Myc cardiomyocytes than in the WT cardiomyocytes of *iMOS*$^{T1\text{-}Myc}$ mosaic hearts (Figure 7B). This increase did not alter the proportion of mononucleated cardiomyocytes (Figure 7C), suggesting that the balance between mononucleated cardiomyocyte division and binucleation is preserved.

To directly assess the involvement of apoptosis in the cardiomyocyte population shift, we analyzed the TUNEL pattern in adult *iMOS*$^{T1\text{-}Myc}$ mosaics; however, we found no significant differences in TUNEL frequency between the *EYFP-Myc* and *ECFP-WT* cell populations. These results suggested that, unlike the situation during development, apoptosis might not be involved in the elimination of WT cardiomyocytes in adults, despite the activation of apoptotic pathways detected by RNA-seq. We then explored whether alternative cell-death pathways could be operating in postnatal cardiomyocytes. Given that p35, in addition to inhibiting apoptotic cell death, can also inhibit autophagic cell death (Martin and Baehrecke, 2004) and that many apoptosis regulators are also involved in autophagic cell death, we tested whether this pathway could be involved in postnatal cardiomyocyte cell competition. Analysis of the autophagic death-specific marker Beclin (Liang et al., 1999) showed rare positive cells in *iMOS*^{WT} hearts (Figures 7D–7D″); however, the frequency of Beclin-positive cells increased by 5-fold in *iMOS*$^{T1\text{-}Myc}$ mosaic hearts (Figure 7E–7E″ and 7F). Moreover, the frequency of Beclin-positive cells within the *iMOS*$^{T1\text{-}Myc}$ mosaics was 9-fold higher in ECFP-WT cells than in EYFP-Myc cells (Figure 7G). These results indicate that autophagic cell death instead of apoptotic cell death is a major contributor to postnatal cardiomyocyte cell competition.

DISCUSSION

In this study, we demonstrate the ability of moderate Myc overexpression to induce cell competition in the developing and adult mouse heart. Previous studies showed that strong Myc

overexpression during fetal life leads to cardiac hyperplasia due to cardiomyocyte hyperproliferation, while overexpression in adults leads to cardiac hypertrophy due to cardiomyocyte overgrowth (Jackson et al., 1990; Xiao et al., 2001). In contrast, we found that the Myc overexpression levels provided by the endogenous promoter of the *Rosa26* locus do not lead to cardiac hypertrophy or hyperplasia. These results agree with previous evidence of ubiquitous $MycER^{T2}$ expression from the *Rosa26* locus, which did not induce cardiac hypertrophy even when two alleles were present (Murphy et al., 2008). A molecular signature typical of the response to cardiac overload however was activated. The activated pathways (Nppa, HGF) are cardioprotective and stimulate benign adaptation to increased cardiac function demands (Kishimoto et al., 2001; Kuhn et al., 2002; Madonna et al., 2012). In particular, the HGF pathway is not only involved in the cardiac overload response but also stimulates cardiac regeneration (Madonna et al., 2012). The activation of these pathways in the absence of cardiac overload, or in the presence of increased cardiac demand due to intense exercise, did not result in functional impairment. In fact, the EGF pathway, involved in pathological cardiac hypertrophy (Lee et al., 2011), was found inhibited in the Myc mosaic hearts. The Myc levels used here therefore can be considered ''homeostatic'' in the heart, since hearts exposed to these levels stay within normal anatomical and functional parameters. Interestingly, these expression levels provided in a mosaic fashion are enough to trigger cell competition, thereby enabling Myc-high cardiomyocytes to eliminate neighboring WT cardiomyocytes and expand to replace them. These results identify a window in which Myc level fluctuations can affect cardiomyocyte behavior to promote homeostatic changes in myocardial cell composition without affecting organ development and function.

These observations highlight the remarkable ability of fetal cardiomyocyte populations to undergo changes in composition without disrupting cardiac function. Previous studies showed that in mosaic hearts composed of wild-type cardiomyocytes and others carrying a deleterious mutation, the wild-type cardiomyocytes overproliferate during development to compensate for the loss of mutant cardiomyocytes (Drenckhahn et al., 2008). These studies indicate that the fetal heart bears sensing mechanisms that detect the loss of functional cardiomyocytes and promote their replacement. Our present results show that this replacement ability can also be stimulated by cell competition, whereby even undamaged wild-type cardiomyocytes can be eliminated and replaced by more competitive cells, without compromising cardiac homeostasis. Interestingly, this ability is retained during adult life, albeit at a notably slower pace with respect to that observed during development. In *Drosophila*, damaged postmitotic cells in the ovary can be eliminated and compensated for by hypertrophy of the remaining healthy cells (Tamori and Deng, 2013), while in the eye, postmitotic cells become refractory to cell competition (Tyler et al., 2007). Here, we found that, despite the predominant postmitotic nature of adult cardiomyocytes, the loss of the outcompeted population is not compensated by hypertrophy of winner cells but through overproliferation.

The mechanisms by which neighboring cells compare their fitness during cell competition in the mammalian embryo remain unknown, but a common theme of cell competition in the epiblast and the developing heart is the elimination of loser cells by apoptosis. In fact, in the fetal heart, we did not observe overt differences in proliferation between the two mosaic populations. This result is in apparent conflict with the fact that overexpansion of *Islet-Cre*-recombined cardiomyocyte population requires overproliferation and with the fact that the relative reduction of the WT cardiomyocyte population in the *Nkx2.5-Cre*-recombined mosaics requires compensatory proliferation to preserve normal heart size. The 5.7× expansion of the *IsletCre*-recombined population, however, involves only 2.5 extra cell cycles per cell in the 11 days between the activation of the driver at E7.5 and birth. This yields a total of 0.22 extra divisions per cell and day. In the case of the studies with the *Nkx2.5Cre* driver, between E8.5 and E11.5, a 60% reduction in the original 25% WT cardiomyocyte population was observed, which represents a 15% of the total cardiomyocyte population. To replace the 15% missing cardiomyocytes, only 0.15 extra cell divisions/cardiomyocyte would be required during the 3-day observation period. The degree of overproliferation required to explain the changes observed is therefore small and might not be experimentally detectable, especially since PHH3 and BrdU alone might not be enough for a full characterization of the cell proliferation rate cell proliferation.

In adult cardiomyocytes, however, we found a clear increase in the proliferative ability of winner cardiomyocytes, which likely contributes to the replacement of the loser population. While this increased proliferation capacity might be essential for the competitive ability, it is clearly not sufficient, and elimination of the loser population is still a requirement for cell competition in the adult heart. In fact, this overproliferation is most likely only compensatory for the loss of WT cardiomyocytes, since the homogeneous overexpression of two *ROSA26-MycER* copies does not lead to overproliferation in the adult heart (Murphy et al., 2008). The compensatory nature of this overproliferation would also explain the absence of cardiac overgrowth upon Myc mosaic overexpression.

These results suggest that fitness comparison between neighbors and death of the less-fit cells is a common theme in cell competition in very different scenarios. The fact that autophagic instead of apoptotic cell death is observed in adult cardiomyocytes could be more related to the specific features of adult cardiomyocytes than to the cell-competition phenomenon. Dying cells are normally eliminated by macrophages, but the size of an adult cardiomyocyte is about 100 times that of a macrophage, so a phase of self-destructive autophagy might be necessary before they can be eliminated by macrophages in a controlled manner. In fact, the typical example of autophagic death in *Drosophila* involves as well the elimination of giant cells of the salivary gland (Martin and Baehrecke, 2004). These considerations are in agreement with the predominance of TUNEL-negative autophagic cardiomyocyte death reported in heart failure patients (Knaapen et al., 2001).

The fact that cardiomyocytes undergo Myc-induced cell competition suggests that cell competition operates during normal heart development for the elimination of impaired cardiomyocytes unable to meet the anabolic rates demanded in the myocardium. Anabolism-induced cell competition thus appears

as a widespread phenomenon in mammalian tissues and not restricted to stem cell pools like the epiblast. There is an important difference, however, between endogenous cell competition in the epiblast and how it might operate during cardiogenesis: whereas epiblast development is characterized by a strong pattern of cell competition-associated apoptosis, during cardiogenesis, cardiomyocyte death is very infrequent (Poelmann et al., 2000). This suggests that while cell competition would work as a cell quality-control mechanism in both scenarios, in the epiblast it functions as a constitutive program, whereas during cardiogenesis it is used contingently, only if impaired cardiomyocytes appear. Since cardiomyocyte competition ability extends into adult life, it will be very interesting in the future to study whether cell competition is involved in maintaining tissue fitness during aging and whether it can contribute to natural or induced repair of cardiac insults in which cardiomyocytes are lost or impaired.

EXPERIMENTAL PROCEDURES

Mouse Strains

The *iMOS*^{WT}, *iMOS*$^{T1\text{-}Myc}$, and *iMOS*$^{T1\text{-}Myc/T2\text{-}p35}$ mouse lines have been described (Clavería et al., 2013). Here, they were used in combination with different Cre-expressing lines to induce genetic mosaics in the developing and adult mouse heart. Experimental embryos or born mice were generated from crosses of homozygous *iMOS* females with males carrying the different Cre drivers: *Nkx2.5Cre* (Stanley et al., 2002), *Islet1Cre* (Yang et al., 2006), and *αMHCmerCremer* (Sohal et al., 2001). Mice were genotyped by PCR (Clavería et al., 2013). To induce recombination in *iMOS*;*αMHCmerCremer* mice, they were fed for 1 month with pellets containing tamoxifen at 40 g/kg (Teklad ref. TD.07262).

Confocal Microscopy

Whole embryonic hearts or histological sections were imaged with a Nikon A1R confocal microscope using 405, 458, 488, 568, and 633 nm wavelengths and 20×/0.75 dry and 40×/1.30 oil objectives. Areas occupied by EYFP and ECFP cells were quantified using the threshold detection and particle analysis tools in ImageJ (NIH; http://rsb.info.nih.gov/ij). To calculate the relative frequency of ECFP cells, the percentage of ECFP area observed was divided by the average percentage in *iMOS*^{WT} mosaics. All percentages were normalized to a 100% value in the WT mosaic. ECFP was scored either by direct identification of native ECFP fluorescence or by subtracting the area of native EYFP from the anti-GFP staining, which detects both EYFP and ECFP.

Immunofluorescence and TUNEL Assay

Embryos were obtained at different days of gestation and fixed overnight at 4°C in 2% paraformaldehyde in PBS. Hearts were either dissected for whole-mount staining or gelatin embedded and cryosectioned. Adult cardiomyocytes were isolated by Langerdorff perfusion with liberase (Roche Applied Science) and plated for confocal imaging as described previously (García-Prieto et al., 2014). Primary antibodies used were anti-phosphohistone H3 (Ser 10), anti-Myc polyclonal antibody (Millipore), Living colors Rabbit polyclonal anti-GFP antibody (Clontech), Beclin1 (Cell Signaling), and Nppa (Millipore). Immunofluorescence was performed following standard procedures. TUNEL was performed on whole-mount embryonic hearts or sections using terminal deoxynucleotidyl transferase (TdT) and biotin-16-2′-deoxy-uridine-5′-triphosphate (Biotin-16-dUTP) (both from Roche), and developed with various streptavidin fluorescent conjugates (Jackson ImmunoResearch).

Statistical Analysis

To compare average percentages of ECFP cells/area between more than two groups, the Kruskal-Wallis test was used (assuming nonnormal distributions). For comparisons of two groups, a Mann-Whitney test was used. To test the correlation between cell size and EYFP expression, a linear regression model was used. All comparisons were made using Prism statistical analysis software. The significance of BrdU^{+} frequency and mononucleated cardiomyocyte frequency comparisons from adult hearts was analyzed using a proportions test as implemented in R.

ACCESSION NUMBERS

The NCBI Gene Expression Omnibus database accession number for the RNA-seq data reported in this paper is GSE58858.

SUPPLEMENTAL INFORMATION

Supplemental information includes Supplemental Experimental Procedures, three figures, and one movie and can be found with this article online at http://dx.doi.org/10.1016/j.celrep.2014.08.005.

ACKNOWLEDGMENTS

We thank J.L. de la Pompa for comments on the manuscript, V. García for mouse work, E. Arza and A.M. Santos for help with microscopy and 3D reconstruction, J. García-Prieto for help with cardiomyocyte isolation, A.V. Alonso for the echocardiography assays, F. Sánchez-Cabo for statistics, and S. Bartlett for text editing. The CNIC Genomics unit performed the RNA sequencing procedures. This work was supported by grants BFU2012-31086 and RD12/0019/0005 (ISCIII) from the Spanish Ministry of Economy and Competition (MINECO) and grant P2010/BMD-2315 from the Madrid Regional Government. C.V. is supported by a FPI grant from the MINECO. The CNIC is supported by the MINECO and the Pro-CNIC Foundation.

Received: February 5, 2014
Revised: April 21, 2014
Accepted: August 1, 2014
Published: September 4, 2014

REFERENCES

Baker, N.E. (2011). Cell competition. Curr. Biol. *21*, R11–R15.

Bondar, T., and Medzhitov, R. (2010). p53-mediated hematopoietic stem and progenitor cell competition. Cell Stem Cell *6*, 309–322.

Clavería, C., Albar, J.P., Serrano, A., Buesa, J.M., Barbero, J.L., Martínez-A, C., and Torres, M. (1998). Drosophila grim induces apoptosis in mammalian cells. EMBO J. *17*, 7199–7208.

Clavería, C., Giovinazzo, G., Sierra, R., and Torres, M. (2013). Myc-driven endogenous cell competition in the early mammalian embryo. Nature *500*, 39–44.

Dang, C.V. (2013). MYC, metabolism, cell growth, and tumorigenesis. Cold Spring Harb Perspect Med *3*.

Davis, A.C., Wims, M., Spotts, G.D., Hann, S.R., and Bradley, A. (1993). A null c-myc mutation causes lethality before 10.5 days of gestation in homozygotes and reduced fertility in heterozygous female mice. Genes Dev. *7*, 671–682.

de Beco, S., Ziosi, M., and Johnston, L.A. (2012). New frontiers in cell competition. Dev. Dyn. *241*, 831–841.

de la Cova, C., Abril, M., Bellosta, P., Gallant, P., and Johnston, L.A. (2004). Drosophila myc regulates organ size by inducing cell competition. Cell *117*, 107–116.

Drenckhahn, J.D., Schwarz, Q.P., Gray, S., Laskowski, A., Kiriazis, H., Ming, Z., Harvey, R.P., Du, X.J., Thorburn, D.R., and Cox, T.C. (2008). Compensatory growth of healthy cardiac cells in the presence of diseased cells restores tissue homeostasis during heart development. Dev. Cell *15*, 521–533.

Durgan, D.J., and Young, M.E. (2010). The cardiomyocyte circadian clock: emerging roles in health and disease. Circ. Res. *106*, 647–658.

Evans, S.M., Yelon, D., Conlon, F.L., and Kirby, M.L. (2010). Myocardial lineage development. Circ. Res. *107*, 1428–1444.

Gallant, P. (2013). Myc function in Drosophila. Cold Spring Harb Perspect Med *3*, a014324.

García-Prieto, J., García-Ruiz, J.M., Sanz-Rosa, D., Pun, A., García-Alvarez, A., Davidson, S.M., Fernández-Friera, L., Nuno-Ayala, M., Fernández-Jiménez, R., Bernal, J.A., et al. (2014). β3 adrenergic receptor selective stimulation during ischemia/reperfusion improves cardiac function in translational models through inhibition of mPTP opening in cardiomyocytes. Basic Res. Cardiol. *109*, 422.

Hay, B.A., Wolff, T., and Rubin, G.M. (1994). Expression of baculovirus P35 prevents cell death in Drosophila. Development *120*, 2121–2129.

Hurlin, P.J. (2013). Control of vertebrate development by MYC. Cold Spring Harb Perspect Med *3*, a014332.

Jackson, T., Allard, M.F., Sreenan, C.M., Doss, L.K., Bishop, S.P., and Swain, J.L. (1990). The c-myc proto-oncogene regulates cardiac development in transgenic mice. Mol. Cell. Biol. *10*, 3709–3716.

Kelly, R.G., Brown, N.A., and Buckingham, M.E. (2001). The arterial pole of the mouse heart forms from Fgf10-expressing cells in pharyngeal mesoderm. Dev. Cell *1*, 435–440.

Kishimoto, I., Rossi, K., and Garbers, D.L. (2001). A genetic model provides evidence that the receptor for atrial natriuretic peptide (guanylyl cyclase-A) inhibits cardiac ventricular myocyte hypertrophy. Proc. Natl. Acad. Sci. USA *98*, 2703–2706.

Knaapen, M.W., Davies, M.J., De Bie, M., Haven, A.J., Martinet, W., and Kockx, M.M. (2001). Apoptotic versus autophagic cell death in heart failure. Cardiovasc. Res. *51*, 304–312.

Kuhn, M., Holtwick, R., Baba, H.A., Perriard, J.C., Schmitz, W., and Ehler, E. (2002). Progressive cardiac hypertrophy and dysfunction in atrial natriuretic peptide receptor (GC-A) deficient mice. Heart *87*, 368–374.

Lee, K.S., Park, J.H., Lim, H.J., and Park, H.Y. (2011). HB-EGF induces cardiomyocyte hypertrophy via an ERK5-MEF2A-COX2 signaling pathway. Cell. Signal. *23*, 1100–1109.

Levayer, R., and Moreno, E. (2013). Mechanisms of cell competition: themes and variations. J. Cell Biol. *200*, 689–698.

Levens, D. (2013). Cellular MYCro economics: Balancing MYC function with MYC expression. Cold Spring Harb Perspect Med *3*.

Liang, X.H., Jackson, S., Seaman, M., Brown, K., Kempkes, B., Hibshoosh, H., and Levine, B. (1999). Induction of autophagy and inhibition of tumorigenesis by beclin 1. Nature *402*, 672–676.

Madonna, R., Cevik, C., Nasser, M., and De Caterina, R. (2012). Hepatocyte growth factor: molecular biomarker and player in cardioprotection and cardiovascular regeneration. Thromb. Haemost. *107*, 656–661.

Martin, D.N., and Baehrecke, E.H. (2004). Caspases function in autophagic programmed cell death in Drosophila. Development *131*, 275–284.

Marusyk, A., Porter, C.C., Zaberezhnyy, V., and DeGregori, J. (2010). Irradiation selects for p53-deficient hematopoietic progenitors. PLoS Biol. *8*, e1000324.

Morata, G., and Ripoll, P. (1975). Minutes: mutants of Drosophila autonomously affecting cell division rate. Dev. Biol. *42*, 211–221.

Moreno, E., and Basler, K. (2004). dMyc transforms cells into super-competitors. Cell *117*, 117–129.

Murphy, D.J., Junttila, M.R., Pouyet, L., Karnezis, A., Shchors, K., Bui, D.A., Brown-Swigart, L., Johnson, L., and Evan, G.I. (2008). Distinct thresholds govern Myc's biological output in vivo. Cancer Cell *14*, 447–457.

Nieminen, A.I., Eskelinen, V.M., Haikala, H.M., Tervonen, T.A., Yan, Y., Partanen, J.I., and Klefström, J. (2013). Myc-induced AMPK-phospho p53 pathway activates Bak to sensitize mitochondrial apoptosis. Proc. Natl. Acad. Sci. USA *110*, E1839–E1848.

Poelmann, R.E., Molin, D., Wisse, L.J., and Gittenberger-de Groot, A.C. (2000). Apoptosis in cardiac development. Cell Tissue Res. *301*, 43–52.

Rana, M.S., Christoffels, V.M., and Moorman, A.F. (2013). A molecular and genetic outline of cardiac morphogenesis. Acta Physiol. (Oxf.) *207*, 588–615.

Sancho, M., Di-Gregorio, A., George, N., Pozzi, S., Sánchez, J.M., Pernaute, B., and Rodríguez, T.A. (2013). Competitive interactions eliminate unfit embryonic stem cells at the onset of differentiation. Dev. Cell *26*, 19–30.

Shah, B.H., and Catt, K.J. (2003). A central role of EGF receptor transactivation in angiotensin II -induced cardiac hypertrophy. Trends Pharmacol. Sci. *24*, 239–244.

Sohal, D.S., Nghiem, M., Crackower, M.A., Witt, S.A., Kimball, T.R., Tymitz, K.M., Penninger, J.M., and Molkentin, J.D. (2001). Temporally regulated and tissue-specific gene manipulations in the adult and embryonic heart using a tamoxifen-inducible Cre protein. Circ. Res. *89*, 20–25.

Soonpaa, M.H., Kim, K.K., Pajak, L., Franklin, M., and Field, L.J. (1996). Cardiomyocyte DNA synthesis and binucleation during murine development. Am. J. Physiol. *271*, H2183–H2189.

Stanley, E.G., Biben, C., Elefanty, A., Barnett, L., Koentgen, F., Robb, L., and Harvey, R.P. (2002). Efficient Cre-mediated deletion in cardiac progenitor cells conferred by a 3'UTR-ires-Cre allele of the homeobox gene Nkx2-5. Int. J. Dev. Biol. *46*, 431–439.

Tamori, Y., and Deng, W.M. (2013). Tissue repair through cell competition and compensatory cellular hypertrophy in postmitotic epithelia. Dev. Cell *25*, 350–363.

Tsai, J.Y., Kienesberger, P.C., Pulinilkunnil, T., Sailors, M.H., Durgan, D.J., Villegas-Montoya, C., Jahoor, A., Gonzalez, R., Garvey, M.E., Boland, B., et al. (2010). Direct regulation of myocardial triglyceride metabolism by the cardiomyocyte circadian clock. J. Biol. Chem. *285*, 2918–2929.

Tyler, D.M., Li, W., Zhuo, N., Pellock, B., and Baker, N.E. (2007). Genes affecting cell competition in Drosophila. Genetics *175*, 643–657.

Vincent, S.D., and Buckingham, M.E. (2010). How to make a heart: the origin and regulation of cardiac progenitor cells. Curr. Top. Dev. Biol. *90*, 1–41.

Vincent, J.P., Fletcher, A.G., and Baena-Lopez, L.A. (2013). Mechanisms and mechanics of cell competition in epithelia. Nat. Rev. Mol. Cell Biol. *14*, 581–591.

Xiao, G., Mao, S., Baumgarten, G., Serrano, J., Jordan, M.C., Roos, K.P., Fishbein, M.C., and MacLellan, W.R. (2001). Inducible activation of c-Myc in adult myocardium in vivo provokes cardiac myocyte hypertrophy and reactivation of DNA synthesis. Circ. Res. *89*, 1122–1129.

Yang, L., Cai, C.L., Lin, L., Qyang, Y., Chung, C., Monteiro, R.M., Mummery, C.L., Fishman, G.I., Cogen, A., and Evans, S. (2006). Isl1Cre reveals a common Bmp pathway in heart and limb development. Development *133*, 1575–1585.